Application of Arterial Spin Labelling as Perfusion Imaging in Acute and Chronic Ischaemic Stroke Patients

Zanariah Binti Mohd
BSc. (Hons), MSc (UK)

Submitted in fulfilment of requirements for the Degree of Doctor of Philosophy

Institute of Neuroscience and Psychology
University of Glasgow

January, 2023

Abstract

Introduction

The assessment of cerebral blood flow (CBF) perfusion is an important measure in clinical practice for evaluating the clinical and imaging outcomes in ischaemic stroke patients. Various imaging methods been applied to measure CBF, including applications of nuclear medicine, computed tomography perfusion (CTP) and contrast-enhanced Magnetic Resonance Imaging (MRI). However, each of these modalities has some disadvantages, such as excess radiation or contraindications to contrast agents, and limited repeatability.

The thesis aimed to explore the clinical application of arterial spin labelling (ASL) as perfusion imaging among acute and chronic ischaemic stroke patients. Clinical and imaging data in this thesis were obtained from two prospective ischaemic stroke databases, namely WHISPER and XILOFIST. Both studies used ASL as one of the perfusion imaging methods.

Methods and results

Before further studies, I conducted various detailed image post-processing steps to acquire the quantitative value of CBF from ASL raw data. The image post-processing steps include structural T1-image processing, creation of grey matter, white matter and lesion masks, distortion correction, and image co-registrations. These post-processing steps were performed using Statistical Parametric Mapping (SPM12) and Bayesian Inference for Arterial Spin Labelling (BASIL) software for studies in Chapter 3 until Chapter 6.

In Chapter 3, two commonly used ASL sequences which were PCASL with multi-post labelling delays (multi-PLDs) and PASL (single-PLD), were compared to investigate their agreement. 35 subjects from WHISPER study underwent ASL scanning for both sequences. Grey matter and white matter CBF for these subjects were compared. Although there was a significant correlation between PCASL and PASL in measuring grey matter ($r=0.997$, $p<0.001$) and white matter ($r=0.991$, $p<0.001$) cerebral perfusion, the Bland-Altman analysis demonstrated

large agreement between these ASL sequences suggesting the several systematic biases. These findings suggested that multi-PLDs PCASL sequence is recommended in patients with delayed blood flow, especially in ischaemic stroke patients.

Further to this work, the assessment of reperfusion status among 63 WHISPER subjects was measured using PCASL sequence. Reperfusion index (RI) was established as a quantitative indicator by calculating the difference between the reperfusion among recanalised and non-recanalised subjects. RI $\leq$ 0 – 0.4 indicated mild reperfusion, RI 0.41 to 0.70 indicated moderate reperfusion and RI 0.71 to 1.0 indicated high reperfusion. Correlation and predictions between ASL reperfusion index and clinical and imaging outcomes were statistically analysed. Reperfusion index was significantly correlated with infarct growth ($r = 0.421$, $p<0.001$) and positively correlated with penumbra salvage ($r = 0.297$, $p=0.021$). Regression analyses showed reperfusion index was a significant independent predictor for early neurological improvement (OR 1.370, 95% CI 0.572 to 16.721; $p<0.036$) and 90-day good functional outcome (OR 49.817; 95% CI 3.097 – 801.435; $p=0.006$).

In Chapter 6, perfusion assessment of white matter hyperintensities (WMH) among 159 chronic ischaemic stroke patients was investigated in XILO-FIST study. Baseline WMH volume and perfusion were calculated. Correlation and predictions between ASL volume and perfusion with associated WMH risk factors and WMH progression were analysed. The result of this study showed WMH perfusion was significantly associated with age and WMH volume. Furthermore, lower WMH perfusion was significantly associated with increased WMH burden as scored using Fazekas score.

Conclusions

The studies presented in this thesis demonstrated the clinical application of ASL in quantifying cerebral blood flow among patients with acute and chronic ischaemic stroke. It is concluded that ASL is a suitable imaging technique for continuous cerebral perfusion assessments as it has no radiation risks and is non-invasive. In addition, the reperfusion index measured by ASL can serve as potential imaging biomarkers in predicting imaging and clinical outcomes.

Table of Contents

List of tables

List of figures

Acknowledgement

A special thank you to Professor Keith Muir for his endless support and guidance through my PhD journey. I may not be able to complete this thesis without his constant encouragement. Not to forget my co-supervisor, Prof. David Potter, for his input on ASL imaging.

Our thanks to Professor Michael Chappell and his team at the University of Oxford for our useful early discussions on arterial spin labelling methods and agree to share the PCASL ASL sequence with University of Glasgow.

Special thanks also to Dr. Viveka Biswas, for her invaluable effort on compiling the clinical and imaging data for WHISPER study.

Thanks to everyone at Imaging Centre of Excellence (ICE), University of Glasgow, especially Dr. Graeme Keith and Tracey Hopkins for helping with the installation of the PCASL ASL sequence from University of Oxford to the MRI clinical scanner in ICE. Thank you to radiographers who help me to compile all the MRI images from the research scanner.

Finally, many special thanks to my mother and my husband for your endless support and financial aid, and my daughter, Maryam, for keeping me sane during the whole 4 years of my PhD journey.

Author's declaration

The data in this thesis was based clinical databases of WHISPER and XILO-FIST studies from University of Glasgow. This thesis comprises my own work, unless otherwise acknowledged and referenced and has not been submitted for any degree at the University of Glasgow or any other institutions.

Zanariah Mohd
January, 2023

Abbreviations

ADC	apparent diffusion coefficient
AIF	arterial input function
AOL	arterial occlusion lesion
ASL	arterial spin labelling
ASPECTS	Alberta Stroke Program Early CT Score
ATT	arterial transit time
BASIL	Bayesian Inference for Arterial Spin Labelling
BP	Blood pressure
BBB	blood-brain barrier
CASL	continuous arterial spin labelling
CBF	cerebral blood flow
CBV	cerebral blood volume
CMRO2	cerebral metabolic rate of oxygen
CPP	cerebral perfusion pressure
CT	computed tomography
CTA	CT angiography
CTP	CT perfusion
CVR	cerebrovascular resistance
DSC	dynamic susceptibility contrast
DTI	diffusion tensor imaging
DWI	diffusion-weighted images
FLAIR	fluid-attenuated inversion recovery
FSL	FMRIB Software Library
Gd	gadolinium
HIR	Hypoperfusion intensity ratio
HU	Hounsfield unit
ICH	intracerebral haemorrhage
IQR	interquartile range
LACS	lacunar stroke
LVO	large vessel occlusion
MABP	mean arterial blood pressure
MCA	middle cerebral artery
MRA	magnetic resonance angiography
MRI	magnetic resonance imaging
mRS	modified Rankin Scale
MTT	mean transit time
NAWM	normal appearing white matter
NCCT	non-contrast computed tomography
NIHSS	National Institutes of Health Stroke Scale
OEF	oxygen extraction fraction
PACS	partial anterior circulation stroke
PASL	pulsed arterial spin labelling
PCASL	pseudo-continuous arterial spin labelling
PET	positron emission tomography
PLD	post-labelling delay
POCS	posterior circulation stroke

PWI	perfusion-weighted imaging
rCBF	relative cerebral blood flow
rCBV	relative cerebral blood volume
SD	standard deviation
SPECT	single photon emission tomography
SVD	small vessel disease
SWI	susceptibility-weighted imaging
T1	T1-weighted MR imaging
T2	T2-weighted MR imaging
TACS	total anterior circulation stroke
TE	echo time
TI	inversion time
TIA	transient ischaemic attack
TTP	time-to-peak
VOF	venous outflow function
WMH	white matter hyperintensities

Chapter 1 Ischemic stroke and white matter hyperintensities

1.1 Introduction

Stroke is a leading cause of death, and it is also a leading cause of long-term disability. In 2019, stroke is regarded as the second leading cause of disability in 50 years and older subgroup (Vos *et al.*, 2020). The Global Burden of Diseases Study 2016 indicated that the global burden of stroke is likely to remain high with equal prevalence between women and men (Johnson *et al.*, 2019). Among the risk factors that contribute to the burden of stroke are high blood pressure, smoking, diabetes, hyperlipidaemia and physical inactivity (Campbell and Khatri, 2020). These risk factors are categorized as modifiable and could be prevented.

Generally, the World Health Organization (WHO) defines stroke as focal disturbance of cerebral functions with rapid developing clinical signs lasting more than 24 hours or leading to death (Aho *et al.*, 1980). However, this general and broad definition of stroke does not consider of the nature and clinical and imaging findings of stroke. In 2013, the stroke definition has been updated by the Stroke Council of the American Heart Association/American Stroke Association based on nature, timing, clinical and imaging findings. The term stroke definition includes all the following: CNS infarction, ischaemic stoke, stroke by intracerebral haemorrhage, stroke by subarachnoid haemorrhage, stroke by venous thrombosis and stroke of not otherwise specified (Sacco *et al.*, 2013).

Despite several definitions of stroke, they share a common basis which is the disruption of blood supply to the brain. The disruption of the blood supply may be due to blood clot blocking the blood vessels which is in the case of ischaemic stroke and deep perforating vasculopathy related to high blood pressure in intracerebral haemorrhage (ICH) (Cordonnier *et al.*, 2018). 85% of stroke accounts for ischaemic stroke while 15% are ICH (Zerna *et al.*, 2018). Ischaemic stroke is caused by large artery disease, cardioembolic, small artery disease including lacunar, and other causes. Ischaemic stroke can be further categorized according to Oxfordshire Community Stroke Project classification. The classification was based on the region of occluded vessels visualised on brain

imaging which are total anterior circulation syndrome (TACS), partial anterior circulation syndrome (PACS), lacunar syndrome (LACS) and posterior circulation syndrome (POCS) (Mead *et al.*, 2000).

Accurate diagnosis and investigation of time of ischaemic stroke onset are very important in determining the treatment types. With the advancement of imaging techniques, structural and physiological information of ischaemic stroke patients can be determined. Clinical trials had established the treatment time window based on imaging techniques such as computed tomography (CT) and magnetic resonance imaging (MRI). The thrombolysis treatment using alteplase is proven to be safely administered within the first 4.5 hours (Hacke *et al.*, 1995) and this treatment could be extended to first 9 hours provided there is imaging evidence of salvageable tissue (Ringleb *et al.*, 2019).

1.2 Pathophysiology and haemodynamic of ischaemic stroke

Oxygen and glucose are the main substrate for brain metabolism. These substrates are supplied to the brain by the cerebral circulation. In ischaemic stroke, the cerebral circulation is occluded and can cause reduction of cerebral blood flow (CBF) and oxygen supply to the brain which consequently disrupt the brain normal function.

Brain cells requires high glucose and oxygen to maintain their function. In region of reduced CBF, the production of energy in form of adenosine triphosphate (ATP) by mitochondria is reduced. This will cause lactic acidosis and disruption of ionic haemostasis. Reduction of CBF below the critical threshold triggers a cascade of mechanism that will lead to cell death that occurs depending on severity of CBF reduction between minutes and several hours. The mechanisms include excitotoxicity, peri-infarct depolarisation, oxidative stress, inflammation, and apoptosis.

Excitotoxicity occurs when there is an increase in glutamate neurotransmitters released from ischaemic brain cells and glia. Glutamate promotes the activation of N-methyl-D-aspartic acid (NMDA), α-amino-3-hydroxy-5-methylisoxazole-4-propionate (AMPA) and kainic acid (KA) receptors. These

receptors are responsible for the cellular ionic imbalance due to increase in the influx of calcium (Ca^+), sodium (Na^+) and Cl^- to the cells through the ion channel. Water flows passively into cells with ion influx and causes cytotoxic oedema. Excitotoxicity also triggers catabolic enzyme activities which will lead to apoptosis and necrosis through series of complex biochemistry mechanisms.

Excessive increase of glutamate and K+ lead ischaemic cells to depolarize. The cells' depolarization is associated with cortical spreading depression (CSD) where the neuro-electrical activity is depressed and results in prolonged cellular depolarization and failure of ionic homeostasis. CSD has been associated with the penumbral region (Strong, Venables and Gibson, 1983) and is known as peri-infarct depolarisation. In the infarct core region, cells will suffer from permanent depolarization and ionic imbalance due to energy failure. However, in penumbral region, cells may continue to repolarize at the expense of energy consumption. If cells do not restore energy supply, cells in the penumbral region may be recruited to the core region caused by CSD.

The ionic imbalance stimulates the production of free radicals which can damage important cell survival molecules such as lipids, proteins, nucleic acid, and carbohydrates (Xing *et al.*, 2012). Eventually, these complex cascades will result in neuronal death.

1.3 **Regulation of cerebral perfusion**

Cerebral perfusion is the process of delivering nutrients to the capillaries in the brain. This process is very important to ensure the brain receives adequate blood supply which carries the nutrients for it to function normally. The haemodynamic state of the cerebral perfusion is regulated by a mechanism called cerebral autoregulation. Cerebral autoregulation maintains the CBF when there are any changes in the cerebral perfusion pressure (CPP). In normal circumstances, the cerebral autoregulation functions at mean arterial blood pressures (MABP) between 60 mmHg and 150 mmHg. Changes in the MABP beyond its limit can cause the CBF to drop or increase extensively (Figure 1-1).

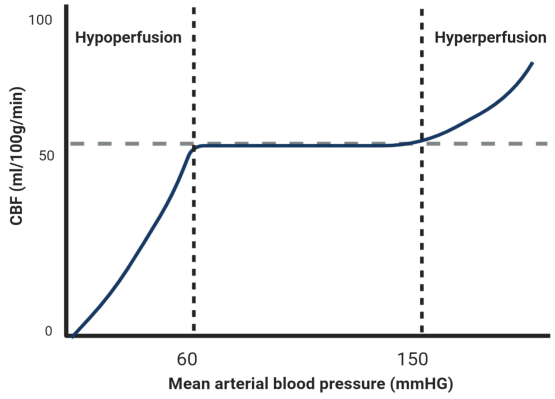

Figure 1-1: Limit of cerebral perfusion pressure.
Figure adopted from Markus, 2004.

Cerebral autoregulation is impaired during ischaemia. The dynamic response of cerebral autoregulation in ischaemic stroke has been extensively reviewed by Markus, 2004. During hypoperfusion state, the brain attempts to maintain its blood flow by dilating the arteries and reduce the cerebrovascular resistance (CVR) in a process called vasodilation. The vasodilatory response caused increase in cerebral blood volume (CBV). At this state, the oxygen extraction fraction (OEF) will increase if the CPP and the CBF continue to fall. The relationship between CPP, CBF, CBV and OEF can be shown in Figure 1-2.

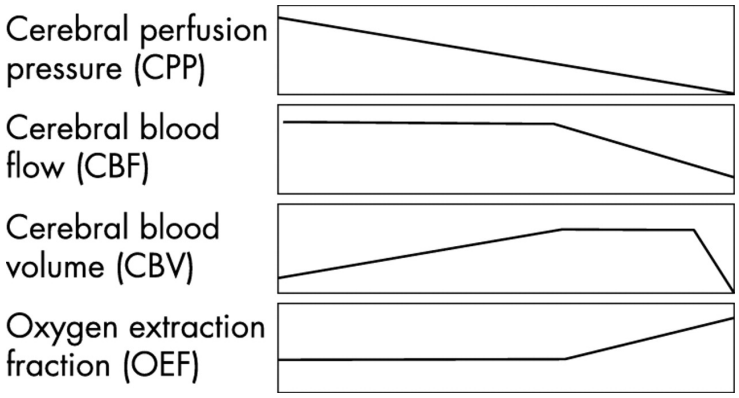

Figure 1-2: Relationship between CPP, CBF, CBV and OEF during hypoperfusion state (Adopted from Markus, 2004).

1.4 Cerebral Perfusion Parameters

1.4.1 Derivation of cerebral perfusion parameters on imaging

The principle of cerebral perfusion parameters is derived from the tissue-time concentration when a contrast bolus enters the cerebral arteries. In stroke imaging, cerebral perfusion parameters are commonly derived using CT perfusion and dynamic susceptibility contrast (DSC) MRI. The general principles of deriving cerebral perfusion parameters such as CBF, cerebral blood volume (CBV) and mean transit time (MTT) are the same for both imaging techniques.

Derivation of the cerebral perfusion parameters starts by tracking the first circulation of the contrast agents through brain tissue after contrast administration. The function of contrast agents or bolus tracking is to measure change in tissue signal or attenuation that allows calculation of arterial, tissue and venous contrast concentration. An assumption is made during the bolus tracking that contrast agents will not be absorbed or diffused during the first pass. In other words, it should remain in the intravascular space. Following this assumption, the concentration of contrast agents in the arterial input is the same concentration at the venous output. The contrast agent concentration in these compartments over time can be translated by plotting the tissue-time concentration curve. The cerebral perfusion parameters such as time-to-peak (TTP), cerebral blood volume (CBV) and CB, mean transit time (MTT) and Tmax

can be derived from the tissue concentration time curve with the aid of automated image post-processing software (Konstas *et al.*, 2009).

Deconvolution technique is a mathematical modelling technique to derive cerebral perfusion parameters from the tissue concentration time curve (Figure 1-3) (Østergaard, 2005). The tissue concentration time curve represents the concentration of contrast agents in tissue after a bolus injection through an artery (arterial input function (AIF)). Several measurable parameters such as arrival time (AT), and full width at half maximum (FWHM) can be derived from the tissue time concentration curve. Perfusion parameters such as CBF, CBV and Tmax can be derived after mathematical deconvolution of the tissue concentration time curve (Figure 1-3b).

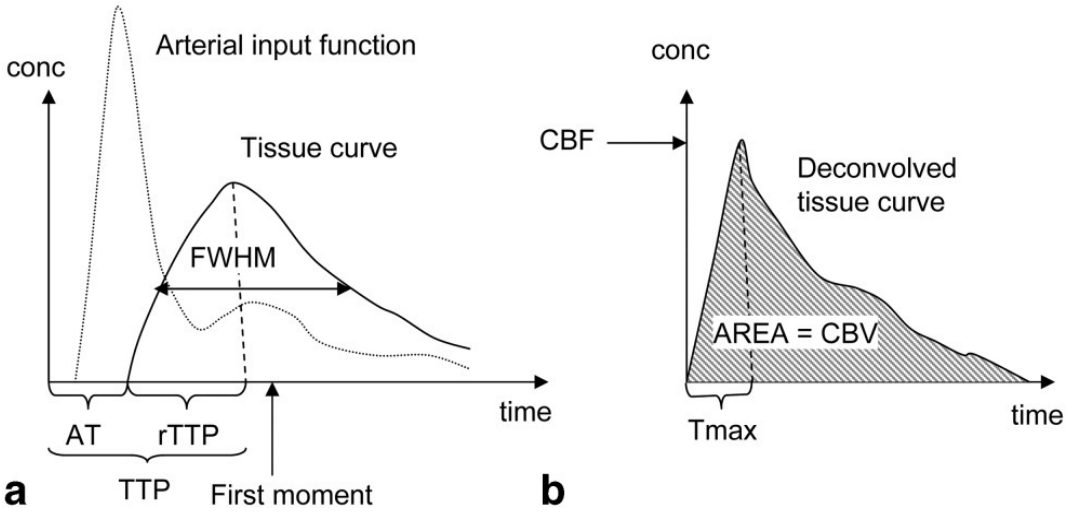

Figure 1-3: Tissue concentration time curve
The measured tissue concentration time curve gives rises to various measures of the transit time that all depend on the local shape of AIF. The arrival time (AT) of the bolus mainly reflects collateral circulation. The time to peak, to some extent, reflects tissue transit time (TTP) and, if arrival delay is included, also reflects collateral circulation (TTP). The first moment (the centre of gravity) and the full width at half maximum (FWHM) of the tissue concentration time curve mainly depend on tissue MTT. b: Deconvolution of the curves in (a) removes the dependence on the arterial input curve and produces the deconvolved tissue curve. In the presence of arterial delays, the deconvolved curve is not maximal at t // 0, but instead is maximal (the tissue impulse response function) after a certain delay (Tmax). CBF is usually taken as the curve height of the deconvolved curve at time Tmax. MTT is calculated as CBV/CBF, where CBV is determined as the area under the deconvolved curve (b) or the tissue curve (a). However, calculation of CBV from the tissue curve requires laborious corrections for tracer recirculation. Reproduced with permission from Østergaard, 2005.

1.4.2 **Mean transit time (MTT)**

MTT is the average of the transit time of blood through a given brain region which is measured in seconds (s) The factors that may affect the MTT are distance travelled between arterial inflow and venous outflow.

1.4.3 **Time to peak (TTP)**

TTP is the time at which contrast enhancement reaches its maximum. TTP is the simplest parameter to measure. TTP maps are usually well-defined and easy to interpret. Besides, it is a reproducible technique which means that TTP measured from one centre to another will be the same for a given data set.

1.4.4 **Cerebral blood flow (CBF)**

CBF is defined as blood volume that flows per unit mass per unit time in brain tissue. It is expressed in unit of ml/100g/min. In healthy adults, the average CBF is 60ml/100g/min. White matter has lower CBF (~20ml/100g/min) as compared to grey matter (~80ml/100g/min). CBF or cerebral perfusion is important in oxygen and substrates delivery and thus maintaining normal brain function and viability.

1.4.5 **Cerebral blood volume (CBV)**

CBV is defined as total volume of blood in each unit volume of the brain. CBV is measured in unit of millilitres of blood per 100 g of brain tissue (mL/100g).

1.4.6 **Tmax**

Tmax is the maximum time of the tissue residue function in each voxel to reach its maximum value after deconvolution. It reflects bolus time arrival.

1.5 Perfusion CBF threshold defining region of ischaemia

Occlusion in cerebral blood vessels causes decrease in CBF in brain parenchyma. Reduction in CBF triggers several ischaemic cascades that disrupts the biochemical, functional, and structural integrity of brain cells. Different components and features of the ischaemic cascade occur at different flow thresholds and may be used to discriminate the irreversible ischaemic core, and ischaemic penumbra which was proposed by Astrup and his colleagues (Astrup, Siesjö and Symon, 1981). While most of the early evidence of CBF thresholds were based on animal stroke models (Branston *et al.*, 1974; Heiss, Hayakawa and Waltz, 1976) only a few validated studies were conducted based on human studies (Bandera *et al.*, 2006). Despite several methods to establish CBF perfusion threshold, Hossmann, 1994, summarised a rank of order of perfusion threshold differentiating the threshold of electrical failure and threshold of membrane failure (Figure 1-4).

CBF threshold is very important to provide the clinicians with the knowledge of underlying physiological function of the brain. Clinical examination alone cannot establish the underlying processes inside the brain. By establishing the CBF threshold in the ischaemic brain, the appropriate treatment could be planned accordingly. The aim of ischemic stroke treatment is to establish perfusion at the region of brain that could be potentially saved and to avoid unnecessary treatments such as reperfusion of ischemic core that could lead to severe haemorrhage.

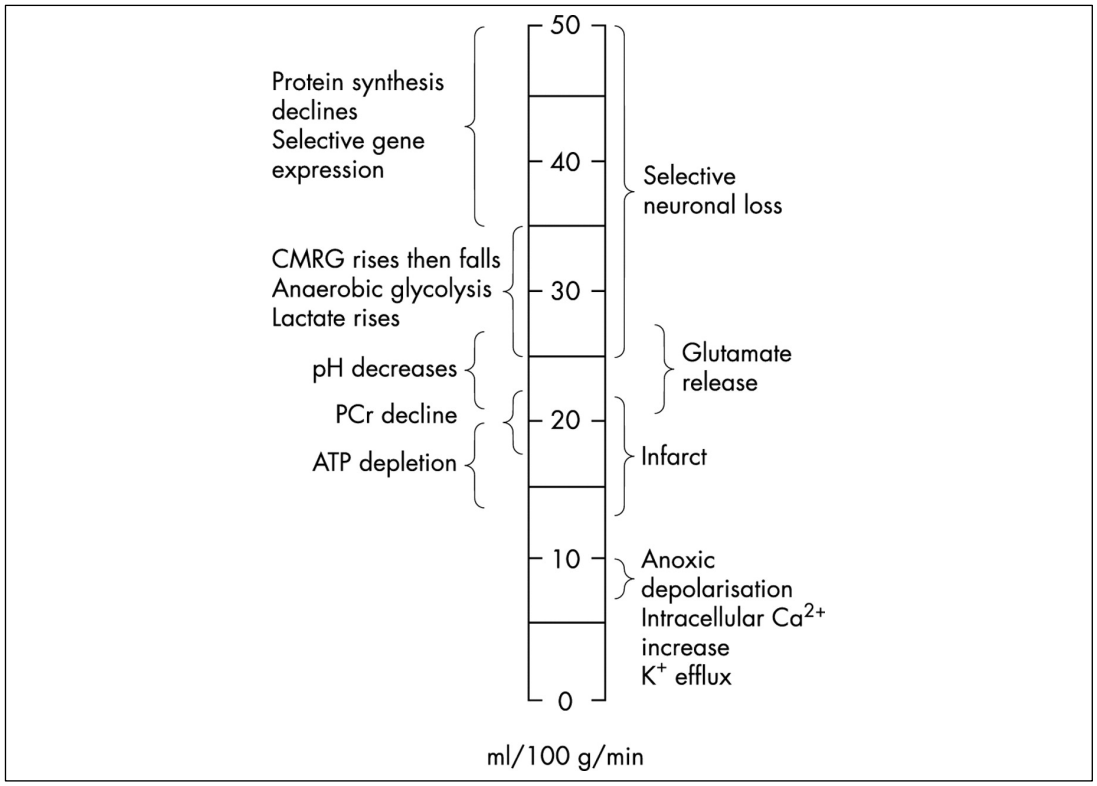

Figure 1-4: CBF flow threshold in relation to biochemical and neuronal changes. Adapted from Markus,2004

1.5.1 **Ischaemic core**

The brain region that suffers the most severe hypoperfusion is called ischaemic core. Ischaemic core can be defined as the region with electrically silence, depletion of energy metabolites and failure of cell membrane which can lead to ionic imbalance and cytotoxic oedema. Damaged cells in this region are regarded as irreversible and could not be treated.

The concept of ischaemic core is historically described based on animal experiments based on the CBF threshold. There is a range of CBF threshold that describes ischaemic core based on the duration of occlusion. The term ischaemic is always interchangeably used in literature between the infarcted brain tissue or hypoperfused brain tissue that is likely to infarct if reperfusion does not occur.

In animal model studies, the range of CBF for the electrical cessation range between 12ml/100g/min to 18 ml/100g/min (Branston *et al.*, 1974; Heiss, Hayakawa and Waltz, 1976) while the loss of ion homeostasis which manifest as massive release of intracellular K+ and influx of Na+ and Ca2+ occur as low as 2

ml/100g/min to 17 ml/100g/min (Astrup *et al.*, 1977). These early animal studies motivated the investigation of CBF threshold in human. Severe ischaemic core was observed at CBF range from 4.8 ml/100g/min to 8.4 ml/100g/min below 6 ml/100g/min in patients with middle cerebral (MCA) occlusion (Kaufmann *et al.*, 1999; Marchal *et al.*, 1999; Heiss *et al.*, 2001).

1.5.2 **Ischaemic penumbra**

The CBF threshold within the core may rises progressively over time to reach a certain threshold where the cellular damages seem to restore, indicating potential recovery of the hypoperfused brain cells. Hypoperfused brain cells within the recovery threshold is called penumbral tissue or ischaemic penumbra which has been the focus in ischaemic stroke diagnosis and therapy.

The ischaemic penumbra has been identified to surround the ischaemic core and this concept has been originally described by Astrup et al., 1981. This area was observed in baboon cortex where the neurons were structurally intact but functionally inactive (Astrup *et al.*, 1977). The penumbral tissue is regarded as potentially salvageable tissue because the energy metabolism is still preserved. The operational definition of ischaemic penumbra includes ischaemic tissue which exhibits high oxygen extraction fraction (OEF), low CBF and low but preserve cerebral metabolic rate of oxygen (CMRO2) (Furlan *et al.*, 1996).

The concept of penumbra should be viewed in various approaches. In early studies the concept of penumbral tissue was discussed in the light of the severity of the CBF reduction and the duration of ischaemia. Evidence of abnormal pattern of neuronal activity in animals was detected at blood flow threshold higher than 18ml/100g/min (Heiss, Hayakawa and Waltz, 1976). These observations suggest the neuronal damage could be reversible without permanent damage. However, poor functional recovery was observed at lower threshold if the duration of ischaemic is prolonged (Heiss and Rosner, 1983). Jones et al., 1981, observed the ischaemic penumbra may exist up to 3 hours after stroke onset in primates. However, ischaemic penumbra in human may last up to 48 hours in human (Read *et al.*, 2000). These studies suggest the dynamic state of penumbra.

While these studies highlighted the severity of CBF reduction and duration of ischaemia, the role of collateral flow in determining the ischaemic penumbra outcome has been identified using advanced imaging techniques. In a multicentre study, large penumbra volume was associated with better collateral flows in untreated ischaemic stroke patients within 24 hours of stroke onset (Vagal *et al.*, 2018).

These evidence forms the basis for the criteria defining the penumbra in which the cerebral blood flow perfusion is less than 20ml/100g/min, shows abnormal neuronal function, develops cellular dysfunction but not death, and the recovery of the tissue is correlated with better clinical outcome (Keith W Muir *et al.*, 2006)

Penumbra region provides beneficial information in ischaemic stroke diagnosis and treatment strategies. There is imaging evidence of persisting penumbra still present from 6 hour to 16 hour after the stroke onset (Marchal, Beaudouin, *et al.*, 1996) which offers delayed treatment opportunities to some patients.

1.5.3 **Oligaemia**

Another hypoperfuse tissue state which less discussed in the literature is oligaemia. Unlike penumbra tissue, oligaemia functions normally and may recover without the need of reperfusion therapy. The oligaemia tissue, which surrounds the penumbra region, is not at risk of infarction. However, oligaemic tissue may be recruited into penumbra region (K W Muir *et al.*, 2006)

The characteristics of oligaemia include high OEF and mild reduction of CBF (Marchal, Furlan, *et al.*, 1996). In imaging, it is difficult to differentiate between penumbra and oligaemia in which the penumbra usually includes the oligaemia. There is also uncertain CBF threshold demarcation between penumbra tissue and oligaemia. Distinguishing oligaemia that is above the threshold of penumbra but below the normal threshold, may be technically difficult due to limited spatial resolution and imprecise bounding thresholds of current imaging. Whether there are pathological consequences of oligaemia (such as selective neuronal loss) requires further investigation.

1.6 Stroke Imaging Techniques

Stroke imaging plays an important role in the evaluation of ischaemic stroke. It has become the essential investigation for stroke assessment as the pathophysiology of stroke differs from individuals. Structural and functional information on the nature of the ischemic stroke could be identified and acts as imaging biomarkers. Various stroke imaging techniques such as nuclear medicine tracers using positron emission tomography (PET) and single photon emission computed tomography (SPECT), conventional computed tomography (CT), perfusion CT (CTP) and magnetic resonance imaging (MRI) with various advanced sequences have been developed and widely used in stroke clinical research.

These imaging techniques works on different principles, and they have their own advantages and disadvantages. Choosing the proper imaging techniques is very crucial and it is based on what type of information is needed in the clinical setting. This is to ensure appropriate decision-making in treating the patient is made in timely manner.

1.6.1 Nuclear medicine tracers

Positron emission tomography (PET) has been utilised widely during in the early years of ischaemic stroke studies both in animals and human. The radionuclide decay emits positron and causes annihilation when the positron collides with electron and produces two equivalent energy of gamma photons (511 keV). These gamma photons are detected with gamma detectors (Powers and Raichle, 1985). The most used radiotracers in stroke imaging are ^{15}O, ^{11}C and ^{18}F and can be used to label metabolic compound such as water which make them as endogenous contrast agents.

Single-photon computed tomography (SPECT), is another nuclear medicine method used in stroke imaging. Like PET, SPECT uses the concept of nuclear decay which emits photons. However, SPECT is less sensitive compared to PET due to the scattering of photons. Thus, SPECT requires a collimator to its detector to focus the scattering photons directly to the camera. The common radiotracers for SPECT in brain imaging are ^{133}Xe ,^{123}Iodine and ^{99}Technetium.

99mTc-DTPA (diethylene triamine penta-acetic acid) offers great advantages as it is lipophilic and able to cross the blood brain barrier.

Both PET and SPECT are able to measure CBF during ischaemia. Non-diffusible SPECT radiotracers only allows semiquantitative (Limburg *et al.*, 1990; Hanson *et al.*, 1993) measurement while diffusible SPECT radiotracers such as ^{133}Xe allows quantitative CBF measurement (Yonas *et al.*, 1991). In relation, PET can provide absolute CBF in its perfusion unit of ml/g/min and able to measure other perfusion parameters such OEF and CBV (Gibbs *et al.*, 1984).

The disadvantage of these nuclear medicine imaging techniques is radiation dose. Due to this, other alternative imaging methods are being used to overcome this issue. Despite its disadvantages, nuclear medicine imaging has provided important information on cerebral perfusion physiological information. The establishment of CBF threshold in cerebral ischaemia as discussed previously has been the reference for current cerebral perfusion measurement in advanced imaging.

1.6.2 **Non-contrast Computed tomography**

Computed tomography (CT) has been widely used in the management of stroke due to its fast acquisition time and availability. In stroke imaging, NCCT serves two purposes, in which NCCT are used to delineate between ischaemic and haemorrhagic lesions and to exclude other stroke mimics such as migraine aura and Moya-Moya disease. NCCT measures the attenuation of X-ray in tissue which is expressed by Hounsfield unit (HU). The HU is calculated based on water density and any tissues which are denser than water such as brain parenchyma and blood will increase the amount of HU and appears hyperdense in CT images. However, the composition of blood changes over time reducing HU density as haemoglobin breaks down. During this time, the ischaemic lesions appear hypodense in NCCT images.

Among the classic NCCT appearance of early ischaemia are parenchymal hypodensity (loss of the insular ribbon), obscuration of the lentiform nucleus,

loss of grey and white matter differentiation and subtle effacement of cortical sulci. In addition, the presence of arterial thrombus can be visualised as the hyperdense artery sign. These early ischaemic changes represent different pathological processes in acute ischaemia and the visualisation of early ischaemic changes can be subtle depending on the time of imaging. Some studies showed poor detection of early ischemic signs using NCCT during the first 3 hours. The hypodense visualisation on NCCT indicate the cytotoxic oedema process in ischemic lesion. The formation of cytotoxic oedema is highly associated at 3 hours after stroke onset in which there was a relationship between the ASPECTS score declines with stroke onset more than 3 hours compared to 0 to 3 hours (Gao *et al.*, 2017). In addition, NCCT provides useful imaging appearances in differentiating ischaemic core (hypodense) and ischaemic penumbra (isodense) within 6 hours from stroke onset (Muir *et al.*, 2007)

Some studies had reported low sensitivity of NCCT in detecting early ischaemic changes although others argue that it depends on the experience of the observer. However, NCCT is still applicable as first line imaging procedure to rule out ischaemic stroke. In major stroke clinical trial, the NINDS trial used NCCT as the only imaging technique for baseline and follow-up radiological examinations to identify intracerebral haemorrhage (The National Institute of Neurological Disorders and Stroke rt-PA Stroke Study Group, 1995). This is followed by other clinical trials include ECASS, ECASS 2 and ECASS 3 in which utilized NCCT to identify early infarct signs in the middle cerebral artery (MCA). Besides, NCCT able to exclude other stroke mimics which include brain tumours and arteriovenous malformation.

NCCT allows the identification of early ischaemic changes using Alberta Stroke Program Early CT Score (ASPECTS) at parenchymal level. One score will be deducted from the full score (10 score) if there is an evident of hypoattenuation in MCA territory. NCCT is important to assess the extent of ischaemic lesions within vascular territory. Evidence of hypodensity more than one-third of MCA is contraindicated for revascularization therapy due to haemorrhagic complications. ASPECTS is significantly correlated with NIHSS and able to predict functional outcome (Barber et al., 2000).

1.6.3 **CT angiography**

CT angiography (CTA) can be performed after ruling out any haemorrhagic sign on NCCT. CTA allows the visualisation of the blood vessels patency in two-dimensions (2D) or three-dimensions (3D) after contrast enhancement through image post-processing. The visualisation of the vessel fillings aid in the assessment of vessel occlusion, collateral flow, and vessel recanalization. Vast developments of CT scanner such as increased number of detectors and number of slices allows the routine application of CTA in acute stroke assessments. CTA is recommended to be included as part of the ischaemic stroke baseline imaging and is widely available (Wintermark *et al.*, 2008). In relation to this recommendation, CTA has been included as one of the imaging tools in major clinical trials (Albers *et al.*, 2018; Ma *et al.*, 2019).

Presence of collateral flow and vessels occlusion can be assessed using CTA. Visual assessment of arterial patency can be graded into collateral score. Collateral score of 3 indicates maximal collateral flow whereas collateral score of 0 indicates no collaterals (Tan *et al.*, 2007). In addition to collateral flow, CTA provides important information on the vessel occlusion. High diagnostic accuracy (with sensitivity range from 87%, and specificity 84%) of vessel occlusion detected by CTA has been reported (Verro *et al.*, 2002)). Furthermore, in 92 patients with proximal intracranial occlusion, favourable functional outcomes (mRS 0-2) were observed in 92 patients with good collateral status assessed using CTA (Miteff *et al.*, 2009. In a large prospective multicentre acute stroke study, CTA has a moderate positive predictive value (PPV) (63% for presence of proximal intracranial occlusion, 66 % for leptomeningeal collaterals and 58 % for carotid of vertebrobasilar occlusion (van Seeters *et al.*, 2015). CTA has shown excellent inter-rater reliability (κ=0.81, P<.001), which reduces the misinterpretation (Menon *et al.*, 2015).

1.6.4 **CT Perfusion**

CT perfusion (CTP) is one of the most widespread techniques to detect acute ischaemic stroke by providing visual and quantitative information on blood flow haemodynamic of CBF, CBV and Tmax. Like CTA, CTP requires the administration of an iodinated contrast agent. The passage of the contrast flow

can be acquired through repeated CT brain scans. Perfusion images and parameters are generated through deconvolution of the tissue-time curve. Visualisation of perfusion maps of CBF, CBV and Tmax helps to estimate the ischemic core region and the penumbral region.

In hypoperfused tissue, the infarcted core is the depicted as area with elevated of MTT and Tmax, and decreased CBF and CBV. While in the penumbral region, the MTT and Tmax are increased and while the CBF is decreased but with normal or increased in CBV. Thresholds are needed to interpret the perfusion parameters. It is accepted that the penumbra region is when the Tmax more than 6 seconds (Tmax>6s) while the core is when the CBF less than 30 % (Heit and Wintermark, 2016). At the core region, the CBV appears plays major role in distinguishing the ischemic core and penumbra region (Lin et al., 2016). This can be achieved by comparing area of CBV and CBF on the CT perfusion map. A study conducted by Wintermark et al., (2005) reported a high accuracy of CT perfusion (86%) in detecting stroke and 94.4% of accuracy in determining the extent of stroke with the use of CT perfusion mapping.

Despite its advantages in stroke assessment, CT perfusion posed some limitations. One of the limitations is CT perfusion maybe difficult to evaluate for specific group of patients. Turk et al., (2007) and Waaijer et al., (2007) studied the application of CT perfusion on stroke patients with carotid stenosis. They found out that the CT maps were inaccurate in calculating the perfusion parameters. However, they acknowledged that the accuracy of CT perfusion maps did depends on the technologists experienced for the post-processing procedures. Another limitation of CT perfusion is radiation dose. The radiation dose in CTP are contributed from two CT perfusion acquisition (at the level of basal ganglia and above basal ganglia up to vertex) needed due to limited brain coverage along the z-axis of the CT scanner.

1.6.5 **MR Diffusion-weighted Imaging**

Diffusion-weighted imaging (DWI) is an MRI sequence which measures the random movement of water molecule (Brownian motion) in tissue. In ischaemic stroke tissue, DWI has been proven to indicate early onset of pathophysiologic changes in ischaemic tissue in animals and humans (Moseley et al., 1990).

DWI is used to assess early ischaemic stroke because its ability to detect cytotoxic oedema by measuring the proton diffusion using the apparent diffusion coefficient (ADC). Decrease in water diffusion will reflect decrease of ADC in the ADC maps. This will result in increasing intensity in DWI (Schaefer et al., 2006). This can be observed within minutes after vascular occlusion. The decrease in water diffusion is caused by the failure of Na+/K+/ATPase ionic pumps which leads to loss ionic gradients and the net transfer of water from the extracellular to the intracellular compartment. ADC will continue to decrease up until 4 days following occlusion and started to increase to its baseline within 1 to 2 weeks reflecting vasogenic oedema. In this chronic phase, mild hyperintensity is visible on the DWI. However, it is important to check with the ADC map because the DWI may include the T2 signal (T2 shine through). This is important to show the process of ischaemic tissue and predict the clinical outcome of stroke patients.

In terms of diagnostic accuracy of DWI, several studies reported high sensitivity and specificity of DWI in detecting hyperacute stroke as early as 2 to 6 hours after onset of symptoms (Van Everdingen et al., 1998; González et al., 1999; Desmond et al., 2001; Saur et al., 2003). Additionally, DWI was superior compared to NCCT in diagnosing acute ischaemic stroke within 12 hours of symptom onset (Chalela *et al.*, 2007). Besides, DWI has the advantage in the evaluation of posterior circulation (Tei et al., 2010) and small volume infarcts (Daniere et al., 2015).

1.6.6 **MR Perfusion weighted imaging**

MR perfusion weighted imaging (PWI) uses bolus-tracking technique in which the paramagnetic contrast agent such as gadolinium (Gd) is dynamically monitored from the cerebral arteries until the veins after being administered intravenously. The most common MR perfusion sequence used in brain is the dynamic susceptibility contrast (DSC). DSC uses T2 or T2*-weighted sequences to measure the signal loss of Gd due to the susceptibility effect. The signal intensities of the contrast agent at those regions are deconvoluted to produce cerebral perfusion map of the relative CBF, relative CBV (rCBV), and Tmax. The principle of this technique has been discussed in previous section.

PWI is valuable in ischemic stroke treatment when used together with DWI. The mismatch region between PWI and DWI revealed the brain tissue that need to be salvage (penumbra) to stop from further ischaemia. The application of MR imaging in identifying suitable patients to receive iv-tPA treatment during 4.5 to 9 hours after stroke onset based on the penumbral mismatch has been used in ECASS 4 (Ringleb *et al.*, 2019). Major ischaemic stroke clinical trials such as DEFUSE-3 and EXTEND used thresholded PWI/DWI (mismatch ratio ≥ 1.8 with mismatch volume ≥ 15 mL for DEFUSE-3, and mismatch ratio ≥ 1.2 and mismatch volume ≥ 10mL for EXTEND) to identify the region of penumbra for patients' selection (Albers *et al.*, 2018; Ma *et al.*, 2019). Patient selection for ischaemic stroke treatment based on PWI/DWI mismatch has been associated with favourable clinical outcomes. This showed that only a group of patients may benefit with the stroke treatment.

However, there are some potential challenges with penumbra measurements. Several studies have demonstrated the overestimation of penumbra by including regions of oligaemia (Heiss, Sobesky and Hesselmann, 2004; Kucinski et al., 2005; Schaefer et al., 2008). Likewise, overestimation of the infarct core also may occur when the mismatch includes the penumbra (Guadagno et al., 2004).

1.7 Perfusion patterns

1.7.1 Cerebral spontaneous reperfusion

Spontaneous reperfusion can be described as increase in CBF in the region of hypoperfusion within the few days or weeks after stroke onset. Jørgensen et al., 1994, described spontaneous reperfusion as presence of hyperperfusion in an infarcted area using SPECT imaging. In their observation, the spontaneous reperfusion occurs within 2 weeks after stroke onset in untreated stroke patients while early reperfusion may occur up to 48 hours (Baird et al., 1996).

The cause of spontaneous reperfusion remains unknown. Hakim et al., 1987, studied the cerebral metabolic in a small cohort of stroke patient within 48 hours of onset. They found that several metabolic parameters such as cerebral metabolic glucose, cerebral metabolic rate for oxygen, CBF, cerebral pH, and CBV changes during spontaneous reperfusion which may suggests the spontaneous reperfusion mechanism.

Cerebral spontaneous reperfusion is associated with improved clinical outcome. This is called nutritional reperfusion as described by Barber et al., 1998, and occurred in 1/3 of his study cohort. Similarly, Marchal et al., 1996, predicted that early spontaneous reperfusion is a marker for favourable tissue outcome.

1.7.2 No reflow phenomenon

No-reflow phenomenon was observed in early animal studies in rabbits where there was absence of normal flow after the ischemia was relieved (Ames *et al.*, 1967). Several mechanisms of no-reflow phenomenon have been proposed which include swelling of endothelial cells, erythrocyte aggregation, pericytes constriction and involvement of neutrophils (Fischer and Ames, 1972; Yemisci *et al.*, 2009; el Amki *et al.*, 2020).

While these mechanisms can be observed in laboratory works, no-reflow phenomenon can be visualised using imaging modalities. In an angiogram study, no-reflow phenomenon was observed as delayed washout of contrast despite recanalisation of occluded artery (Hussain *et al.*, 2013). In other imaging study,

Schiphorst et al., 2021, defined no-reflow as 40% reduction of CBF at 24 hours on ASL imaging.

1.8 Chronic hypoperfusion - white matter hyperintensities

Chronic hypoperfusion of deep white matter can lead to disruption of blood brain barrier leading to chronic leakage of plasma into the white matter. Axonal degeneration and demyelination cause increase in interstitial water and appears hyperintense in DWI imaging. The hyperintense signal of white matter in DWI is known as white matter hyperintensities (WMH). WMH or also known as leukoariosis, is the diminution of white matter density (Hachinski, Potter and Merskey, 1987). WMH is a feature of small vessel disease and has been associated with other names such as white matter lesions, leukoencepholathy and white matter disease (Shi and Wardlaw, 2016a). These terms are interchangeably used in the literature and may cause confusion to the reader. The STRIVE guideline has come with a recommendation to differentiate the spectrum of small vessel disease (SVD) based on their features in neuroimaging (Wardlaw *et al.*, 2013)

WMH are commonly seen in the elderly and progress with age. The Rotterdam Scan Study, which is a large-scale longitudinal study, investigates the brain changes in elderly starting from 1995 and continued until 2016 (Ikram *et al.*, 2015). The results of the study showed that the frequency of WMH occurrence increasing with age and can be detected as early as 45 years old. In other multicentre and multinational study, The Leukoaraiosis and Disability Study (LADIS), found out that the progression of WMH over 3 years (WMH progression based on Rotterdam Progression score) increased by 2 points (Gouw *et al.*, 2008)

Several hypotheses related to pathogenesis of WMH have been reviewed by Pantoni and Garcia, 1997. Among the causes of WMH is the reduction in CBF. There has been conflicting discussion on the relationship between CBF with white matter lesions. Some suggested that low CBF causes white matter lesions and their progression overtime. In 21 patients with late-onset dementia, the deep white matter hypoperfusion was caused by capillary dysfunction with 67%

OEF increase which can lead to white matter injury (Dalby *et al.*, 2019). In addition, low NAWM CBF at baseline (9.2 mL) increases the WMH volume (11.96 mL) after 18-month follow-up in 40 patients with minor ischaemic stroke (Bernbaum *et al.*, 2015). On contrary, there was an argument that chronic hypoperfusion did not caused WMH but due to less normal cerebral tissue that requires less oxygen supply in brain with more WMH. This hypothesis was supported in a large longitudinal study, where there was no association between baseline parenchymal CBF with WMH progression after 3.9 years in 575 patients with arterial disease (van der Veen *et al.*, 2015). It is important to note that various hypotheses on WMH pathogenesis were based on broad range of studies cohort (Alzheimer's disease, cognitive impairment, or ischaemic stroke patients), methods of investigation (histology or brain imaging) and study design (cross-sectional or longitudinal).

1.8.1 **Radiological features of WMH**

Imaging can help to structurally and functionally identify WMH. The radiological features of patchy low attenuation at the periventricular region and deep white matter in CT was originally described by Hachinski and collegues (Hachinski, Potter and Merskey, 1987). The reduction of CT's Hounsfield unit reflects the demyelination of the axon's myelin sheath.

In MRI, WMH appears hyperintense on T2, proton density, FLAIR and T2* but hypointense in T1. In contrast to CT, MRI is more sensitive in detecting the subtle alterations in water content using the DWI sequence with ADC map. The most sensitive MRI sequence is FLAIR. FLAIR can differentiate between WMH and lacunar infarcts (lacunes) which appear as a 'hole' surrounded with white rim. Advanced application of MRI such as diffusor tensor imaging (DTI) allows the visualisation of axonal tracts in white matter. Mean diffusivity (MD) is the biomarker to measure the diffusion magnitude of water molecules (Basser and Pierpaoli, 1996).

The severity of WMH is graded using visual rating scales. Among the common visual rating scales are Fazekas scores (Fazekas, Chawluk and Alavi, 1987) and Scheltens scale (Scheltens *et al.*, 1993). The Fazekas scores describes the white matter lesions as caps, smooth halo or irregular at the periventricular

region and differentiate between puncate, beginning confluent or large confluent at the deep white matter region. On the other hand, the Scheltens scale rates the WMH based on the brain anatomical regions.

Chapter 2 Arterial Spin Labelling

2.1 Principles of arterial spin labelling

ASL is an alternative to DSC MRI where it uses blood as an endogenous contrast to measure cerebral perfusion. ASL takes an advantage from the long T1 decay rate, which allows the detection of perfusion of tissue and microvasculature. From its name, arterial spin label, the proton spins of the arterial blood water were “labelled” or “tagged” using 180° radiofrequency (RF) pulse. During the labelling period, the proton spins are inverted 180° to the opposite direction, and thus create a label (Figure 2-1). After a certain amount of time, or post-labelling delay (PLD), the labelled blood reaches the capillaries at the region of interest and exchange with tissue water occurs. To differentiate between labelled magnetization signal and static tissue signal, a control image is acquired without applying any RF pulse. The difference between the labelled image and control image, creates the perfusion signal which is then captured using MR imaging rapid acquisition techniques such as echo planar imaging (EPI), gradient and spin echo imaging (GRASE) and 3D fast spin echo imaging.

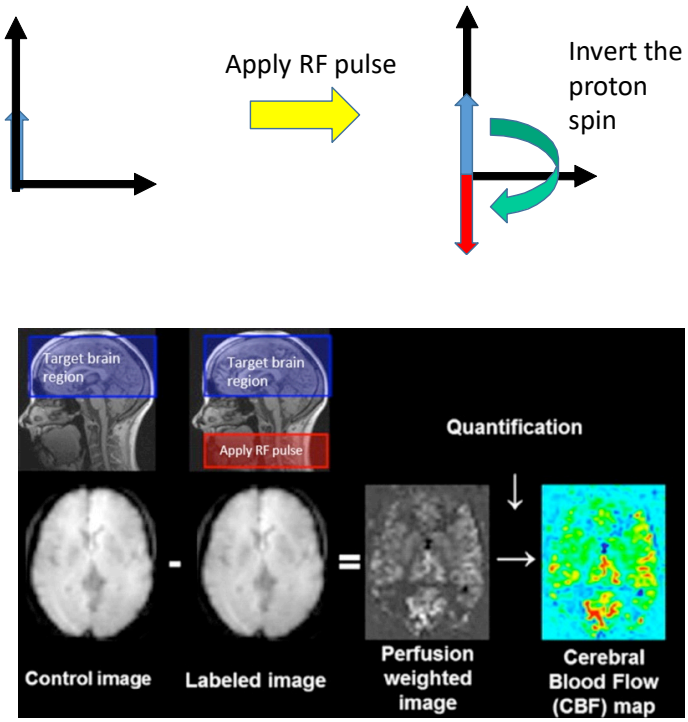

Figure 2-1: General principles of ASL (Adapted from Ferré et al., 2013)

The difference in signal intensity between labelled blood water and the control are subtracted to produce the ASL perfusion images. The difference between perfusion signal intensity is proportional to CBF and is expressed as the volume of blood per volume of tissue per minute (ml/100g/min). However, the ASL signal is very low, accounting for 0.5 to 1.5% of the full perfusion signal. This explains why ASL has low signal-noise-ratio (SNR). There are several ASL labelling strategies such as continuous ASL (CASL), pulsed ASL (PASL), and pseudo-continuous ASL (pCASL).

2.2 ASL labelling approaches: CASL, PCASL and PASL

There are many approaches to acquire ASL images including continuous ASL (CASL) pseudo-continuous ASL (PCASL) and pulsed ASL (PASL) (Figure 2-2 and Figure 2-3). These techniques differ in terms of excitation methods (Alsop *et al.*, 2015) and the labelling duration (Belani *et al.*, 2020).

CASL is the early ASL approaches of non-invasive perfusion method. It uses long continuous RF pulse (≈ 2 seconds) to invert the blood during labelling period, in which the continuous RF pulse is applied at the frequency of the main magnetic field. This method is also known as flow-driven adiabatic inversion (Dixon *et al.*, 1986). Though CASL provides with high SNR compared to PASL, the long application of RF pulse causes more heat deposited to the tissue or high specific absorption rate (SAR). This problem is more prominent in higher field of MRI scanner. Besides, the long RF pulse does require additional hardware such as additional neck or surface coil to provide the long RF pulse.

CASL also is prone to magnetization transfer effect from adjacent tissue. This magnetization effect reduces the signal of the labelled blood. To overcome this problem, additional coil to separate between the labelling plane and another coil for imaging plane has been introduced in rat brain imaging (Silva *et al.*, 1995). However, this solution may not be practical in clinical applications due to subject movement and limited space in the MR scanner. The magnetization effects caused in CASL were overcome with PCASL. PCASL uses larger gradients during the inversion which will increase the resonant offset of the pulses relative to the brain tissue. Furthermore, PCASL is compatible with existing RF amplifiers without additional coil.

PASL was implemented to overcome the long continuous RF pulse used in CASL. PASL uses single short 180° adiabatic RF pulse with a thick labelling slab (≈10 – 20cm) applied proximally that inverts inflowing spins. The control sequence repeats the 90°spoiler saturation of static tissue in the imaging plane to produce control images. There are variants of PASL sequences designed to overcome the low ASL signal in PASL (Table 2-1).

PASL sequence produce relatively short temporal width with unknow labelling time. Thus, it is difficult to estimate the duration of the inversion flow that will leave the labelling plane and it could cause underestimation of CBF perfusion at the capillaries. This limitation could be overcome by using QUIPSS-II modification technique developed by Wong, Buxton and Frank, 1998b, to remove the tail end of the labelled blood.

The choice of ASL labelling sequences and its parameters is critical in CBF quantification. Theoretically, CASL/PCASL has longer labelling duration and higher SNR compared to PASL. It has been established that PCASL has the advantage of high SNR with less hardware required and low SAR (Detre *et al.*, 2012). In the white paper for clinical applications of ASL perfusion, it is recommended that PCASL should be adopted as the routine ASL protocol (Alsop *et al.*, 2015). However, the choice of the ASL sequence used depends on the availability on the MRI scanner. Not all MRI scanners are installed with PCASL sequence, and this may result in different study outcomes using ASL.

Table 2-1: PASL variants

Name	Acronym
Flow Sensitive Alternating Inversion Recovery (Kim, 1995)	FAIR
Echo-planar Imaging And Signal Targeting With Alternating RF (Edelman *et al.*, 1994)	EPISTAR
Proximal Inversion With A Control For Off-Resonance Effects (Wong, Buxton and Frank, 1997)	PICORE
Pulsed Star Labelling Of Arterial Regions MENDELEY CITATION PLACEHOLDER 1	PULSAR
Double Inversions With Proximal Labelling (Jahng *et al.*, 2003)	DIPLOMA

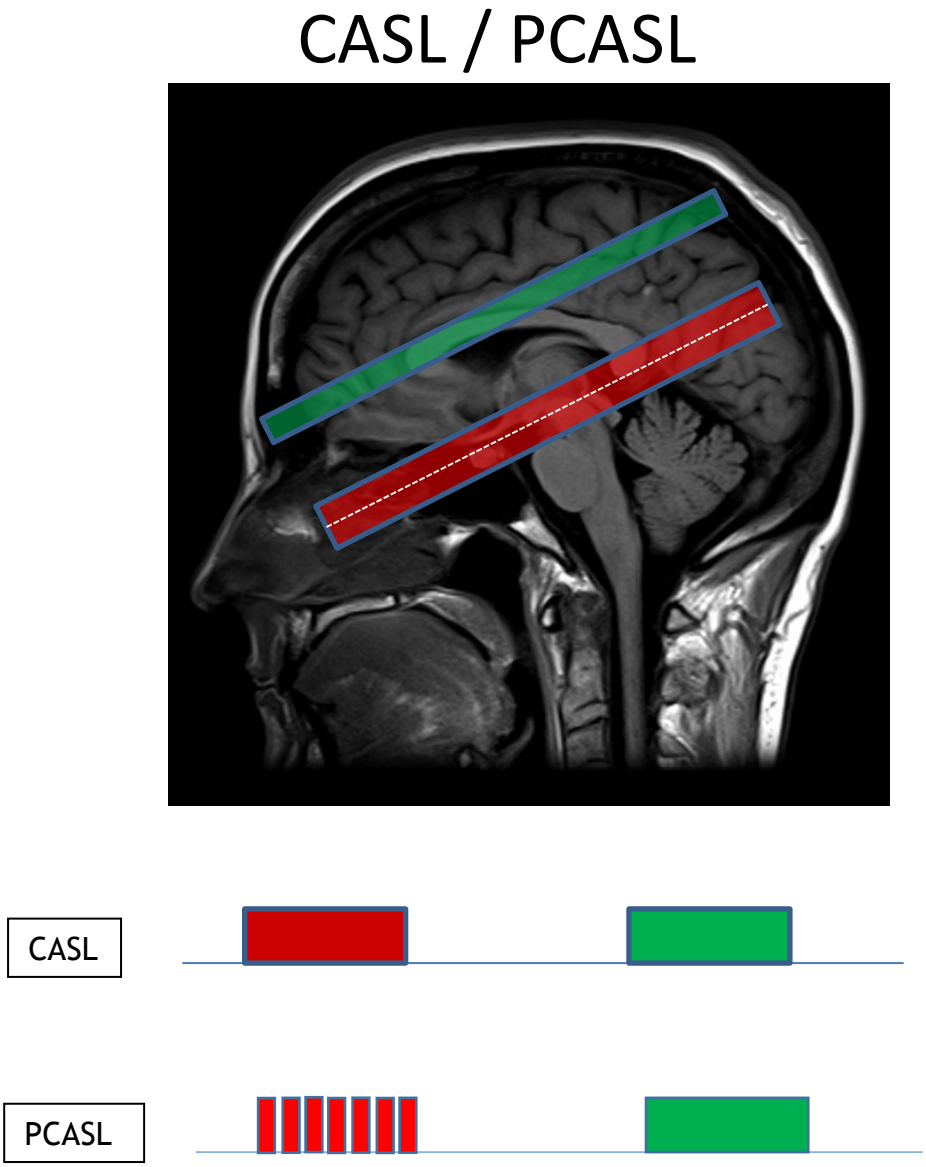

Figure 2-2: CASL or PCASL labelling and imaging plane

Figure 2-3: PASL labelling and imaging plane

2.2.1 **Additional ASL labelling modifications**

There are various ASL labelling modifications has been introduced to answer various clinical questions. These modifications were developed based on the PASL and CASL/PCASL labelling techniques. Vessel-encode ASL (VE-ASL) was developed based on PCASL to improve the SNR by mapping the vascular territories (Wong, 2007) (Figure 2-4). However, these additional ASL labelling methods are seldomly used particularly in clinical cohort due to limited availability on clinical MR scanners.

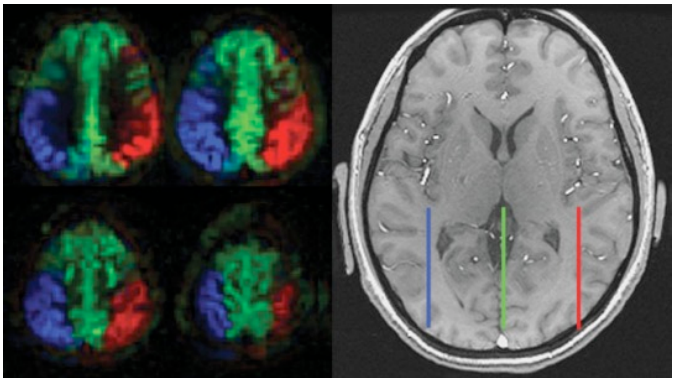

Figure 2-4: Vessel-encode ASL. Different colours (red, blue and green) represent different blood vessels supplies. Image adapted from Wong, 2007.

2.3 General kinetic model

The CBF perfusion in ASL is measured based on general kinetic model developed by Buxton (1998). This model is based on several assumptions:

i. All the labelled blood is delivered to the target tissue.

ii. There is no outflow of the labelled blood.

iii. The relaxation of the labelled blood spins is determined by the blood T1.

Based on the general kinetic model, CBF in each voxel is quantified using the formula depending on the ASL approached used (Figure 2-5 and Figure 2-6). Generally, the perfusion measurements can be obtained by dividing the difference in signal intensity with the initial magnetization.

$$CBF = \frac{6000\lambda(Scontrol - Slabel)\, e^{PLD/T1}}{2\alpha . T_1 . S_{PD}(1 - e^{-\tau/T1})}$$

where:

$S_{control}$ – S_{label} = the result of label-control subtraction

S_{PD} = the magnitude of the proton-density-weighted image

PLD = post labelling delay

τ = label duration

T1 = arterial blood, taken from literature to be 1.65 seconds at 3T

α = pCASL labelling efficiency, sets at 0.85

λ = single whole-brain partition coefficient value, sets at 0.9

Figure 2-5: CBF quantification for PCASL

$$CBF = \frac{6000\lambda(Scontrol - Slabel)\, e^{TI/T1}}{2\alpha . TI_1 . S_{PD}}$$

where:

$S_{control}$ – S_{label} = the result of label-control subtraction

S_{PD} = the magnitude of the proton-density-weighted image

TI = inversion time

T1 = arterial blood, taken from literature to be 1.65 seconds at 3T

TI_1 = timing of QUIPSS II pulse, sets at 800 ms

α = PASL labelling efficiency, sets at 0.98

λ = single whole-brain partition coefficient value, sets at 0.9

Figure 2-6: CBF quantification of QUIPSS II PASL

2.4 **ASL labelling efficiency (α)**

ASL imaging is very dependent to its labelling efficiency (α). In ASL, the signal comes from the difference between the inverted proton in labelled water and in the control image. The labelling efficiency is how well or how perfect of an ASL labelling approach to invert the proton during the labelling period. Generally, PASL has higher labelling efficiency, 97% compared to PCASL/CASL due to their difference RF pulse approach used (Figure 2-7).

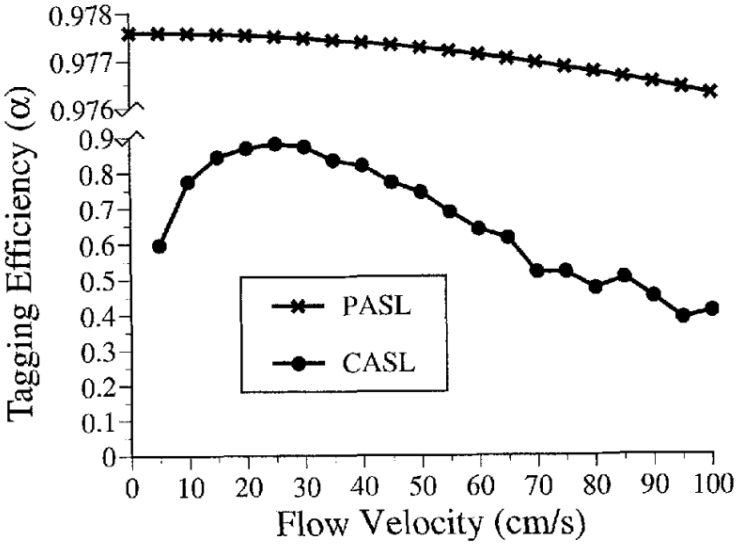

Figure 2-7: PASL and CASL/PCASL labelling efficiency.
Adopted from (Wong, Buxton and Frank, 1998a).

2.5 Arterial spin labelling as emerging techniques in perfusion imaging in ischaemic stroke.

The idea of measuring CBF started with the dilution theory developed by Kety and Schmidt, using nitrous oxide as a tracer (Kety and Schmidt, 1945). This idea provides the basis of ASL that used magnetically labelled water as a natural endogenous diffusible tracer. Subsequently, more perfusion experiments using animal models and humans were developed to measure regional CBF (Williams *et al.*, 1992; Roberts *et al.*, 1994). These studies discovered the potential use of ASL in human especially in stroke.

2.5.1 Alternative to DSC

There is a concern regarding the accumulation of gadolinium in brain region such as globus pallidus and dentate nucleus, and within the cerebrospinal fluid (McDonald *et al.*, 2015; Nehra *et al.*, 2018). With the advent of technology, ASL offers an alternative imaging technique to DSC. ASL provides comparable results when compared with DSC in assessing ischaemic stroke patients. A strong agreement (κ = 0.8) between the ASL (PCASL sequence) and DSC in assessing the reperfusion status of 24 iV-tpa treated ischaemic stroke patients at 24 hours of follow-up imaging (Mirasol *et al.*, 2014).

ASL able to derive perfusion parameters such as CBF, CBV and ATT comparable to DSC. A study by Wang et al. showed significant correlations between ASL and DSC in measuring CBF ($r = 0.7$, $p < 0.01$) and CBV ($r = 0.45$, $p < 0.01$) in 24 patients with acute middle cerebral artery stroke (Wang *et al.*, 2013)

In addition, ASL has higher sensitivity value of 80% on localising large vessel occlusion compared to DSC (sensitivity 64%) (McCullough-Hicks *et al.*, 2021). In this study, the large vessel occlusion is seen as bright vessel signal in ASL as compared to blooming susceptibility vessel sign.

2.5.2 **ASL as ischaemic penumbra identification**

During the baseline imaging, the presence of ischaemic penumbra is important to estimate the volume of salvageable tissue that could be an advantage of reperfusion. Conventionally, the presence of ischaemic penumbra can be identified and estimate using CTP (Tmax) and DSC. Alternatively, the estimation of penumbral mismatch could also be done using ASL. The presence of the ischaemic penumbra on ASL are defined based on qualitative criteria (hyperperfusion) (Bivard *et al.*, 2013) and quantitative criteria (relative CBF (rCBF) compared to contralateral side)(Niibo *et al.*, 2013)

Validation of penumbra region identification using ASL were compared using various DSC perfusion parameters. Niibo et al., 2013, used DSC MTT, Bivard et al., 2014, used Tmax>6s, whereas Bokkers et al., 2012 used TTP for penumbral region estimation. In addition to this, Wang et al., 2012, compared both MTT and Tmax>6s with ASL CBF and found consistencies between Tmax>6s, MTT and ASL CBF. Thus, the findings of these validation studies generally indicated the suitability of ASL to identify ischaemic penumbra region in stroke patients. However, there are no ASL CBF threshold are the best to estimate the ischaemic penumbra. The range of ASL CBF threshold used for penumbra estimation were CBF<20% (Niibo *et al.*, 2013) and CBF<40% (Bivard et al., 2014).

The penumbra region identification was also has been identified using DWI-ASL mismatch. Dongmei et al., 2020, used DWI-ASL mismatch to select patients who likely to benefit the thrombectomy. However, this study was

conducted on a very small sample size (12 patients) and further validation study should be conducted on larger cohort.

2.5.3 CBF quantification in the evaluation of ASL hyperperfusion

One of the applications of ASL in acute ischaemic stroke patients is the evaluation of hyperperfusion. Hyperperfusion, or luxury perfusion, is increased CBF in brain tissue above normal baseline values after a period of vascular occlusion either through spontaneous arterial recanalisation or collateral circulation. Previously, SPECT and PET were used to evaluate hyperperfusion in ischaemic stroke patients (Marchal, Furlan, *et al.*, 1996; Barber *et al.*, 1998). In a recent study, ASL has been found useful in detecting luxury perfusion presented with hyperperfusion in acute infarct (Belani *et al.*, 2020).

Hyperperfusion may also be associated with haemorrhagic transformation (HT) which could happen after recanalisation therapy. In a large study, Yu et al. (2015) investigated ASL hyperperfusion in 221 stroke patients who had received recanalisation therapy, scanned within 24 hours within the time of stroke onset (Yu et al., 2015). The results showed that the CBF value was 1.7 times higher at the infarcted region (70 mL/100g/min) compared to the normal contralateral region (43 mL/100g/min). This study showed a significant association between hyperperfusion with HT (OR=3.5, $p<0.001$). They found that ischaemic stroke patients presenting with hyperperfusion were approximately three times as likely to experience HT with patients without hyperperfusion. However, this study did not report the clinical outcome for the patients and thus limiting the clinical impact of hyperperfusion. The results of this study correspond with other study where focal hyperperfusion was associated with HT (OR=9.3, $p<0.001$) when compared with SPECT (Okazaki *et al.*, 2017).

Serial assessment of brain perfusion could provide prognostic information on reperfusion status in ischaemic stroke patients (Deibler *et al.*, 2008). Crisi et al., 2018, investigated the significance of regional hyperperfusion using ASL in 22 untreated stroke patients at 24 to 36 hours after the stroke onset and found an increment of CBF up to 99 mL/100g/min (Crisi, Filice and Scoditti, 2018). The National Institutes of Health Stroke Scale (NIHSS) score for these patients were significantly reduced from admission score of 4.5 to 3.0 at discharged. No stroke

symptom was observed after 1-month and 6-month follow. The result of this study was in sync with other study by Bivard et al., 2013, in which they observed a significant reduction in NIHSS score in patients with ASL hyperperfusion 24 hours after stroke onset (Bivard *et al.*, 2013).

2.5.4 **Regional CBF quantification**

Another application of ASL is to measure differences in CBF values according to the area of ischaemic lesion. As for now, there are limited number of studies that uses ASL to measure the CBF at different brain regions in patients with ischaemic stroke. Guo et al., 2014 measured the CBF value using ASL in 21 acute ischaemic stroke patients at specific brain regions which were brain cortex, white matter, external/internal capsule, basal ganglia, thalamus, brainstem and cerebellum(Guo *et al.*, 2014). The result showed that the CBF values reduced from the brain cortex to the deep brain region such as white matter and internal and external capsule.

Similarly, Harston et al., 2017, investigated the CBF at different site of stroke region which are the ischaemic core, early infarct core, late infarct core, peri infarct and the contralateral region (Harston *et al.*, 2017). This study provides some insights in the pathophysiology of ischaemic stroke where the regions surrounding the ischaemic core had CBF values <20 ml/100g/min at 24 hours after the symptom onset. This phenomenon suggested facilitated diffusion from early vasogenic oedema and a more serious injury.

2.6 Summary and aims of thesis

Several perfusion imaging markers based on contrast perfusion imaging methods (CTP and DSC) has been established to investigate the association of imaging markers with clinical outcomes. While these techniques may require the usage of contrast agents, CTP and DSC are not suitable for patients with renal dysfunction and contrast allergy. Arterial spin labelling MRI (ASL-MRI) has emerged to provide a safe alternative method, without the administration of contrast agents, which makes is safe for ischaemic stroke patients who are having or at risk of renal failure. Although ASL does not routinely used in stroke clinical studies, its ability to quantitatively measure CBF provides more information on cerebral perfusion. Thus, this thesis aims to explore the clinical application of ASL as perfusion imaging marker among acute and chronic ischaemic stroke patients.

The specific objectives of the thesis are:

1. to measure the agreement between two commonly used ASL sequences in clinical scanner;

2. to establish an ASL imaging marker (reperfusion index) and how does it associate with clinical and radiological outcomes among recanalised and non-recanalised ischaemic stroke patients;

3. to investigate the association of moderate and high index with infarct growth volume, early neurological improvement and 90-day good functional outcome among recanalised ischaemic stroke patients;

4. to explore the association between ASL perfusion in white matter hyperintensities among chronic ischaemic stroke patients.

Chapter 3 Agreement between different ASL labelling sequences in quantifying CBF among ischaemic stroke patients

3.1 Introduction

ASL is increasingly applied in neuroimaging. Given its advantage on able to provide the absolute perfusion measurement without contrast agent, ASL has shown comparable results with DSC in CBF quantification (Nael *et al.*, 2013; Niibo *et al.*, 2013). Constant technical refinement of ASL methods has been conducted since early 1990's of its application (Williams *et al.*, 1992) to improve its performance (Wang *et al.*, 2021; Zhang *et al.*, 2021). Moreover, new ASL sequences such as Territorial ASL (TASL) allows perfusion measurement at selected vessels in patients with patients with carotid stenosis (Yamamoto et al., 2017; Wang et al., 2021). However, these studies were based on ASL sequences that are still under research purposes and not routinely available in clinical scanners.

Despite the advancement of ASL sequences, PASL and PCASL sequences remains relevant in clinical settings as these are the most common ASL labelling techniques used. Several studies have investigated the reliability and reproducibility of PASL and PCASL within a centre (Chen, Wang and Detre, 2011), and across different centres (Petersen, Mouridsen and Golay, 2010). They found that both sequences were reliable and reproducible among healthy volunteers. Nevertheless, there were limited studies investigate the agreement between these two ASL sequences, especially in clinical cohort. It is important to investigate the agreement between the ASL sequences as it allows the causes behind underestimation or overestimation of perfusion measurement. Or, in other words, it allows to explore the potential systematic errors between PASL and PCASL sequences.

Therefore, the aim of this study is to investigate the agreement of common ASL sequences in measuring the cerebral perfusion among ischaemic stroke patients using Bland-Altman analysis (Bland and Altman, 1999).

3.2 Methods

3.2.1 Data source – WHISPER study

The subjects recruited in this study were part of prospective ongoing clinical trial, Whole Human Ischaemic Stroke Perfusion and Extended Re-canalisation (WHISPER). The ethics approval for WHISPER study was sought from NHS Greater Glasgow and Clyde Ethics Board on 29th March 2018 (R & D reference: GN17ST571; REC reference: 18/SS /0001)

WHISPER study was a prospective single-centre cohort study of adult patients (>18 years old) with clinical diagnosis of acute stroke presented within 24 hours of stroke onset or time last seen well. Patients underwent routine baseline stroke imaging protocol which include non-contrast CT, CT angiogram and CT perfusion. A follow-up MR imaging examinations were conducted at 48 to 72 hours after last seen well. The follow-up MRI imaging used standard stroke protocols (T1, T2, DWI, SWI, FLAIR, time of flight MRA) and additional ASL scans.

Access application for the usage of MRI images (including ASL) of the WHISPER study for this PhD work has been approved by the Research and Development, NHS Greater Glasgow and Clyde on 21st May 2019. The ASL scans were screened for the criteria in Table 3-1.

Table 3-1: Inclusion and exclusion criteria for agreement study

Inclusion criteria	Exclusion criteria
• Both ASL sequences (PASL and PCASL) performed in each patient.	• ASL scans which do not have calibrated image (M0) for CBF quantification. • Subjects with incomplete MRI-stroke sequence. • Distorted MR T1-weighted and ASL images.

3.2.2 **MRI data type**

All the MRI images were acquired using 3.0T MRI PRISMA (Siemens, Erlangen, Germany). The MRI images were anonymised prior transferring to personal workstation. The MRI images were in Digital Imaging and Communications in Medicine (DICOM) format (.dcm) and converted into Neuroimaging Informatics Technology Initiative (NIFTI) format (.nii) for further image processing.

3.2.3 **ASL imaging sequence**

The PASL sequence used was a commercially available PASL PICORE Q2TIPS product sequence (Wong, Buxton and Frank, 1998). The PASL sequence parameters were TR/TE = 3000/11, bolus duration = 700 ms, TI = 1800 ms, slice thickness = 4 mm, flip angle = 90°, number of averages = 1 and 29 slices. A total of 100 ASL images (50 pairs of label and controls) and 1 calibration image (M0) were acquired for 5 minutes 14 seconds scan time.

The PCASL sequence used in this study was acquired from Nuffield Department of Clinical Neurosciences Medical Sciences Division, University of Oxford. The PCASL sequence parameters were TR/TE = 4100/14 ms, bolus duration = 1400 ms, PLD = 250 ms, 500 ms, 750 ms, 1000 ms and 1500 ms, slice thickness = 4.5 mm, flip angle = 90°, number of averages = 1 and 24 slices. A total of 96 ASL images (48 pairs of label and controls) and 1 M0 image were acquired for 6 minutes 39 seconds scan time. The image readout for both sequences were acquired using 2D echo-planar imaging (EPI) with no background suppression.

Scan planning was aligned to the anterior commissure-posterior commissure (AC-PC) line in the transversal plane orthogonal to the T1 sagittal plane. The coverage of the entire cerebrum including the vertex. The imaging plane for both sequences was oriented perpendicular to the blood vessel. The order of the ASL sequence were not specified and it could be in any order (PCASL first or PASL first). Patients underwent both ASL sequences if their conditions

allowed. Each ASL scans were conducted one after another sequence without delay to minimize the time required for the subjects inside the scanner and to avoid subjects' movement.

Table 3-2: ASL imaging parameters for PCASL and PASL

	PCASL	PASL
Repetition time (TR), ms	4100	3000
Echo time (TE), ms	14	11
Bolus duration, ms	250, 500, 750, 1000, 1500	700
Inversion time (TI), ms	1400	1800
Slice thickness, mm	4.5	4.0

3.2.4 **Image processing software**

Statistical Parametric Mapping (SPM12) was used for image format conversion. FSL software developed by the FMRIB Analysis Group, Oxford, UK, was used for T1 image post-processing. Bayesian Inference for Arterial Spin Labelling (BASIL) was used for analysis of ASL data (Chappell *et al.*, 2009).

3.2.5 **Structural T1-weighted image processing**

The structural T1-weighted image for each subject was automatically processed using the fsl_anat command in FSL software. The T1-weighted imaging pipeline include the reorientation of the T1-weighted image to the standard MNI orientation. Next, a bias-field correction was applied. Then the oriented T1-weighted image was registered to 2mm-MNI standard space through linear registration (12 degree of freedom) and non-liner registration (T1-MNI).

The extracted brain T1-weighted image was used for tissue type segmentation. Three tissue types were grey matter (GM), white matter (WM) and cerebrospinal fluid (CSF). The segmented tissues were used as mask for creation of ASL CBF perfusion image. The steps of the T1-weighted image post-processing were outlined in Figure 3-1.

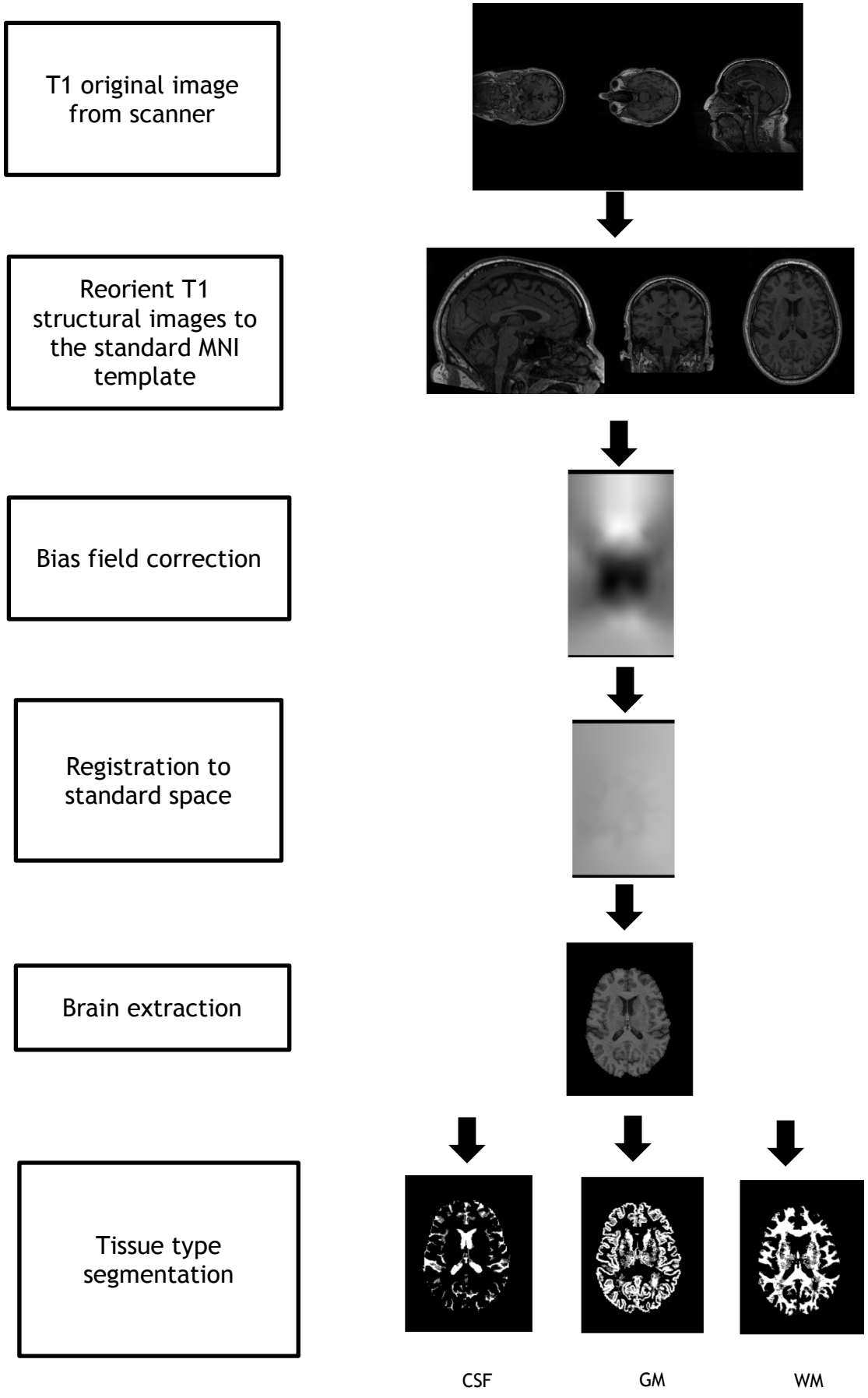

Figure 3-1: T1 anatomical image processing pipeline

3.2.6 **ASL CBF post-processing and quantification**

The CBF perfusion was calculated using BASIL graphical user interface (Figure 3-2) (Chappell *et al.*, 2009). BASIL performed automated post-processing steps to create the CBF perfusion map based on the input data needed. These input data were filled based on the subjects for this study (Table 3-3):

i. Input data: Details of the ASL acquisition such as type of ASL sequence, bolus duration and number of PLD.

ii. Structural input: The structural T1-weighted image used for creation of masks and image registration created by the fsl_anat command.

iii. Calibration image (M0): The M0 used to produce images of absolute perfusion in ml/100g/min.

The CBF perfusion measurement for GM and WM were calculated by BASIL using general kinetic model described in Chapter 2 for each PASL and PCASL sequence.

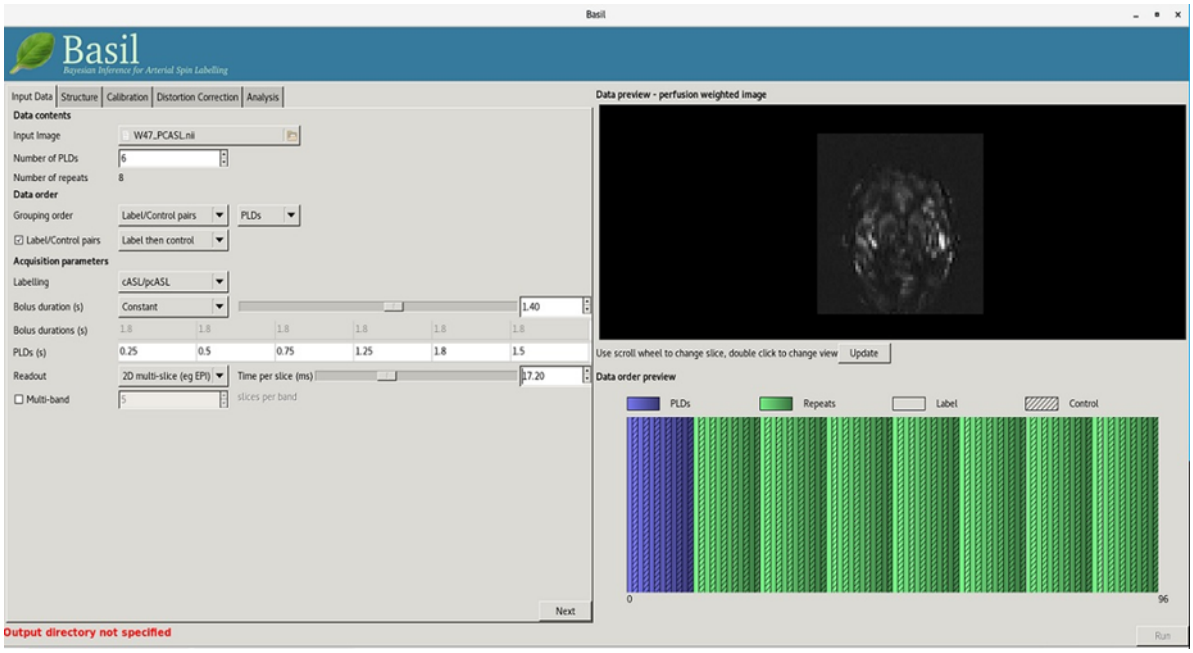

Figure 3-2: BASIL graphical user interface for automated CBF perfusion measurement

Table 3-3: Details of the input data needed for BASIL

Input Data	PCASL	PASL
Data contents	PCASL label-control images	PASL label-control images
PLDs, ms	250, 500, 750, 1000, 1500	700
Number of repeats	8	50
Grouping order	Label/control pairs	Label/control pairs
TI, seconds	1.4	1.8
Readout	2D multi-slice (EPI) with time per slice 17.2ms	2D multi-slice (EPI) with time per slice 45.2ms

General ASL image processing pipeline include the distortion correction, motion correction, registration to a structural image, partial volume correction and quantification (Table 3-4 and Figure 3-3).

Table 3-4: ASL perfusion map pipeline

Pipeline	Description
Distortion correction	Set the ASL images to the centre of each image.
Motion correction	Realign ASL images to the first ASL image.
Slice timing correction	Registration of the M0 image to the mean images generated during motion correction.
Spatial smoothing	Co-registration of the ASL images to the T1 image

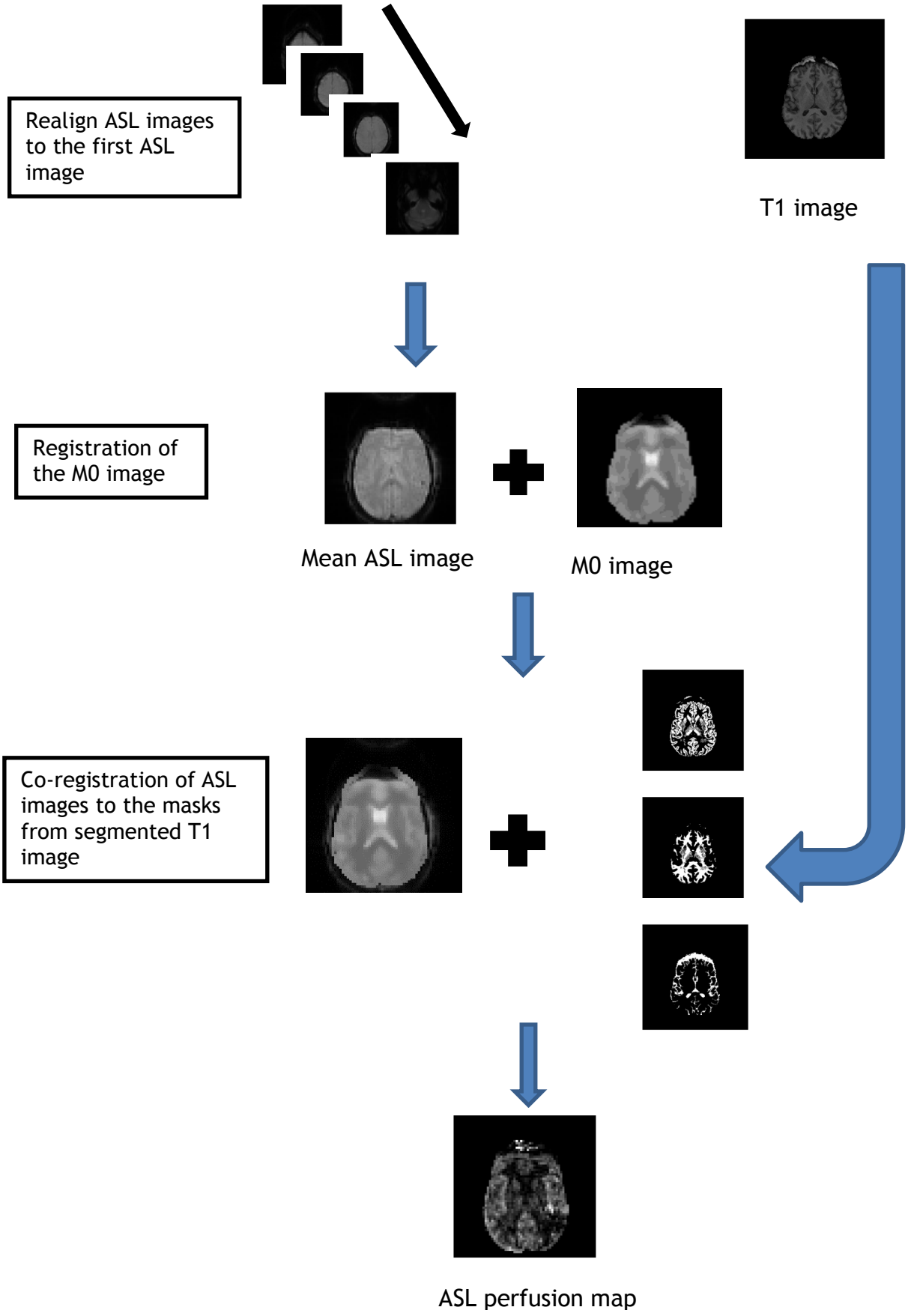

Figure 3-3: Automated ASL image post-processing pipeline using BASIL

3.2.7 **Statistical analysis**

All statistical analysis were performed using an IBM SPSS Statistics for Windows, version 22.0 software (IBM CORP., Armonk, N.Y., USA). Shapiro-Wilk was used to test for normality. The data was considered normal when the p-value of Shapiro Wilk was significant ($p>0.05$). Parametric statistical tests were conducted for all normal variables, unless stated otherwise.

Paired t-test was used to statistically compare between the GM and WM between ASL sequences. The Pearson's correlation test was used to know the correlation between PCASL and PASL. The Bland-Altman plot was plotted to quantify the agreement between CBF measured both by PCASL and PASL. The mean difference (bias) between two methods were calculated. The upper and lower limit of 95% confidence interval were calculated by multiplying the value of 1.96 with ± of the standard deviation.

3.3 **Results**

A total 57 patients' scans were screened for study eligibility (Figure 3-4). Among them, only 35 were scanned with both PCASL and PASL sequences and included in analysis. Twenty-two patients were excluded because there were no ASL images and some of them were only scanned with only one ASL sequence. Major demographic and clinical characteristics are reported in Table 3-3.

The grey matter and white matter mask created by both ASL sequence were not identical in terms of pixels when they were overlapped with similar position together (Figure 3-5).

The Shapiro-Wilk test indicated normal distribution for all CBF perfusion. The paired-t test showed statistically higher mean GM CBF of 43 ± 8 ml/100g/min in PCASL compared to PASL which was 42 ± 8 ml/100g/min ($p<0.001$). The PCASL also showed statistically higher mean WM CBF, 18 ± 3 ml/100g/min, compared to PASL which was 16 ± 3 ml/100g/min ($p<0.001$)

The Pearson's correlation showed a significant strong correlation between PCASL and PASL in for both GM ($r=0.95$, $p<0.001$) and WM ($r=0.76$, $p<0.001$). The agreement of PCASL and PASL in grey and white matter is shown in the Bland-Altman plots of Figure 3-9. The mean difference for GM is 0.72 ± 10 ml/100g/min and 1.04 ± 5 ml/100g/min for WM. The 95% limits of agreement for both grey matter (-7.0 to 8.15) and white matter (-3.25 to 5.83) contains almost all perfusion measurements.

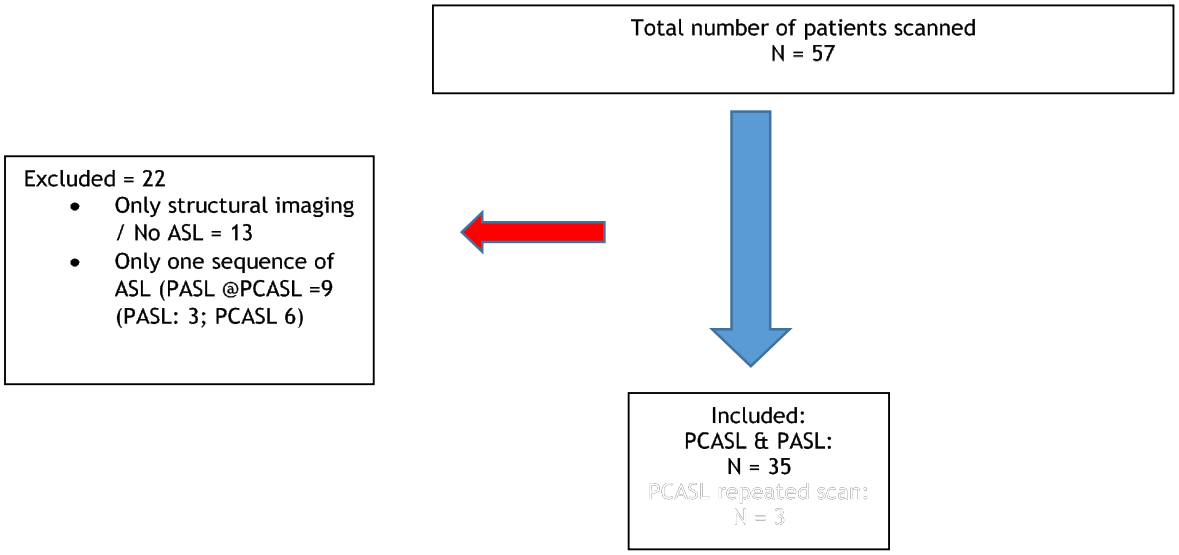

Figure 3-4: Number of included patients

Table 3-5: Patients' characteristics

Characteristics	Cohort (n=35)
Demographic	
Age, mean (SD)	66 (12)
Gender, n (%)	
Male	24 (69)
Female	11 (31)
Time from onset to MRI imaging, hour, mean (SD)	51 (19)
Evidence of occlusion on CTA, n (%)	17 (49)
Stroke severity	
Baseline NIHSS, median (IQR)	6 (2-8)
Follow-up NIHSS, median (IQR)	2 (0-5)
Vascular risk factors, n (%)	
Hypertension	17 (52)
Diabetes	7 (15)
Atrial fibrillation	4 (12)
Myocardial infarction history	4 (12)
Past stroke	4 (12)
Smoking	7 (21)
Alcohol	1 (3)

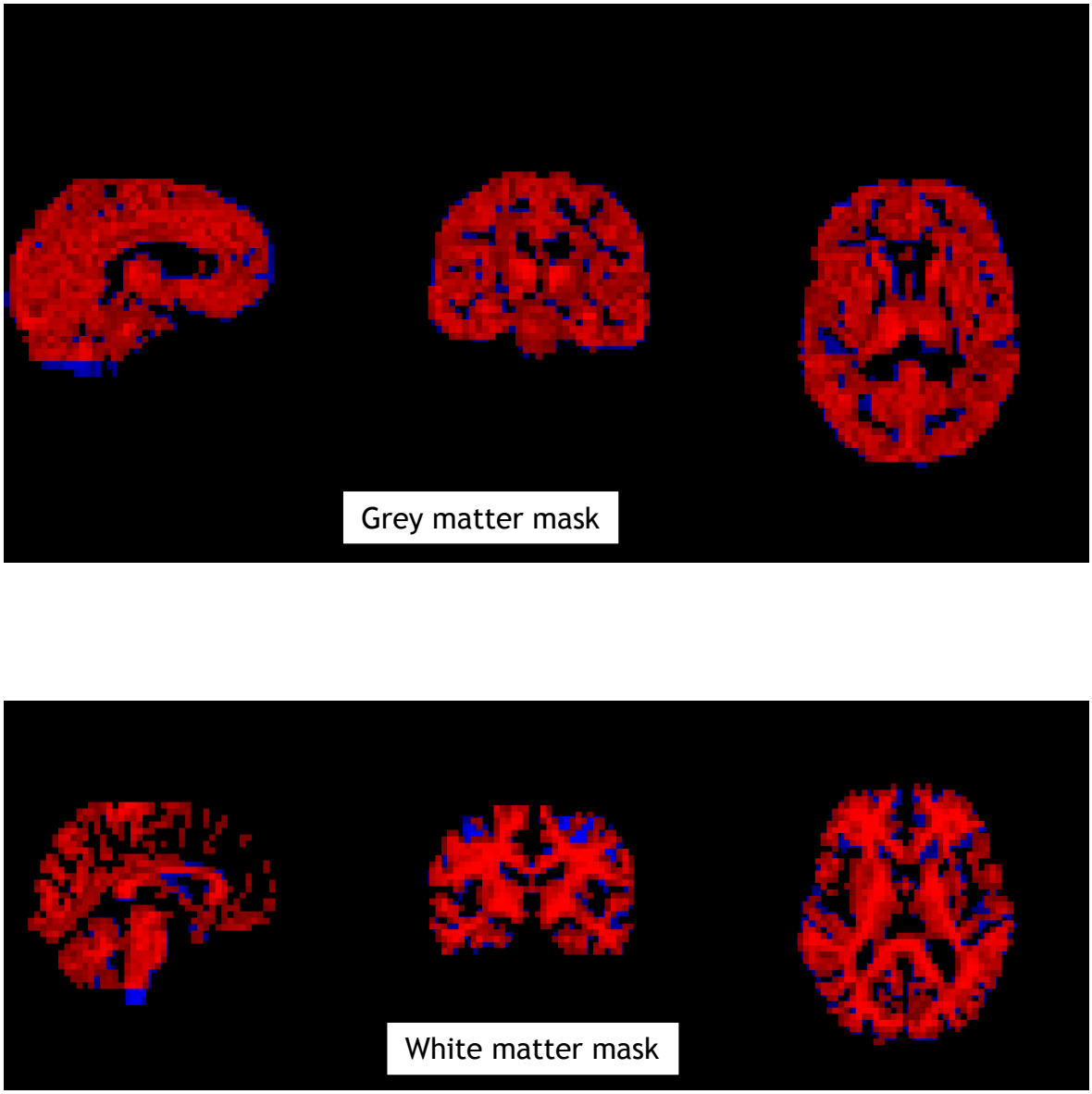

Figure 3-5: Comparison between grey matter and white matter masks for PCASL (blue) and PASL (red).

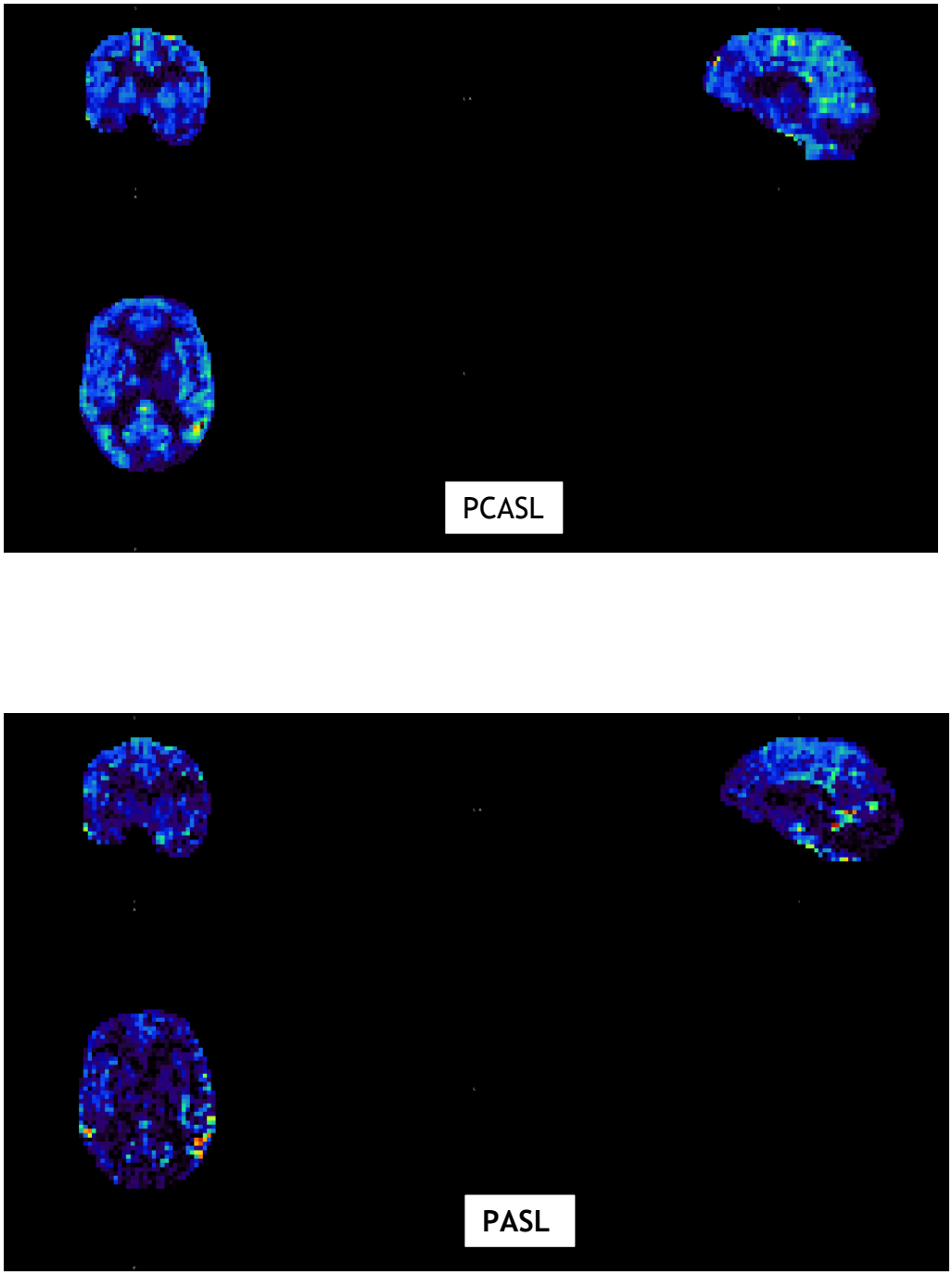

Figure 3-6: CBF perfusion map for PCASL and PASL.

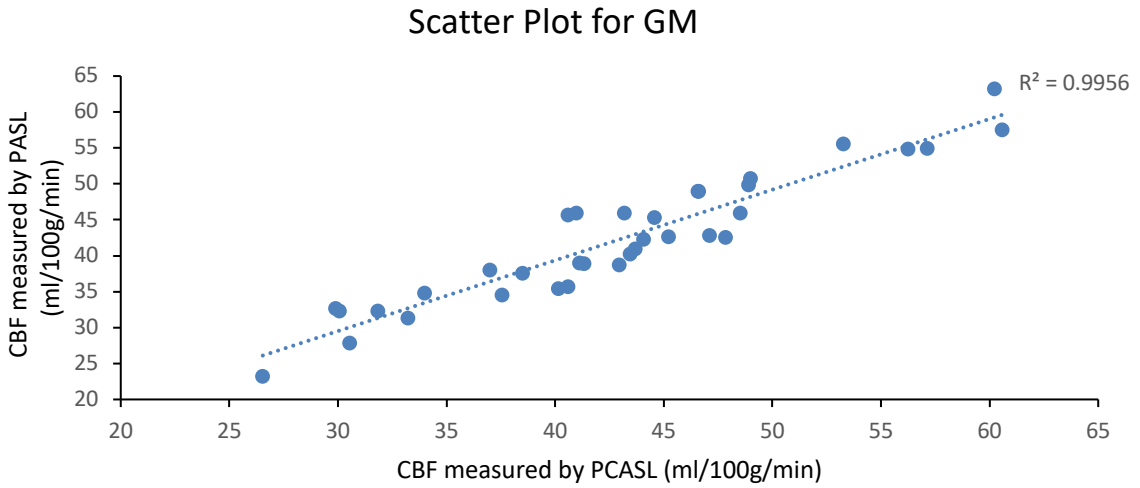

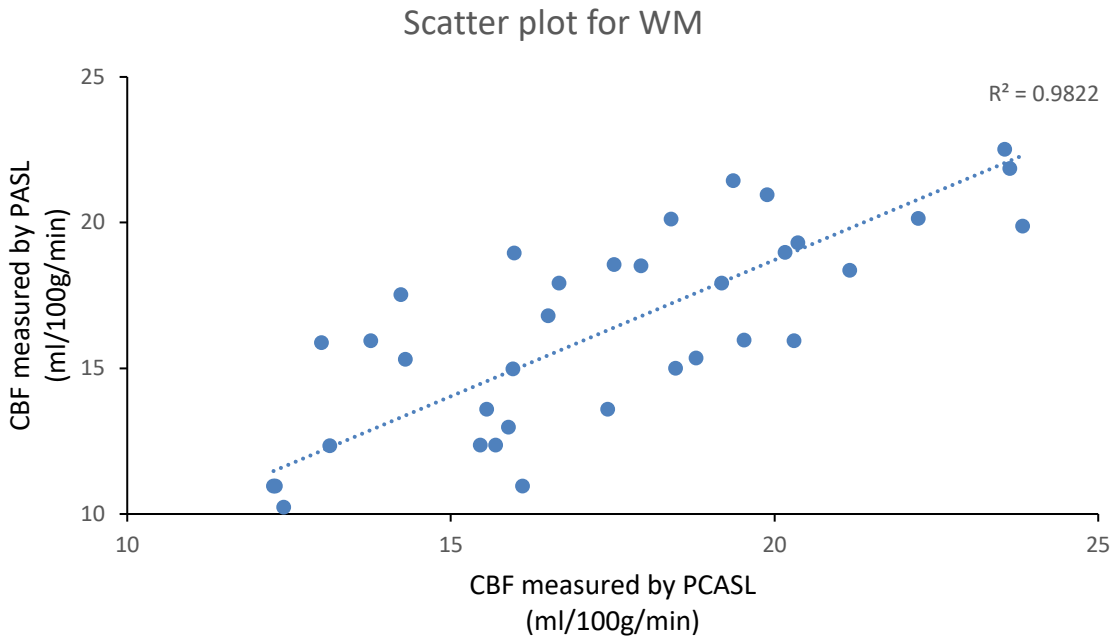

Figure 3-7: Correlation between PCASL and PASL

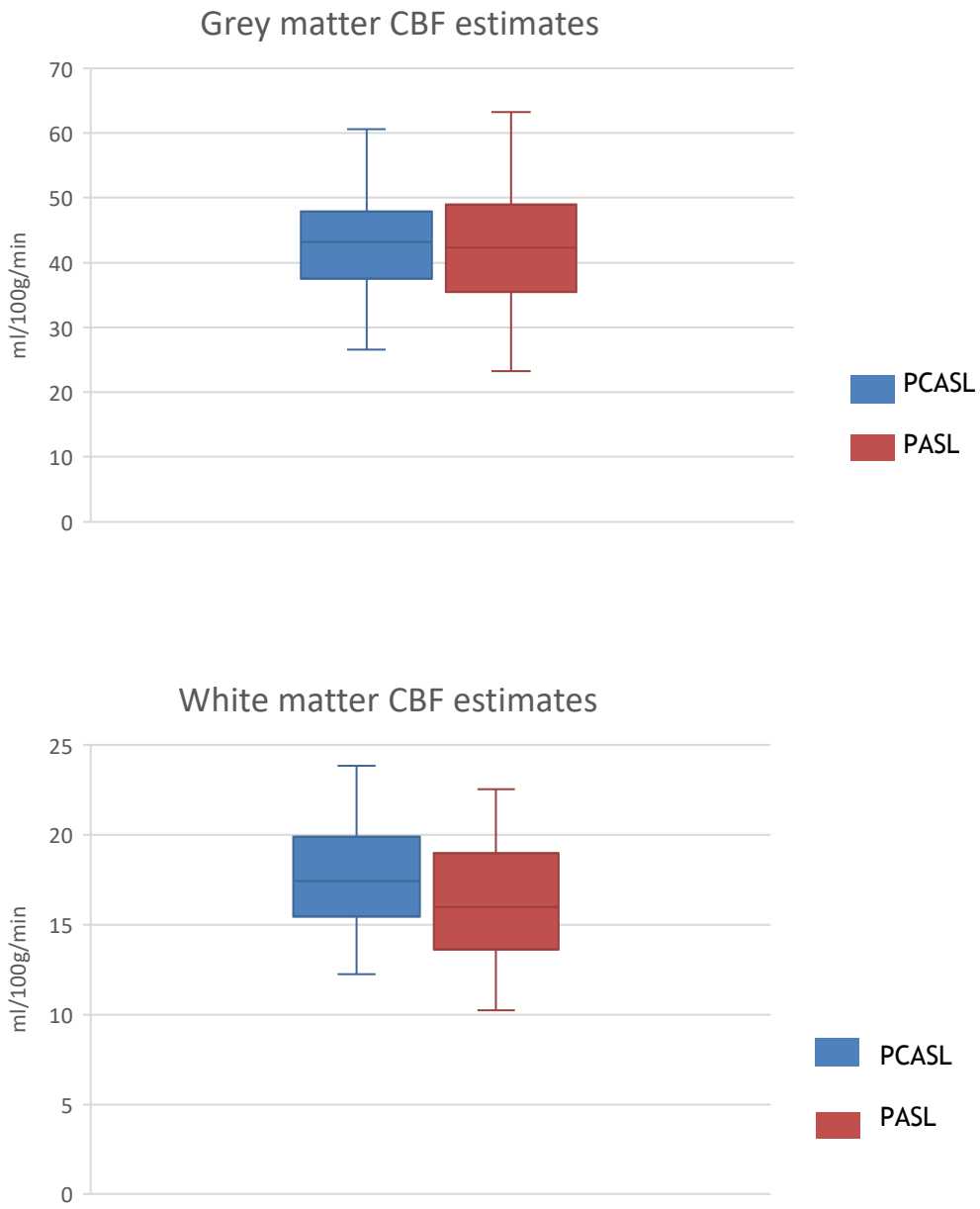

Figure 3-8: CBF estimates for grey matter and white matter between PCASL and PASL

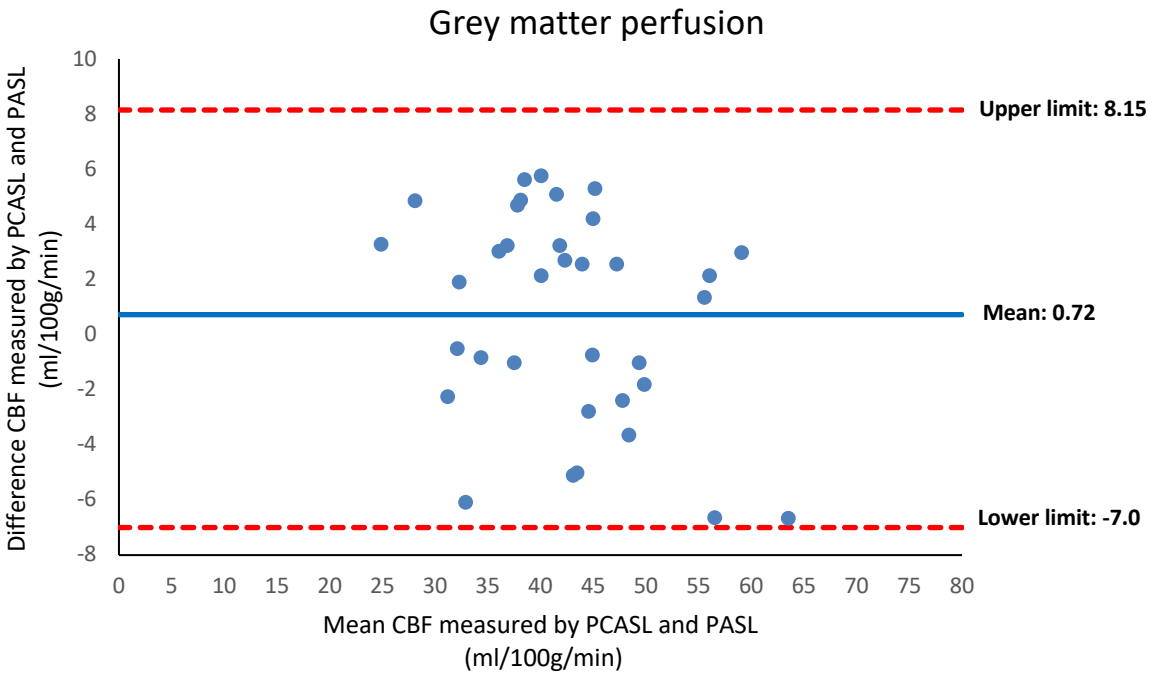

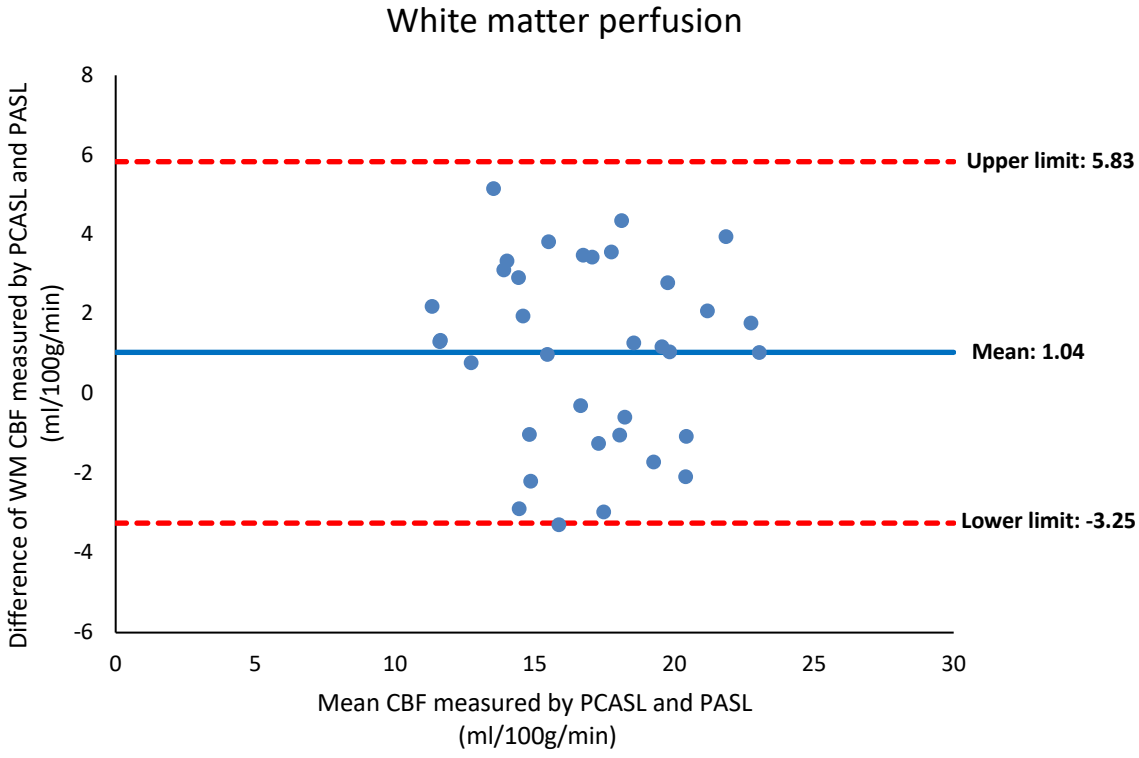

Figure 3-9: Bland-Altman plot to assess the limit of agreement between PCASL and PASL for grey matter and white matter perfusion.

3.4 **Discussion**

This study explored the relationship and agreement of two common types of ASL acquisition methods which are PCASL and PASL in ischaemic stroke patients. It is difficult to compare the results of this study with previous literatures as there were no ASL comparative study conducted in ischaemic stroke patients. Although reproducible CBF measurements using different ASL labelling sequences had been reported in previous literatures, these studies were conducted using healthy volunteer and the agreement between ASL sequences were underexplored.

The result of this study showed that there were significant correlations between PCASL and PASL in measuring the perfusion of grey and white matter. However, the Bland-Altman analysis demonstrated the large agreement between the ASL sequences suggesting the systematic errors in measuring CBF. Bland-Altman argued that correlations coefficient was a measurement of association rather than agreement (Altman and Bland, 1983). Thus, correlations were not the appropriate way to compare two methods or instruments.

This study also showed high mean CBF perfusion in PCASL for both grey and white matter compared to PASL. This result was in line with previous ASL comparison study which suggesting overestimate of CBF perfusion in PCASL compared to PASL among the mild cognitive impaired subjects (Dolui *et al.*, 2017). The CBF overestimation can be explained by high temporal resolution and SNR in PCASL. However, Wong and colleague claimed that estimation of CBF perfusion in PASL was more accurate because it has higher inversion efficiency and independent of the blood flow velocity (Wong, Buxton and Frank, 1998a). Nevertheless, it is difficult to tell which ASL sequence is more accurate because there was no comparison against the gold-standard perfusion imaging method, which is the PET imaging.

The large estimates of error between ASL sequences may results from several systematic biases. Among the biases are differences in labelling or inversion efficiency for both sequences. The inversion efficiency used in this study were 0.85 and 0.98 for PCASL and PASL respectively. PASL has higher inversion efficiency because it uses thick RF pulse slab (approximately 10 cm –

20cm) as compared to thin slice-selective RF pulse at the labelling plane. Another potential bias is the number of PLD used. In this study, multi-PLD was applied in the PCASL sequence while only one labelling delay was applied in the PASL. The reason for the multi-PLD PCASL used in this study was because it is recommended to use among patients with cerebrovascular disease to compensate with the delay of blood flow to the imaging plane (Alsop et al., 2015).

Non-uniformity of perfusion signal is another source of systematic bias. It was reported that PASL sequence yielded a higher ASL signal at both top and bottom slices than the middle slices. This observation was due to perfusion signal from residual intravascular labelled blood and chemical shift effect across the imaging slices (Jahng, Weiner and Schuff, 2007). In another observation, variations of ASL perfusion signal were seen at the posterior flow territory though the ASL scans were conducted based on near identical ASL sequences of different vendors (Mutsaerts *et al.*, 2015).

Variations of CBF perfusion between patients were confounded by several factors such as age (Parkes *et al.*, 2004), stroke severity, reperfusion status of the patients and patient's motion during the follow-up scan. These factors are called perfusion-modifiers (Clement *et al.*, 2018) and may explain why there was large limits of agreement for both ASL sequences. Evidence of occlusion and reperfusion of the blood vessels varies from one patient to another. Some patients may have occluded blood vessels and reperfused while others are not. Besides, ASL is sensitive to motion. Hence, head motion will also affect the perfusion signal, thus a potential systematic bias for ASL. In this study, motion correction was applied during the post-processing to minimize the motion artefact.

There were several limitations of this study. First, this study complies with the recommendations of the consensus paper with fixed labelling efficiency for both ASL sequences, while the labelling efficiency may differ between individuals(Wu *et al.*, 2007). Furthermore, the results of this study were based on small sample size and replication in larger sample size is needed. Finally, there was no preliminary study conducted among healthy volunteers in

establishing the CBF perfusion using the ASL sequences installed in the clinical scanner.

3.5 **Conclusion**

In conclusion, there is a large agreement of perfusion measurement between PCASL and PASL sequences although they showed significant correlations with each sequence. The differences in agreement between these ASL sequences are mainly due to various systematic biases. PASL estimates lower perfusion in grey and white as compared to PCASL due to single PLD used. PCASL has the advantage of multi-PLD to estimate late blood flow at distal capillaries. Thus, multi-PLD PCASL sequence is recommended in patients with delayed blood flow especially in ischaemic stroke patients.

Chapter 4 Relationship between ASL reperfusion index and follow-up clinical severity, follow-up imaging endpoints and good functional outcome in acute ischaemic stroke patients

4.1 Introduction

In acute ischemic stroke, the re-establishment of flow through the blocked blood vessels (recanalisation) is strongly associated with improved chances of tissue rescue and good clinical outcome (Rha and Saver, 2007). Recanalisation of occluded vessels is necessary to restore blood flow to more distal capillary beds (reperfusion), and it is the process of reperfusion that salvages the ischaemic penumbra and prevents penumbral tissue being recruited to the ischaemic core. The restoration of neuronal tissue function on reperfusion of ischaemic tissue is observed in animal studies and subsequently in humans, underpins the concept of the penumbra (Branston *et al.*, 1974)

The ischemic stroke lesion is a dynamic process that changes overtime. Brain perfusion provides information on factors that may associated with radiological and clinical outcomes (Chen *et al.*, 2017). Furthermore, data from clinical trials showed that perfusion imaging is helpful in treatment management for subgroup of stroke patients (Lansberg *et al.*, 2012; Ma *et al.*, 2019).

Advanced imaging such as CTP and PWI are widely used modalities for assessing perfusion. However, these techniques require the use of contrast agents that may be contraindicated in patients with renal dysfunction or contrast allergy. These perfusion imaging techniques are valuable in providing additional imaging markers such as early infarct growth rate (Sarraj *et al.*, 2021) and hypoperfusion intensity ratio (Olivot et al., 2014).

Arterial spin labelling has been applied as an alternative for perfusion imaging. The application of ASL in ischaemic stroke has been explored in estimation of penumbral tissue in acute ischaemic stroke (Lyu *et al.*, 2022) and quantifying reperfusion status within severely damaged tissue (Yu *et al.*, 2020). The studies did not use ASL as follow-up perfusion imaging and did not quantify

the degree of reperfusion at follow-up and did not explore the relationship of reperfusion and other imaging biomarkers.

This study investigated the reperfusion status of acute stroke patients using reperfusion index as quantitative indicator. The concept of reperfusion index has been used proposed based on CTP, as the difference in hypoperfused tissue volumes between baseline and follow-up (Soares *et al.*, 2010; Lin *et al.*, 2017).

Therefore, the aims of this chapter are to:

1. To investigate the relationship between ASL reperfusion index and infarct growth volume and penumbra salvage, and early neurological improvement.

2. To examine which baseline predictors, predict early neurological improvement and 90-day good functional outcome.

4.2 Methods

4.2.1 Study cohort

Data in this study were obtained from the WHISPER study as described in Chapter 3. Similar inclusion and exclusion criteria for subjects' eligibility in WHISPER study were applicable in this study. However, there were some additional inclusion and exclusion criteria applied in this study (Table 4-1)

Table 4-1: Inclusion and exclusion criteria for Chapter 4

	Inclusion criteria	Exclusion criteria
• Prespecified from WHISPER study	• Age 18 years and above • Male or non-pregnant females • Clinical diagnosis of stroke • Patient whom thrombectomy not planned. • Scan to be obtained within 24 hours of last being seen well. • No contraindication to IV contrast • Informed consent from patient or proxy (if patient lacks capacity)	• Renal impairment with eGFR less than 30ml/min • Known allergy to IV contrast. • Patient not expected to survive until or to be available for, final follow-up due to stroke or other comorbidities. • Intracranial haemorrhage or non-stroke diagnosis on initial CT • Contraindication to MRI scanning • NIHSS = 0 or 1 at time of imaging
• Criteria for this study (Chapter 4)	• Only subjects scanned with PCASL sequence. • Subjects with large vessel occlusion	• Incomplete clinical data/follow-up information • Incomplete imaging at baseline and follow-up

4.2.2 **WHISPER imaging studies**

The imaging studies for WHISPER can be divided into baseline imaging and follow-up imaging (Table 4-2). Baseline imaging was performed using CT and was conducted during the first visit less than 24 hour from onset of symptom. The baseline imaging examinations included non-contrast CT, CTP and single-phase CTA.

The ischemic core volume was defined as tissue with Tmax>6s and relative CBF<30% - while ischaemic penumbra was defined as delay of the residue function, Tmax>6s. Mismatch volume was calculated as the ratio between CBF<30% and Tmax>6s. All baseline imaging parameters were assessed using CTP automated software (RAPID, iSchemaView)

The follow-up imaging was conducted using an MRI scanner, 3 Tesla Magnetom Prisma (Siemens Healthcare, Erlangen, Germany). Follow-up MR imaging was conducted during second visit, 48 – 72 hours after stroke. Non-contrast CT, CTP and CTA scans were conducted during the follow-up if the patients had contraindications to MRI.

Table 4-2: Types of imaging studies

Baseline imaging	
Imaging studies	**Description**
NCCT	• To identify intracerebral haemorrhage
CTA	• To demonstrate any occlusion • To evaluate the carotid and vertebral arteries
CTP	• To measure cerebral perfusion parameters such as CBF, CBV, MTT • To obtain thresholded penumbra map
Follow up imaging	
T1	• As a structural imaging
T2	• To exclude any pathological lesion
DWI	• To measure final infarct volume
SWI	• To delineate intracranial haemorrhage
Time of flight (TOF) MRA	• To detect any intravascular occlusion • To assess recanalization
ASL	• To measure the brain perfusion in CBF

4.2.3 **Clinical data**

Clinical data included age, gender, vascular risk factors, baseline, and follow-up mRS and NIHSS, and times from symptom onset to first imaging and follow-up imaging.

4.2.4 **Category of occluded vessels**

The occluded blood vessels were grouped into large vessel occlusion and distal vessel occlusion based on the arterial occlusion sites (Table 4-3).

Table 4-3: Category of occluded vessels

Occlusion types	Arterial occlusion sites
Large vessels	• ICA-L • ICA-T • Proximal M1 • Distal M1 • PCA
Distal vessels	• M2 1 branch • M2>1 branch

ICA-L: Internal carotid artery, L-shaped
ICA-T: Internal carotid artery, T-shaped
Proximal M1: Proximal (<10mm from ICA-MCA bifurcation) M1 portion of middle cerebral artery
Distal M1: Distal (> 10 mm from ICA-MCA bifurcation) M1 portion of middle cerebral artery
PCA: Posterior cerebral artery
M2 1 Branch: M2 portion of middle cerebral artery, 1 branch involved
M2>1 branch: M2 portion of middle cerebral artery, more than one branch involved

4.2.5 **ASL perfusion definition**

The CBF threshold for hyperperfusion was defined as perfusion ratio >1.5 of the affected side compared to the contralateral side (Okazaki *et al.*, 2017). The CBF threshold of 20% (CBF 20%) relative to the contralateral side was used to indicate the hypoperfused brain tissue (Niibo *et al.*, 2013).

4.2.6 **ASL reperfusion index**

Reperfusion index was calculated based on Equation 1. The reperfusion index was then categorized into three categories based on their values as in Table 4-4.

$$\boldsymbol{Reperfusion\ index = \frac{Tmax > 6s\ volume - ASL\ hypoperfusion\ volume}{Tmax > 6s\ \ volume}}$$

Equation 1: Calculation on reperfusion index
Tmax > 6s: Hypoperfusion volume calculated by CTP

Table 4-4: Reperfusion index categories

Reperfusion index values	Category
≤ 0 – 0.4	No reperfusion / mild reperfusion
0.41 to 0.7	Moderate reperfusion
0.71 to 1.0	High reperfusion

4.2.7 **Radiological and clinical and outcome**

The radiological outcomes were assessed using infarct growth and penumbra salvage. Infarct growth was calculated based on the difference of baseline ischaemic core (CBF<30%) volume and follow-up DWI volume.

The neurological severity was assessed using the National Institutes of Health Stroke Scale (NIHSS) at baseline and at 24-hours follow-up. Changes of NIHSS were defined as difference in NIHSS at baseline to the follow-up baseline (ΔNIHSS = $NIHSS_{baseline}$ – $NIHSS_{followup}$) (Heitsch *et al.*, 2020). Early neurological improvement was defined as decrement of NIHSS of ≥ 3 points at 24-hours follow-up.

The modified Rankin Scale (mRS) (Table 4-5) was used to evaluate the stroke disability or functional outcome for baseline and follow-up record (Banks and Marotta, 2007). The mRS is graded from 0 with patients without symptoms and increase 1 grade for increasing significant disability. Patients who died prior before the endpoint were graded as 6. The functional outcome was categorized as good (mRS 0-2) and poor clinical outcome (mRS 3-6) at 90 days or 3 months.

Table 4-5: Modified Rankin Scale disability description

Scale	Description
0	No symptoms at all
1	No significant disability; despite symptoms and able to carry out usual duties and activities
2	Slight disability; unable to perform all previous activities but able to look after own affairs without assistance
3	Moderate disability; requiring some help but able to walk without assistance
4	Moderate disability; unable to walk without assistance and unable to attend to own bodily needs without assistance
5	Severe disability; bedridden, incontinent and requiring constant nursing care and attention
6	Death

Reproduced with modification from Banks and Marotta, 2007.

4.2.8 **Image processing software**

Statistical Parametric Mapping (SPM12) was used for image format conversion. Bayesian Inference for Arterial Spin Labelling (BASIL) MRI was used for analysis of ASL data for quantification of perfusion.

4.2.9 **Creation of lesion masks**

The lesion mask was created using the DWI images. The ischaemic core region on DWI images was automatically delineated using RAPID software based on the optimal ADC<620 x 10-6 mm2/s threshold (Purushotham *et al.*, 2015)

4.2.10 ASL lesion CBF quantification

ASL imaging data were carefully selected for further image post-processing and CBF quantification. ASL images with poor motion artifact were excluded from the analysis. The CBF quantification of ischemic lesion was processed and calculated using BASIL software (Figure 4-1).

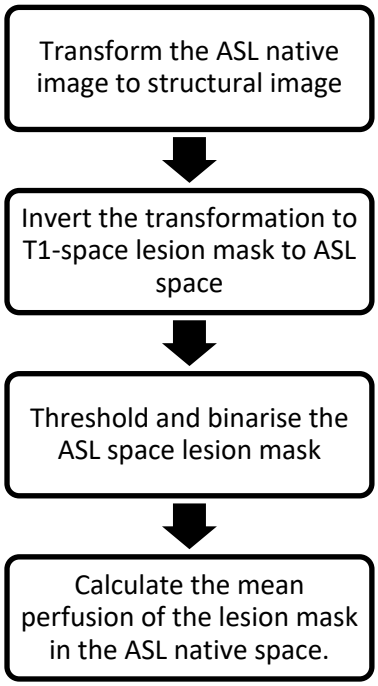

Figure 4-1: Automated BASIL software process to calculate the CBF for ischemic lesion

4.2.11 Statistical analysis

Statistical analysis was performed with IBM SPSS Version 28 (IBM Corp, Armonk, NY, USA). Continuous variables were compared to Spearman's rank correlation. Radiological variables were dichotomised by their median. For categorical outcome variables, normally distributed continuous variables were tested with independent t-tests, and non-normally distributed continuous variables with independent samples Mann-Whitney U tests. Normality was tested with Shapiro-Wilk test. Results are expressed as mean (standard deviation, SD) unless otherwise stated. Multiple linear and multivariable logistic regression models were used to know the association reperfusion index with radiological outcomes and clinical outcomes. The statistical significance was set at $p < 0.05$.

4.3 Results

4.3.1 Study population

A total of 130 subjects was enrolled from February 2020 until December 2021 after the imaging centre was equipped with PCASL sequence. Sixty-seven subjects were excluded from this study because of incomplete clinical information (8 subjects), no identified occlusion being detected on CTA (52 subjects), no MRI follow-up images (7 subjects), no ASL scans (7 subjects) and failed CTP processing (3 subjects). Sixty-three subjects were therefore included in the final analysis (Figure 4-2).

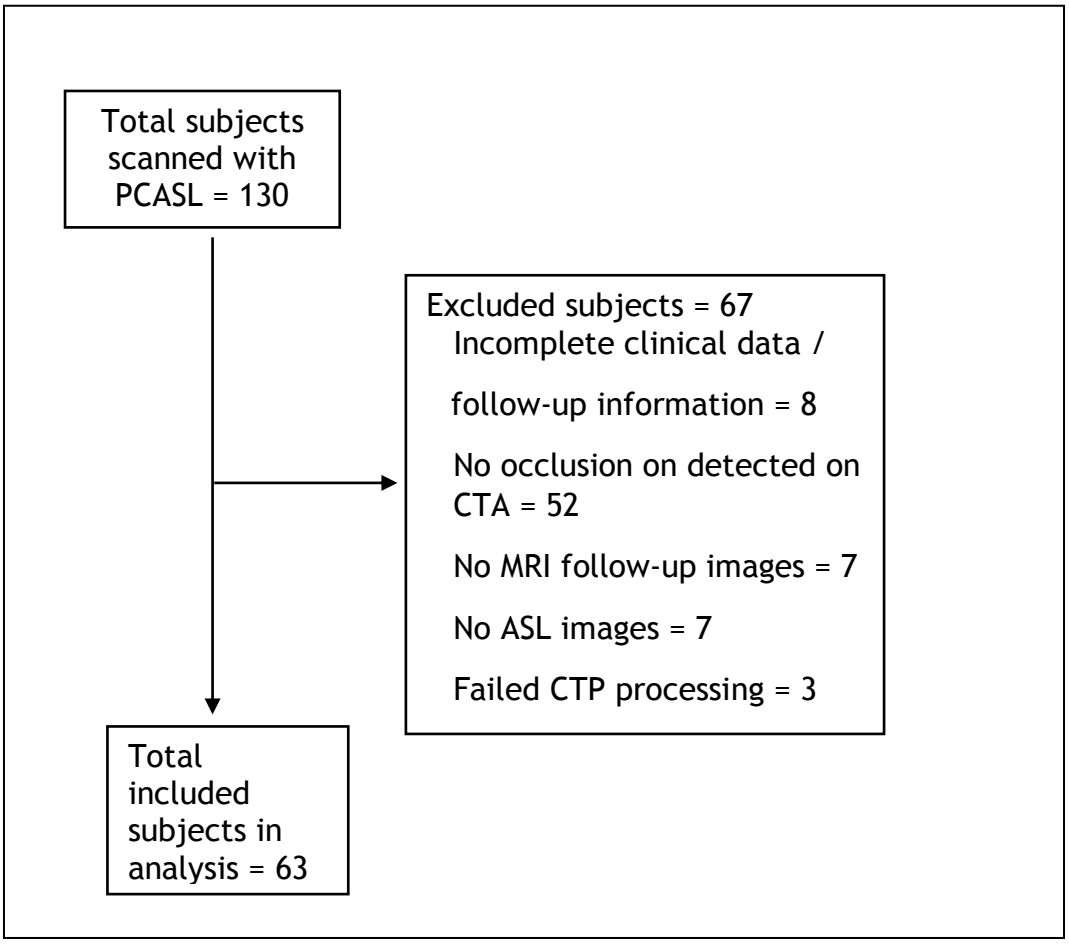

Figure 4-2: Total of included subjects

4.3.2 Baseline and follow – up clinical and imaging characteristics of study population

The study population had mean age of 67 ± 13.6 years with median baseline NIHSS of 7 (IQR: 4 - 11) and was functionally independent prior to the incident stroke (median mRs 0). Forty-one subjects (63%) received thrombolysis treatment during the initial visit. Forty-five percent of the population had hypertension while 19 % had atrial fibrillation and were current smokers. Other risks factors included diabetes mellitus (15%), history of stroke (14%), history of myocardial infarction (9%) and excessive alcohol consumption (6%).

Most of the study population were categorised as partial anterior circulation stroke (PACS) (59%) by the OCSP and only 1 patient had lacunar stroke (LACS), consistent with the selection of patients with vessel occlusion visualised on CTA. Among this population, 51% had distal vessel occlusion and 49% had large vessel occlusion detected on CTA.

The median follow-up NIHSS of the subjects was 3 (IQR: 1-8). The median time from onset to baseline imaging was 3.1 hours (IQR: 1.9 – 5.4). The median ischemic core volume (CBF<30s) detected by CTP was 0ml while the median Tmax>6s hypoperfusion lesion was 63ml (IQR: 18.5-125). The median mismatch volume between the CBF<30% and Tmax>6s was 46ml (IQR: 11-119).

At follow-up, fifty subjects (79%) had an AOL score of II or III. The mean time from onset to follow-up MRI imaging was 59.2 hours (SD: 23.6). The median follow-up ischemic core volume detected by DWI was 11.3ml (IQR: 4 – 58.9) and the median infarct growth was 8.1ml (IQR: 2.05 – 17.15). The median ASL perfusion within the DWI lesion was 46.7 ml/100g/min (IQR: 15.8 - 60) and the median hypoperfusion volume was 25.4 ml (IQR: 10.1-65.4).

Forty subjects (64%) had good functional outcome (mRS-90 of 0-2) while 23 subjects (36%) had poor functional outcome (mRS-90 of 3-6) at the final visit. The summary of baseline clinical and imaging characteristics is detailed in Table 4-5.

Table 4-6: Baseline and follow-up characteristics

Baseline Characteristics (N=63)	
Clinical characteristics	
Age, mean (SD), y	67 (13.6)
Gender, n (%)	
Male	37 (58.5)
Female	26 (41.5)
NIHSS at admission, median (IQR)	7 (4-11)
mRS at admission, median (IQR)	0 (0)
Thrombolysis received, n (%)	41 (63.1)
Vascular risk factors, n (%)	
Diabetes mellitus	10 (15.4)
Hypertension	29 (44.6)
Artrial fibrillation	12 (18.5)
Smoker	12 (18.5)
Excessive alcohol consumption	4 (6.2)
History of stroke	9 (13.8)
History of myocardial infarction	6 (9.2)
Stroke syndrome	
PACS	36 (58.5)
TACS	18 (27.7)
POCS	8 (12.3)
LACS	1 (1.5)
Types of strokes occlusion, n (%)	
Small vessels	33 (50.8)
Large vessels	32 (49.2)
Baseline imaging characteristics	
Time of onset to baseline imaging, median (IQR), hr	3.1 (1.9-5.4)
CBF<30% lesion volume, median (IQR) ml	0 (0 - 12)
Tmax>6s, median (IQR), ml	53 (18.5-125)
Tmax>10s, median (IQR), ml	15 (3.5-53.5)
Mismatch volume, median (IQR) , ml	46 (11-119)
Hypoperfusion intensity ratio (HIR), median (IQR)	0.32 (0.06-0.52)
CTA collateral score, median (IQR)	15.5 (11-18.25)
CT ASPECTS, median (IQR)	8 (6-9)

Follow-up imaging outcomes	
Time of onset to follow-up imaging, mean (SD), hr	59.2 (23.6)
DWI lesion volume, median (IQR),ml	11.3 (4 – 58.9)
Infarct growth, median, ml	8.1 (2.05 – 17.15)
ASL perfusion, median (IQR), ml/100g/min	46.7 (15.8 - 60)
ASL hypoperfusion volume, median (IQR), ml	25.4 (10.1-65.4)
DWI ASPECTS, median (IQR)	6 (3-8)
AOL score, n (%)	
0 - I	13 (20.6)
II - III	50 (79.4)
Clinical outcomes	
Follow-up NIHSS, median (IQR)	3 (1-8)
mRS-90, median (IQR)	2 (1-3)
Good functional outcomes (mRS 0-2), n(%)	40 (63.5)
Poor functional outcomes (mRS 3-6), n (%)	23 (36.5)

Table 4-7: Baseline and follow-up characteristics of patients based on reperfusion index categories

Variables (n =63)	No reperfusion / mild reperfusion (RI ≤ 0 – 0.4) N = 15	Moderate reperfusion (RI 0.41 to 0.7) N = 29	High reperfusion (RI 0.71 to 1.0) N = 19	p-value
Clinical characteristics				
Age, mean (SD), years	66 (18)	66 (14.2)	69 (8.2)	0.69
Gender, n (%)				0.887
Male	8 (12.7)	18 (28.6)	11 (17.5)	
Female	7 (11.1)	12 (19.1)	7 (11.1)	
Thrombolysis treatment, n(%)				*0.013
Yes	5 (7.9)	19 (30.2)	15 (23.8)	
No	10 (15.9)	11 (17.5)	3 (4.8)	
Stroke types, n (%)				*0.029
PACS	4 (6.3)	23 (36.5)	9 (14.3)	
TACS	8 (12.7)	3 (4.8)	7 (11.1)	
POCS	3 (4.8)	3 (4.8)	2 (3.2)	
LACS	0	1 (1.6)	0	
Occlusion type, n (%)				0.135
Large vessels	11 (17.5)	13 (20.6)	8 (12.7)	
Distal vessels	4 (6.3)	17 (26.7)	10 (15.9)	
Previous stroke, n(%)	2 (3.2)	6 (9.5)	1 (1.6)	0.381
Atrial fibrillation, n(%)	4 (6.3)	8 (12.7)	0	0.05
Diabetes, n(%)	4 (6.3)	4 (6.3)	2 (3.2)	0.415
hypertension, n(%)	8 (12.7)	11 (17.5)	8 (12.7)	0.56

Smoker, n(%)	1 (1.6)	6 (9.5)	5 (7.9)	0.301
Baseline NIHSS, median (IQR)	8 (2 – 17)	6 (4 – 8.25)	10.5 (5.25 – 16.25)	0.095
Baseline mRS, median (IQR)	0	0	0	0.418
Baseline imaging				
CBF<30, median (IQR), ml	11 (0 – 15)	0 (0 – 7)	5 (0 – 13.75)	*0.034
Tmax>6s, median (IQR), ml	72 (11 – 145)	43 (12.5 – 110.75)	79 (27.8 – 133)	0.455
Mismatch volume, median (IQR), ml	35 (11 – 132)	43 (10 – 92.75)	51 (23.25 – 130.75)	0.533
Time to baseline imaging, median (IQR), min	3.1 (0.02 – 5)	3.2 (1.95 – 4.86)	162.5 (2.7 – 5.7)	0.807
Time to followup imaging, mean (SD), hours	58.01 (21.1)	56.4 (24.2)	66.8 (23.2)	0.296
CTA collateral score, median (IQR)	11.5 (10 – 18.5)	16 (11 – 20)	17 (12.25 – 18.75)	0.368
Hypoperfusion intensity ratio (HIR), median (IQR)	0.43 (0.16 – 0.54)	0.28 (0 – 0.52)	0.24 (0- 0.55)	0.623
Follow-up imaging				
DWI lesion volume, median (IQR),ml	33.6 (11.3 – 71.4)	10.7 (3.9 – 24.1)	8.56 (3.27 – 15.35)	*0.008
Infarct growth, median (IQR), ml	19.65 (6.6 – 60.4)	7.4 (2 – 15.8)	3.1 (-0.35 – 15.5)	*0.01
Penumbral salvage, median (IQR), ml	5.25 (-8.47 – 53.6)	34.9 (-1.10 – 80.90)	49.5 (6.6 – 104.80)	*0.008
AOL score, median	0	3 (2 -3)	3 (2 -3)	*<0.001
ASL CBF lesion, mean (SD), ml/100g/min	11. 4 (3.9)	55.4 (26.6)	58.3 (19.7)	*<0.001
ASL hypoperfusion volume, median (IQR), ml	118 (19.8 – 204)	25.8 (10 – 63.5)	18.2 (8.3 – 32.8)	*0.01
Follow – up clinical				

Follow-up NIHSS	11.5 (2.75 – 19.75)	2 (1 – 6)	2 (0 - 6)	*0.005
Change in NIHSS, median	1 (- 1.75 – 2.25)	3 (1 – 4)	7.5 (2 – 11)	*0.001
Early neurological recovery, n (%)	3 (4.8)	18 (28.6)	14 (22.2)	*0.005
Follow-up mRS, median (IQR)	3 (1 – 4)	2 (1 – 3)	1.5 (0 – 2)	*0.017
Follow – up mRS category, n (%)				*0.036
Good functional outcomes, mRS 0-2, n(%)	6 (9.5)	19 (30.2)	15 (23.8)	
Poor functional outcomes, mRS 3-6, n (%)	9 (14.3)	11 (17.4)	3 (4.8)	

*** Indicates significant p-value <0.05**

Compared with those with no or slight reperfusion, patients with moderate and high reperfusion index had significant smaller ischemic core volume ($p = 0.034$), smaller follow-up DWI volume ($p = 0.008$), less infarct growth ($p = 0.01$), large penumbral salvage ($p = 0.008$, higher AOL score ($p < 0.001$), lower follow-up NIHSS ($p = 0.005$), early neurological recovery ($p = 0.005$) and good functional outcome ($p = 0.036$).

4.3.3 Relationship between ASL reperfusion index and radiological outcomes – Infarct growth and penumbra salvage

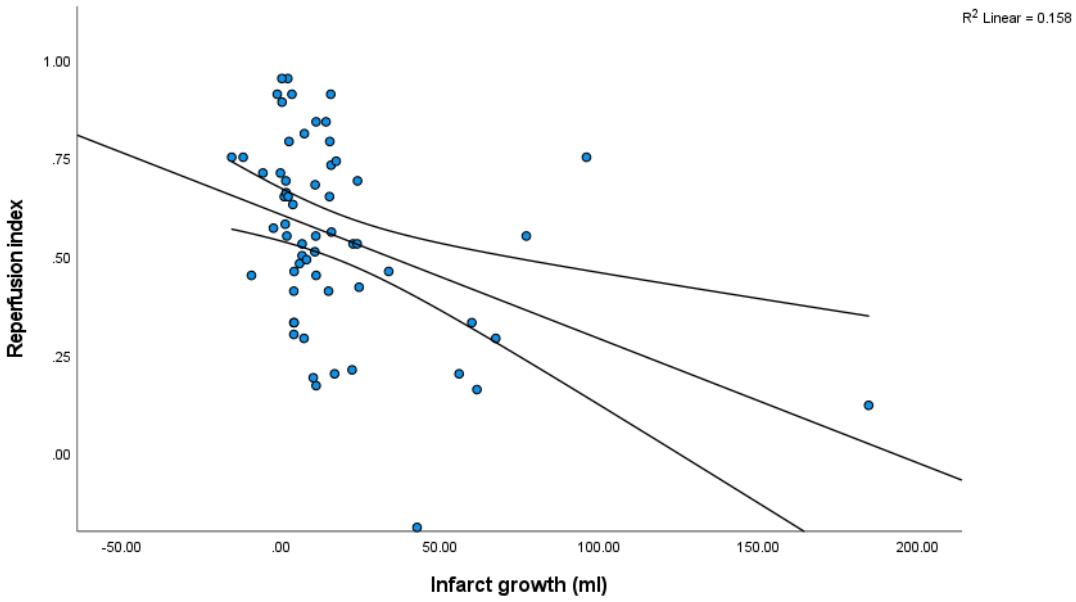

(a)

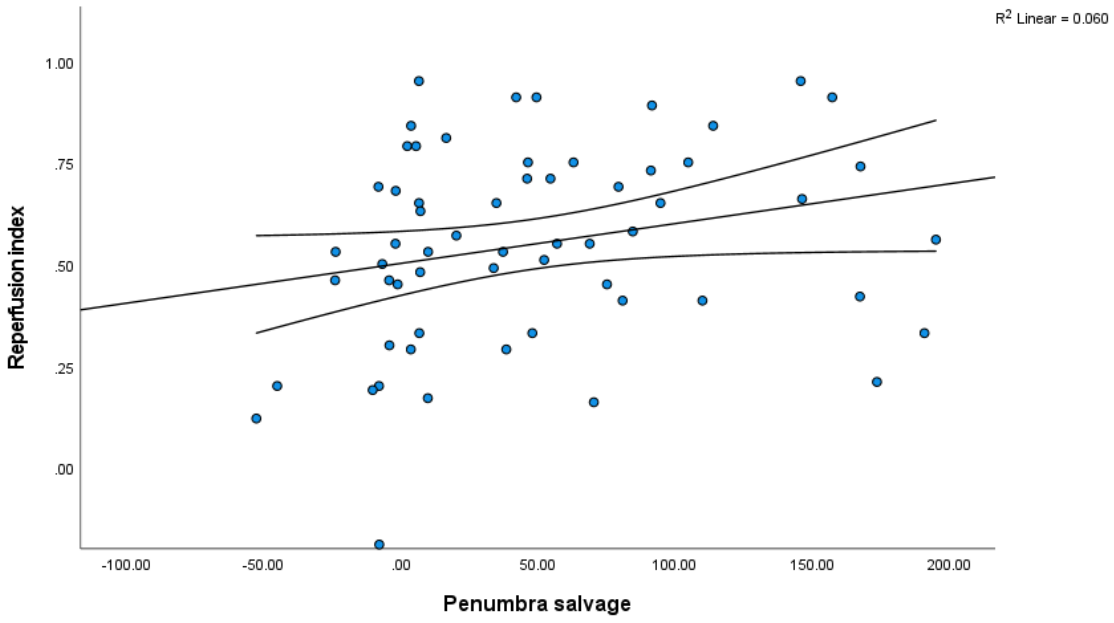

(b)

Figure 4-3: Relationship between reperfusion index and radiological outcomes; a) infarct growth; (b) penumbra salvage.

Reperfusion index was significantly negative correlated with infarct growth (r = -0.421, p < 0.001) and positively correlated with penumbra salvage (r = 0.297, p= 0.021) (Figure 4-3)

4.3.4 **Relationship between ASL reperfusion index and early neurological improvement.**

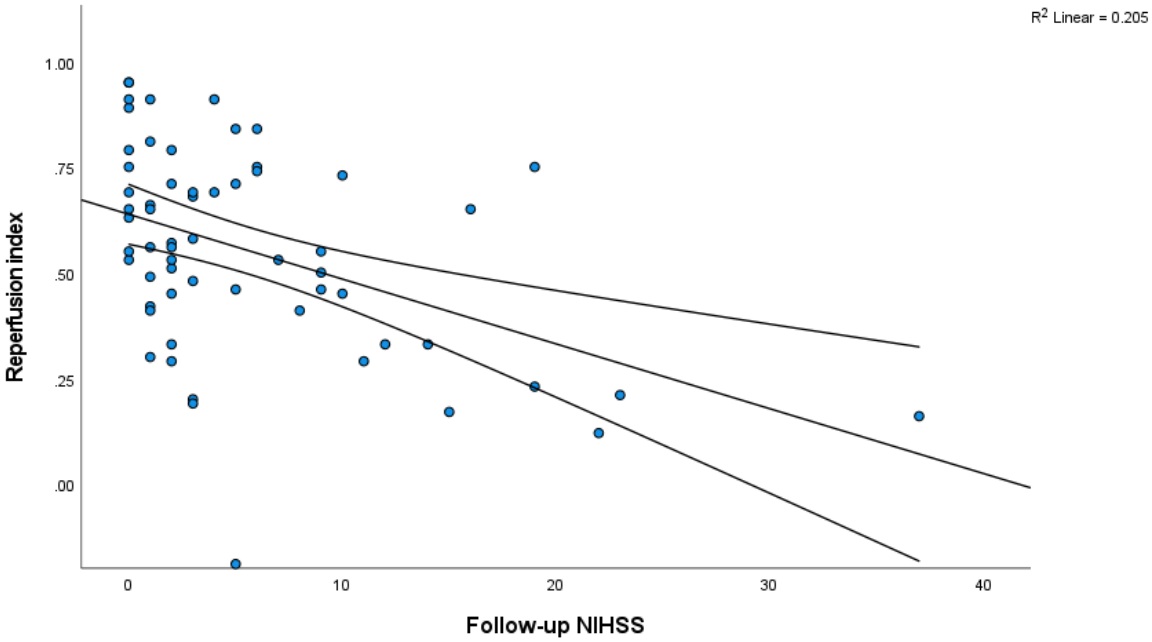

Figure 4-4: Correlation between reperfusion index with follow-up NIHSS

Reperfusion index was significantly negative correlated with follow-up NIHSS score (r = -0.452, p < 0.001) (Figure 4-4).

4.3.5 What are the association between reperfusion index and functional outcome?

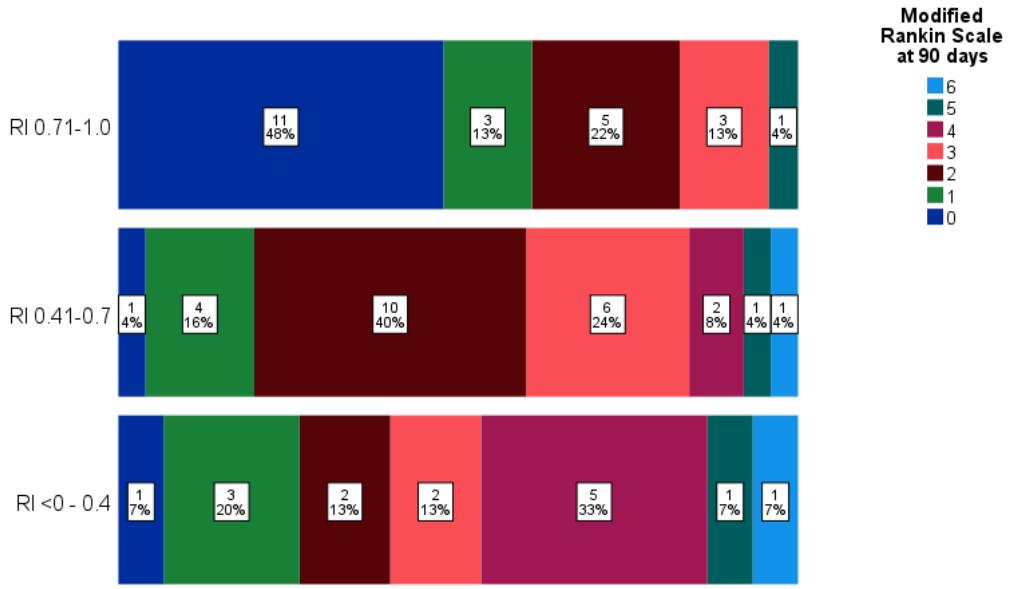

Figure 4-5: Functional outcome at day 90 stratified by reperfusion index.
RI = reperfusion index

Figure 4-5 shows the functional outcome at day 90 (mRS-90) stratified by reperfusion index groups. There were 15 subject who had mild or no reperfusion (RI <0 – 0.4), 29 subjects who had moderate reperfusion (RI 0.41 – 0.7) and 19 subjects who had high reperfusion (RI 0.71 – 1.0). Fourty-eight percent of who had high reperfusion index showed no disabilities (mRS 0) while 33% who had mild, or no reperfusion showed moderate disability (mRS 3) at day 90. Fourty-percent of subjects who had moderate reperfusion showed slight disability (mRS 2) at day 90.

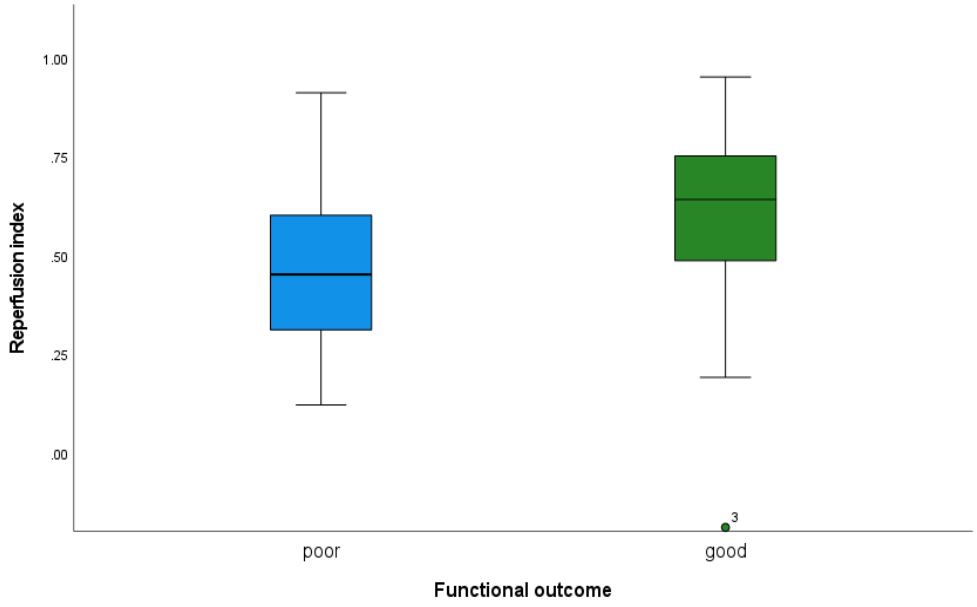

Figure 4-6: Relationship between reperfusion index and functional outcome categorized as good functional outcome (mRs 0-2) and poor functional outcome (mRs 3-6).

There was a significant association ($p<0.008$) between the median reperfusion index for poor functional outcome was 0.45 (IQR: 0.29 – 0.65) and 0.66 (IQR 0.48 – 0.75) for good functional outcome (Figure 4-6).

4.3.6 What are the predictors for radiological outcomes of infarct growth and penumbral salvage?

Table 4-8: Multivariate linear regression analysis predicting infarct growth

Predictors	Standardized Coefficients β	OR (95% CI)	p-value
Age	-0.017	0.983 (-0.555 – 0.482)	0.887
Baseline NIHSS	0.179	1.196 (-0.501 – 2.381)	0.196
HIR score	0.053	1.054 (-40.273 – 29.221)	0.751
Mismatch volume	0.321	1.378 (0.009 – 0.304)	*0.038
Thrombolysis treatment	-0.213	0.808 (-32.666 – 6.176)	0.117
AOL score	-0.017	0.983 (-10.823 – 9.911)	0.930
Reperfusion index	-0.329	0.719 (-82.991 – 0.075)	0.050

***Indicates significant p-value <0.05**

Table 4-9: Multivariate linear regression analysis predicting penumbral salvage

Predictors	Standardized Coefficients β	OR (95% CI)	p-value
Age	0.008	1.008 (-0.482 – 0.555)	0.887
Baseline NIHSS	-0.090	0.914 (-2.381 – 0.501)	0.1956
HIR score	-0.027	0.973(-41.002 - 27.369)	0.691
Mismatch volume	0.870	2.387 (0.696 – 0.991)	*<0.001
Thrombolysis treatment	0.107	1.113 (-6.176 – 32.666)	0.177
AOL score	0.008	1.008 (-9.911 – 10.823)	0.930
Reperfusion index	0.165	1.179 (- 0.075 – 82.991)	0.050

***Indicates significant p-value <0.05**

In multiple linear regression analyses (Table 4-8 and Table 4-9), mismatch volume was a significant independent predictor for infarct growth (OR 1.378, 95% CI: 0.009 – 0.304; p = 0.038), and penumbral salvage (OR 2.378, 95% CI: 0.696 – 0.991; p<0.001) after adjusting for age, baseline NIHSS, HIR score, thrombolysis treatment, AOL score and reperfusion index.

4.3.7 **What are the predictors for early neurological improvement?**

Table 4-10: Multiple binary logistic regression analysis predicting early neurological improvement

Predictors	Adjusted β	Adjusted OR (95% CI)	p-value
Age	-0.048	0.953 (-0.121 – 0.477)	0.647
Baseline NIHSS	-0.023	0.977 (-0.315 – -0.435)	*< 0.001
HIR score	-0.055	0.946 (-5.027 – 8.039)	0.646
Mismatch volume	-0.265	0.767 (-0.056 – 0.001)	0.061
Thrombolysis treatment	0.039	1.039 (-3.159 – 4.221)	0.774
AOL score	0.226	1.254 (-0.649 – 3.306)	0.184
Reperfusion index	0.315	1.370 (0.572 – 16.721)	*0.036

***Indicates significant p-value <0.05**

Multiple binary logistic regression analysis in Table 4-10 shows baseline NIHSS (OR 0.977, 95% CI -0.315 – -0.435; p < 0.001) and reperfusion index (OR 1.370, 95% CI 0.572 – 16.721; p < 0.036) significantly predict early neurological improvement (reduce NIHSS score by 3 points) after adjusted for age, HIR score, mismatch volume, thrombolytic treatment, and AOL score.

4.3.8 **What are the predictors for 90-day good functional outcome?**

Table 4-11: Multiple logistic regression analysis predicting independent recovery

Predictors	Adjusted ß	Adjusted OR (95% CI)	p-value
Age	-0.019	0.981 (0.96 – 1.003)	0.087
HIR score	-3.370	0.034 (1.102 – 767.967)	*0.044
Mismatch volume	0.016	1.016 (0.973 – 0.997)	*0.012
Thrombolysis treatment	0.327	1.386 (0.154 – 3.384)	0.678
Reperfusion index	3.908	49.817 (3.097 – 801.435)	*0.006

***Indicates significant p-value <0.05**
**** Each variable are run as entered**

In multiple logistic regression, HIR score (adjusted OR 0.034, 95% CI 1.102 – 767.967, p = 0.044), mismatch volume (adjusted OR 1.016, 95% CI 0.973 – 0.997, p = 0.012) and reperfusion index (adjusted OR 49.817, 95% CI 3.097 – 801.435, p = 0.006) were independently associated with 90-day good functional outcome (Table 4-11).

4.4 Discussion

This study assessed the relationship between the reperfusion index measured by ASL with radiological endpoints (infarct growth and penumbral salvage), early neurological improvement (reduction in NIHSS by 3 points) and functional outcomes at 90-days. In this study, the follow-up NIHSS scores were taken at 48 to 72 hours after stroke onset. The early neurological improvement was defined as reduced NIHSS score by 3 points from baseline NIHSS. The choice of this cut-off point for early neurological improvement differs from previous stroke trials because the median baseline NIHSS score presented in this study was lower compared to other major stroke trials (Christensen *et al.*, 2019).

The correlation analysis between reperfusion index and infarct growth demonstrates a significant inverse relationship between these two variables. Reperfusion index higher than 0.4 was significantly associated with lower infarct growth compared with lower reperfusion index. Moreover, patients with high reperfusion index had significant smaller follow-up DWI volume compared with patient with lower reperfusion index. The association between reperfusion and infarct growth has been previously demonstrated in a subset of DEFUSE 3 trial data in which absence of reperfusion was associated with increased infarct growth beyond 24 hours of stroke onset (Tate *et al.*, 2021).

The correlation analysis also demonstrates a significant positive correlation between reperfusion index and penumbral salvage. The result suggests that there is evidence of persistent target mismatch even at late time window (after 48 hours of stroke onset). This result also confirms data from previous study which showed that the ischaemic penumbra in human may still exist beyond 48 hours after stroke onset (Read *et al.*, 2000). Preservation of the ischaemic penumbra at later time point may be contributed by the collateral flow. The regression analysis shows a trend of low HIR score (good collateral) with higher penumbral salvage.

In the multivariate linear regression analyses, reperfusion index was not significant as an independent predictor for either of the radiological outcomes (infarct growth and penumbral salvage) after adjusting for age, baseline NIHSS,

HIR score (as an index of collateral status), mismatch volume, thrombolysis treatment and AOL score, but there was a trend consistent with greater infarct growth and lower penumbral salvage with lower reperfusion index.

Reperfusion index was significantly negatively correlated with follow-up NIHSS. In relation, the multiple binary logistic regression analysis showed patients with lower baseline NIHSS, and higher reperfusion index had significant high odds of early neurological improvement after adjusted for age, HIR score, mismatch volume, thrombolytic treatment, and AOL score. Data from Saver and Altman, 2012, showed fluctuations of NIHSS score during few hours (1 hour up to 24 hours after stroke onset) indicating underlying recovery or deterioration of neurological mechanism following cerebral ischaemia. Restoration of blood flow at distal capillary bed can occur via arterial recanalization or collateral pathway. However, degree of reperfusion may differ although in successful recanalisation and thus results in different clinical outcomes.

Reperfusion at tissue level benefited the as demonstrated with reduction of DWI core and increase penumbral salvage at follow-up. These factors are translated into improvement in early neurological recovery. The results are consistent with DEFUSE and EPITHET studies which support the high reperfusion as markers of good clinical outcome (Albers *et al.*, 2006; Davis *et al.*, 2008)

In this study, reperfusion index was a significant predictor of independent recovery assessed by modified Rankin Scale at day 90. This result is in concordance with Lu et al., 2020, in which ASL reperfusion was one of the independent variables in predicting good functional outcome. Previous clinical trials evaluating endovascular mechanical thrombectomy in anterior circulation large vessel occlusion have also shown that quality of reperfusion at the end of a procedure is strongly associated with functional outcome (Liebeskind *et al.*, 2019).

The strength of this study was the application of ASL as follow-up perfusion imaging which is underexplored in other studies. Stratification of reperfusion index in this study is similar with most of reperfusion imaging analysis used modified Thrombolysis in Cerebral Infarction (TICI) score measured

angiographically with 3 grading score, with score of 0 (no reperfusion), score 2 (partial reperfusion) and score 3 (complete reperfusion)(Higashida *et al.*, 2003).

The limitation of this study was the reperfusion index in this study was calculated using two different techniques (CTP perfusion at baseline and ASL perfusion at follow-up) which may not be accurate due to different voxel sizes between CTP and ASL. Thus, ASL should be used as baseline and follow-up perfusion imaging technique to improve the calculation of reperfusion index. Reperfusion assessments should be conducted at multiple time points (during first visit, immediately after reperfusion treatment and 24 to 48 hours after treatment) to capture the dynamic changes of cerebral reperfusion.

4.5 Conclusion

In summary, reperfusion index measured using ASL was correlated with radiological outcomes (infarct growth and penumbral salvage) and clinical outcome. A well-designed study using ASL as baseline and follow-up perfusion imaging at several time-points may yield more accurate reperfusion index and serve as a potential imaging marker of tissue level reperfusion in ischemic stroke. Reperfusion index using ASL across different stroke severity (mild to severe ischemic stroke) is recommend in future studies to provide better understanding on the pathophysiology of reperfusion mechanism in different ischemic stroke patients.

Chapter 5 Reperfusion assessment among recanalized ischemic stroke patients – an investigation using ASL reperfusion index

5.1 Introduction

The main goal of current acute stroke therapy is to open the blocked vessel (recanalisation) and restore flow to the distal capillaries (reperfusion) to prevent brain tissue damaged. Ideally, recanalisation should lead to reperfusion at tissue level with restoration of oxygen and nutrient supply. Reperfusion of the initial infarct at 24 hours was observed angiographically in 79% of patients who underwent thrombectomy (Albers *et al.*, 2018).

However, reperfusion of the distal blood vessels at capillary level may not occur despite complete angiographic recanalisation. The phenomenon known as futile recanalisation was proposed to denote the failure to make good clinical recovery despite apparently complete angiographic recanalisation, and potential mechanisms reviewed by el Amki and Wegener, 2017. Mechanisms for futile recanalisation may be include “no-reflow” phenemenon of recanalised blood vessels or arterial re-oocclusion. The no-reflow concept was introduced in 1967 based on studies of the brain in rabbits’ subjected to global cerebral ischaemia (Ames *et al.*, 1967). Perfusion defects were observed as carbon filling-defects in the post-ischaemic brains even after relief of vessel obstruction. From this study, it was suggested that the failure of flow in the microcirculation after reperfusion post-ischemia might be attributable to post-ischaemic hypotension, an increase in blood viscosity and blood vessels stenoses. These observations were supported by a histology study which found that continuous contraction of pericytes could cause microvascular impairment despite successful recanalisation of an occluded cerebral artery (Yemisci *et al.*, 2009).

On the other hand, arterial re-occlusion is defined as occlusion of recanalised blood vessels characterised by brief clinical improvement and followed by deterioration in clinical condition in the absence of intracranial haemorrhage (el Amki and Wegener, 2017). In addition, Rubiera et al., 2005, investigated the early arterial re-occlusion after thrombolysis via iv-tPA and

found that 25% patients who recanalised were worsened (increase of NIHSS ≥4 points) after an initial improvement (decrease of NIHSS ≥4 points).

The degree of reperfusion is important to predict the clinical outcome (at 24 hours after stroke onset) and late functional outcome (90-day functional outcome). Previous study assessed the degree of reperfusion based on single threshold, more than 50% reduction in the volume of baseline perfusion lesion in DEFUSE 2 using PWI. (Lansberg *et al.*, 2012). Similarly, EPITHET reperfusion was defined as 90% or more on PWI (Davis *et al.*, 2008). Thus, there is a need to quantitatively assessed the reperfusion status among recanalised ischaemic stroke patients using non-invasive imaging method.

The follow-up ASL perfusion data offer the opportunity to explore the relationships between angiographic status, tissue perfusion, and clinical and radiological outcomes. In particular, the potential for reperfusion to offer a more relevant measure of outcome than angiographic outcomes will be explore by focusing on those patients with favourable angiographic recanalisation. Therefore, the aims of this chapter are to:

1. to investigate the association of moderate and high index with infarct growth volume, early neurological improvement, and 90-day good functional outcome among recanalised ischaemic stroke patients.

2. To establish the predictors for early neurological improvement, increase infarct growth volume and good functional outcomes among patients with complete recanalisation.

5.2 Methods

The methods used in this chapter is the same as described in Chapter 4.

5.2.1 Baseline and follow-up imaging

Baseline imaging was performed using CT and was conducted during the first visit less than 24 hour from onset of symptom. The baseline imaging examinations included non-contrast CT, CTP and single-phase CTA.

The ischemic core volume was defined as tissue with Tmax>6s and relative CBF<30% - while ischaemic penumbra was defined as delay of the residue function, Tmax>6s. Mismatch volume was calculated as the ratio between CBF<30% and Tmax>6s. All baseline imaging parameters were assessed using CTP automated software (RAPID, iSchemaView).

The follow-up imaging was conducted using an MRI scanner, 3 Tesla Magnetom Prisma (Siemens Healthcare, Erlangen, Germany). Follow-up MR imaging was conducted during second visit, 48 – 72 hours after stroke. Non-contrast CT, CTP and CTA scans were conducted during the follow-up if the patients had contraindications to MRI.

5.2.2 Study population

The study population in this chapter was selected from included subjects in Chapter 4 who had AOL score of II or III.

5.2.3 Recanalisation assessment

Recanalisation was assessed angiographically by experienced neuroradiologists using the arterial occlusion lesion (AOL) score, Table 5-1. The AOL were dichotomously categorized into two groups. Group 1 was those with no recanalisation or incomplete with no distal flow recanalisation (AOL 0-I), and Group 2 for those with complete recanalisation or incomplete with distal flow (AOL II-III).

Table 5-1: AOL score categories

AOL score	Description
0	No recanalisation
I	Incomplete or partial recanalisation with no distal flow
II	Incomplete or partial recanalisation with distal flow
III	Complete recanalisation of the primary occlusion with distal flow

Adapted from **(Khatri *et al.*, 2005)**

5.2.4 **Statistical analysis**

Statistical analysis was performed with IBM SPSS Version 28 (IBM Corp, Armonk, NY, USA). Continuous variables were compared to Spearman's rank correlation. Radiological variables were dichotomised by their median. For categorical outcome variables, normally distributed continuous variables were tested with independent t-tests, and non-normally distributed continuous variables with independent samples Mann-Whitney U tests. Normality was tested with Shapiro-Wilk. Results are expressed as mean (standard deviation, SD) unless otherwise stated. The statistical significance was set at $p < 0.05$.

Correlation analyses were performed to find the relationship between two variables. Binary multivariate logistic regression analyses were performed with good outcome as a dependent variable, and baseline clinical data, comorbidities, stroke severity, collateral status, baseline imaging parameters, and treatment information as independent variables.

5.3 Results

5.3.1 Arterial occlusion assessment

MRA results were available for a total of 63 subjects who satisfied the inclusion and exclusion criteria based on Chapter 4. Among the 63 subjects, 49 subjects with baseline vessel occlusion had recanalized (AOL II-III) while 14 subjects did not recanalise (AOL 0-I) (Table 5-2). To address the question of whether tissue reperfusion was associated with different clinical and radiological outcomes, analyses were undertaken on the subgroup with good recanalisation (AOL II-III). One subject who did not reperfuse (RI -0.19) was excluded from the statistical analyses because it may decrease the statistical power. However, clinical and imaging data of the subject were presented for an example of patient who did not reperfuse but recanalised.

Table 5-2: Number of patients according to recanalisation category

Category	Not recanalised (AOL 0-I)	Recanalised (AOL II-III)	Total
No reperfusion/ mild reperfusion	14	1 (no reperfusion)	15
Moderate reperfusion	0	30	30
High reperfusion	0	18	18
Total	14	49	63

5.3.2 Baseline and follow – up clinical and imaging characteristics of study population

The mean age of the study population was 67 ± 12.0 with median admission NIHSS of 8 (IQR: 5 - 11). 35 subjects (71%) received thrombolysis treatment during the initial visit. Twenty subjects (42.9%) had large vessels occlusion and 33 (67.3%) had PACS stroke as classified by the Oxford Community Stroke Project classification system. Subjects had small median CBF<30% volume of 0 ml (IQR: 0 – 12ml) and follow-up median DWI volume of 10.7ml (IQR: 3.6 – 25.2ml). The mean reperfusion index was 0.67 (SD: 0.16). Thirty-four subjects (94.3%) had early neurological recovery. Baseline and follow-up characteristics are listed in Table 5-3.

Table 5-3: Baseline and follow-up characteristics

Variables	N= 48
Clinical characteristics	
Age, mean (SD), years	67 (12)
Gender, n (%)	
Male	29 (61)
Female	19 (39)
Thrombolysis treatment, n(%)	
Yes	35 (71)
No	13 (29)
Stroke types, n (%)	
PACS	33 (67.3)
TACS	9 (20.4)
POCS	5 (10.2)
LACS	1 (2)
Occlusion type, n (%)	
Large vessels	20 (42.9)
Small vessels	28 (57.1)
Atrial fibrillation, n(%)	9 (16.3)
Diabetes, n(%)	6 (12.2)
Hypertension, n(%)	19 (38.8)
Smoker, n(%)	11 (22.4)
Baseline NIHSS, median (IQR)	8 (5 – 11)
Baseline mRS, median (IQR)	0
Baseline imaging	
CBF<30%, median (IQR), ml	0 (0 – 12)
Tmax>6s, median (IQR), ml	51 (21 – 119)
mismatch volume, median (IQR), ml	46 (14.5 – 108.5)
Time to baseline imaging, median (IQR), hr	3.1 (1.6 – 5.1)
Time to follow-up imaging, mean (SD), hr	60.5 (23.9)
CTA collateral score, median (IQR)	15 (11 - 18)
Hypoperfusion intensity ratio (HIR), median (IQR)	0.37 (0.06 – 0.52)
Follow-up imaging	
DWI lesion volume, median (IQR),ml	10.7 (3.6 – 25.2)

Infarct growth, median (IQR), ml	6.7 (1.6 – 15.7)
ASL CBF, mean (SD), ml/100g/min	53.6 (24.6)
ASL hypoperfusion volume, median (IQR), ml	18.4 (9.2 – 52.7)
Reperfusion index, mean (SD)	0.64 (0.16)
Follow-up clinical characteristics	
Follow-up NIHSS, median (IQR)	2 (1 – 5.8)
Change in NIHSS, median (IQR)	3 (1 – 7)
Early neurological recovery, n (%)	
Yes	34 (94.3)
No	14 (57.7)
Follow-up mRS-90, median (IQR)	2 (0)
Follow – up mRS-90 category, n (%)	
Good functional outcomes mRS 0-2, n(%)	35 (87.5)
Poor functional outcomes mRS 3-6, n (%)	13 (60.9)

Table 5-4: Association between reperfusion index among patients with recanalised blood vessels.

Variables (n = 48)	Moderate reperfusion RI = 0.41 – 0.7 N = 30	High reperfusion RI = 0.71 – 1.0 N = 18	p-value
Clinical characteristics			
Age, mean (SD), years	65 (14.34)	69 (8.05)	0.441
Gender, n (%)			
Male	19 (37.5)	10 (22.9)	0.694
Female	11 (22.9)	8 (16.67)	
Thrombolysis treatment, n(%)			0.491
Yes	20 (39.6)	15 (31.3)	
No	10 (20.8)	3 (8.3)	
Stroke types, n (%)			0.419
PACS	23 (45.8)	10 (20.8)	
TACS	3 (6.3)	6 (14.6)	
POCS	3 (6.3)	2 (4.2)	
LACS	1 (2.1)	0	
Occlusion type, n (%)			0.702
Large vessels	12 (25.0)	8 (16.7)	
Small vessels	18 (35.4)	12 (35.4)	
Atrial fibrillation, n(%)	8	1	0.203
Diabetes, n(%)	3	2	0.880
hypertension, n(%)	11	9	0.484
Smoker, n(%)	5	6	0.438
baseline NIHSS, median (IQR)	6 (4 – 8)	11 (6 – 16)	*0.029
baseline mRS, median (IQR)	0 (0)	0 (0)	0.112
Baseline imaging			
CBF<30, median (IQR), ml	0 (0 – 10)	5 (0 – 13)	0.098
Tmax>6s, median (IQR), ml	44 (13 – 110)	53 (24 – 128)	0.079
Mismatch volume, median (IQR), ml	44 (10 – 87)	49 (21 – 125)	0.639
Infarct growth rate, median (IQR), ml/hr	0 (0 – 3.62)	2.03 (0 – 5.95)	0.435
time to baseline imaging, median (IQR), min	3.1 (1.75 – 4.65)	2.95 (1.72 – 6.17)	0.873
Time to followup imaging, mean (SD), min	52.8 (22.88)	68.2 (23.32)	0.153
CTA collateral score, median	17 (12 – 19)	12 (10 – 18)	0.240

(IQR)			
Hypoperfusion intensity ratio (HIR), median (IQR)	0.25 (0 – 0.52)	0.42 (0.19 – 0.53)	0.461
Follow-up imaging			
DWI lesion volume, median (IQR),ml	9.4 (3.55 – 24.68)	13.4 (3.5 - 25.2)	0.067
Infarct growth, median (IQR), ml	6.7 (1.85 – 15.7)	3.5 (0.1 – 15.45)	*0.048
Penumbral salvage, median (IQR), ml	34.4 (-1.28 – 81.82)	49.5 (6.66 – 104.8)	0.086
ASL CBF lesion, median (IQR), ml/100g/min	53.71 (43.16 – 61.36)	63.32 (54.28 – 69.36)	*0.017
ASL hypoperfusion volume, median (IQR), ml	10.79 (7.25 – 27.35)	10.0 (2.31 – 12.36)	0.11
Follow – up clinical			
Follow-up NIHSS	2 (1 – 7.25)	2 (0 – 6)	0.741
Change in NIHSS, median	3 (1 – 4)	8 (2 – 11)	*0.014
Follow – up mRS category, n (%)			0.205
Good functional outcomes mRS 0-2, n(%)	18 (37.5)	16 (33.3)	
Poor functional outcomes mRS 3-6, n (%)	10 (22.9)	3 (6.25)	

***Denotes significant value at p<0.05**

Table 5-4 shows the characteristics of the patients with good recanalisation (AOL II-III) divided into two groups based on reperfusion index (moderate and high RI). The subjects with high RI had significantly higher baseline NIHSS ($p<0.029$), smaller infarct growth volume ($p<0.048$) and larger change of NIHSS ($p<0.014$) compared to subjects with moderate RI.

5.3.3 Example of subjects who did not reperfused, but recanalized

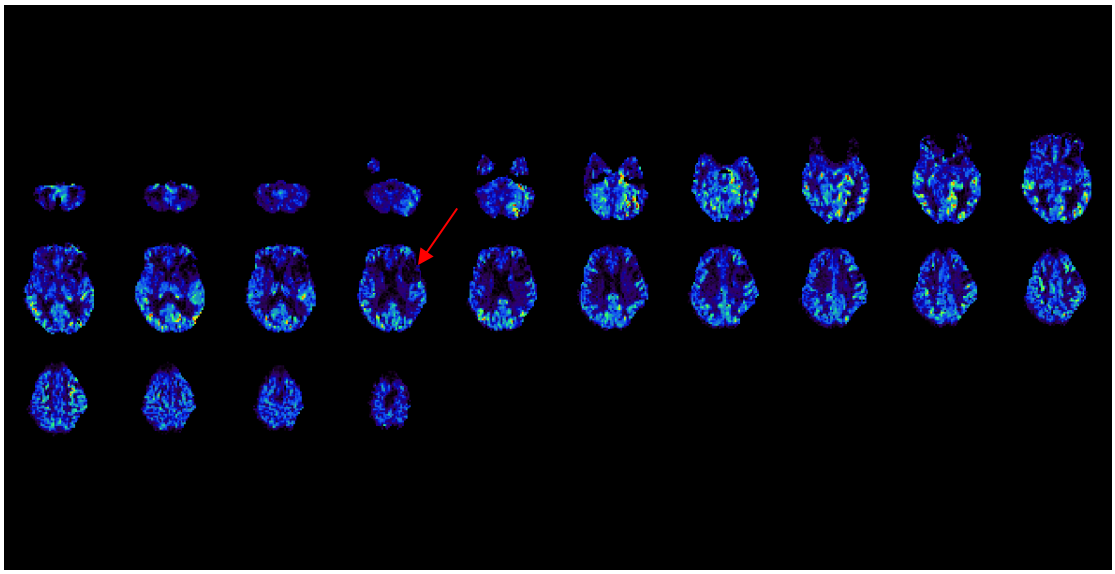

a)

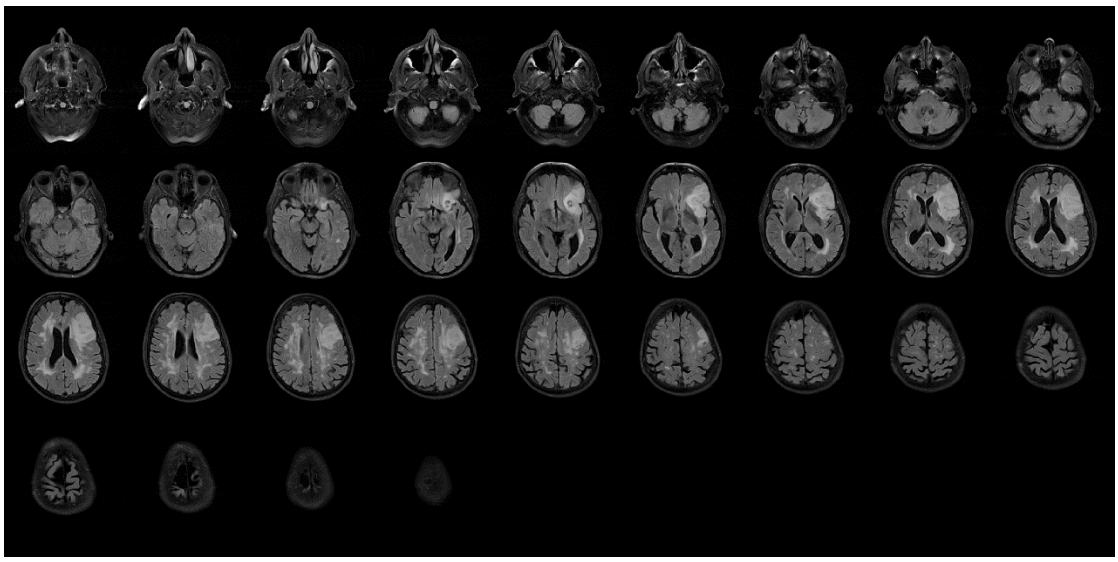

b)

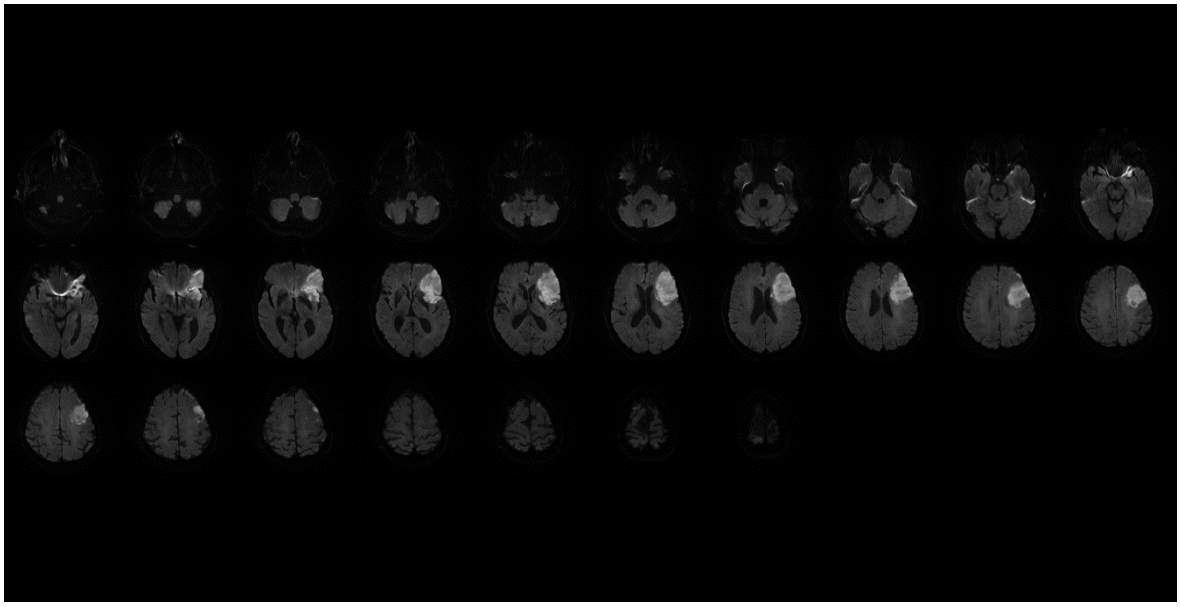

c)

Figure 5-1: Patient with AOL score of III but did not reperfused (reperfusion index of -0.19). a) ASL CBF map showing non-reperfused region (red arrow) with the b) FLAIR map and c) DWI map.

Figure 5-1 shows the ASL perfusion map, FLAIR and DWI of a subject who did not re-perfuse despite an AOL score of 3. The subject was a 76-year-old male who had been thrombolysed 2.6 hours after stroke onset. His baseline NIHSS was 8 and baseline mRS of 1. The CTA revealed an occlusion of the left middle cerebral artery M2 branch and CTA collateral score of 11.

His CTP results showed CBF<30% volume of 37ml and the Tmax>6*s* was 72ml with hypoperfusion intensity ratio of 0.5. His follow-up DWI volume was 79ml with infarct growth of 42ml. His reperfusion index was -0.19. His follow-up NIHSS was 5 and his mRS-90 was 2.

5.3.4 **Example of subject with moderate reperfusion index**

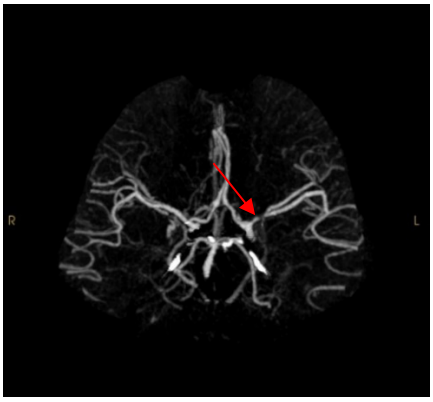

a)

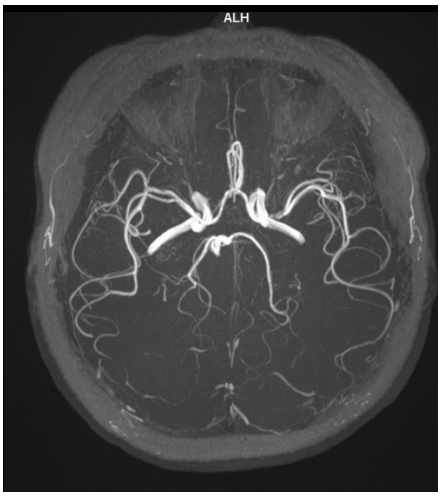

b)

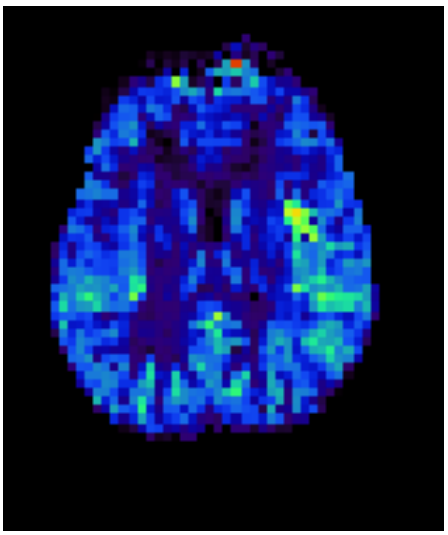

c)

Figure 5-2: Patient with AOL score of II and had moderate refusion index (RI = 0.49). a) CTA showing occluded artery (red arrow) with the b) MRA showing recanalised artery and c) ASL showing moderate hyperperfusion at left side of the brain

Figure 5-2 shows the radiological images for a subject who had reperfusion and partial recanalisation (AOL score II). The subject was 41-year-old female who had been thrombolysed at 3 hours after stroke onset. Her baseline NIHSS was 4 and baseline mRs of 0. The CTA revealed an occlusion at left proximal middle cerebral artery, M1, and the CTA collateral score of 17.

Her CTP results showed CBF<30% of 0ml and the Tmax>6s was 42ml with hypoperfusion intensity ratio of 0. Her follow-up DWI volume was 8.10 ml with infarct growth of 8.10 ml. Her reperfusion index was 0.49. Her follow-up NIHSS was 1 and his mRs-90 was 1.

5.3.5 **Example of subject with high reperfusion index**

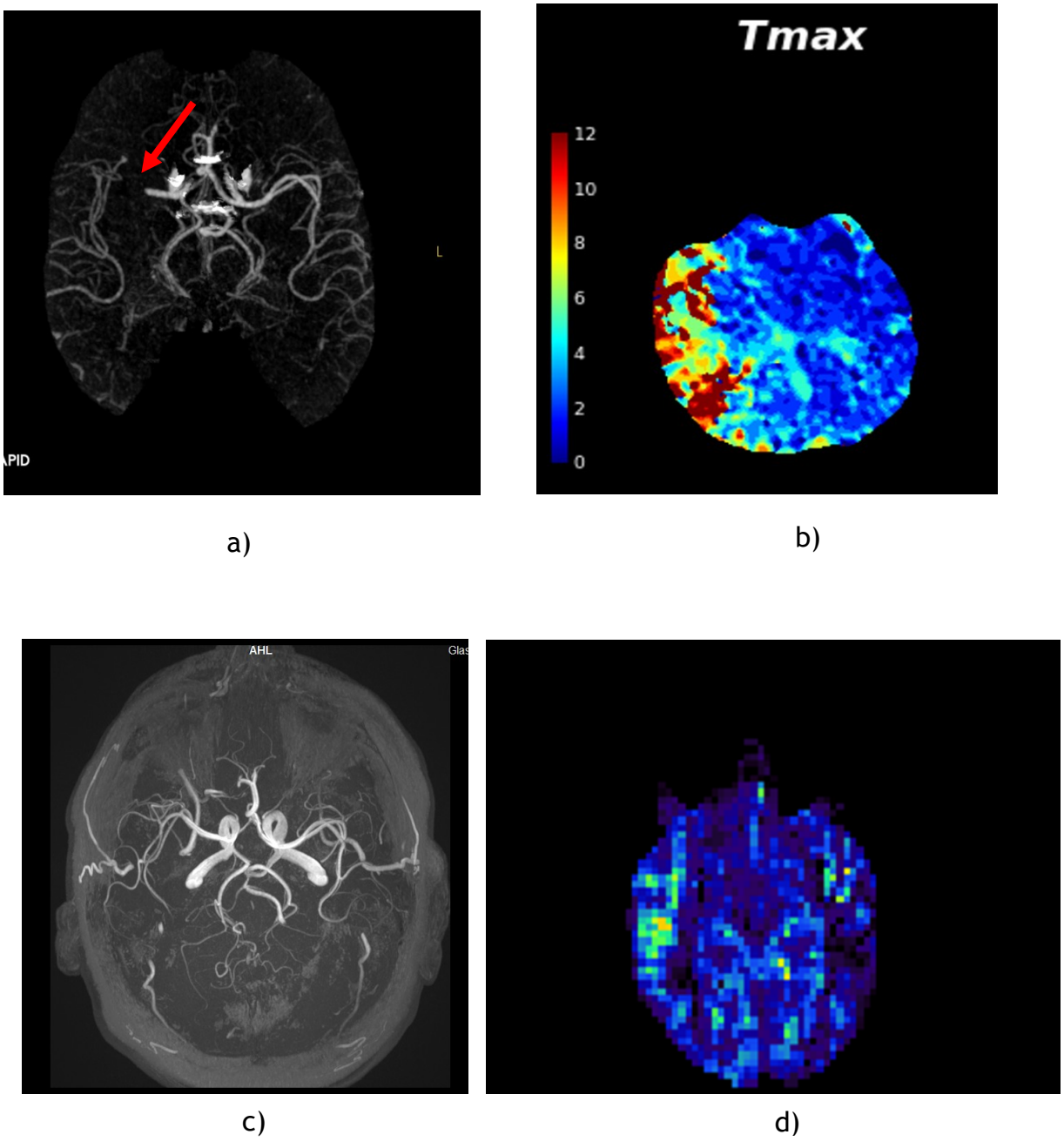

Figure 5-3: Patient with AOL score of III and had high refusion index (RI = 0.77). a) CTA showing occluded artery (red arrow) with the b) Tmax>6s of CTP, c) MRA showing recanalised artery and d) ASL showing hyperperfusion at right side of the brain.

Figure 5-3 shows the radiological images for a subject who had successful reperfusion and recanalisation (AOL score III). The subject was 55-year-old male who had been thrombolysed at 2 hours after stroke onset. His baseline NIHSS was 18 and baseline mRs of 0. The CTA revealed an occlusion at right proximal middle cerebral artery, M1, and the CTA collateral score of 10.

His CTP results showed CBF<30% of 0ml and the Tmax>6s was 185ml with hypoperfusion intensity ratio of 0.4. His follow-up DWI volume was 17.4ml with infarct growth of 17.4ml. His reperfusion index was 0.77. His follow-up NIHSS was 6 and his mRs-90 was 2.

5.3.6 Relationship between degree of reperfusion and infarct growth volume

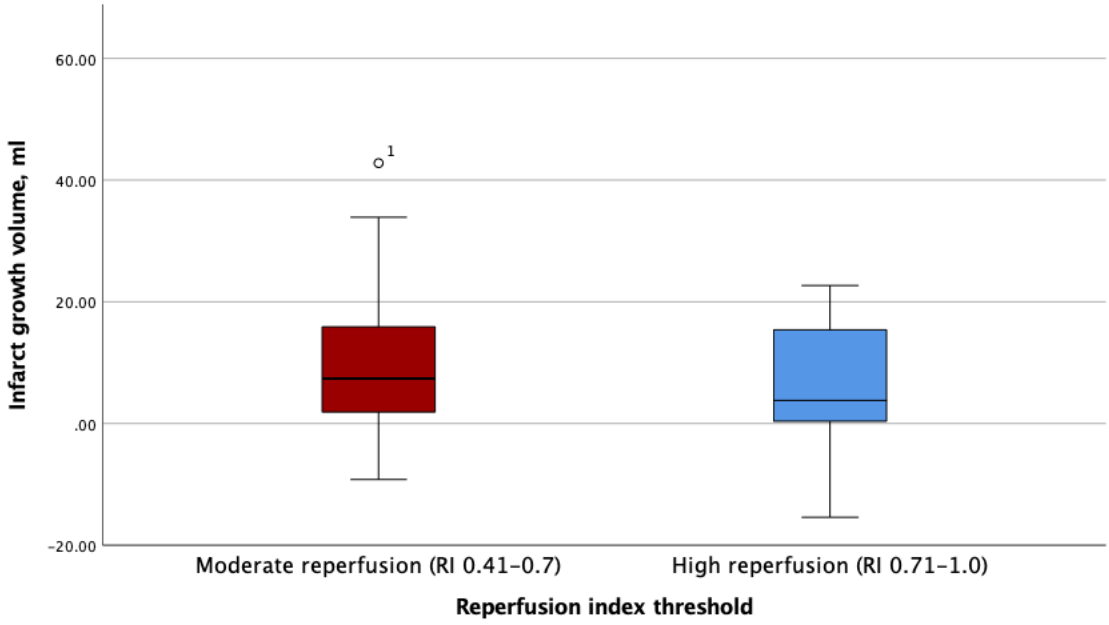

Figure 5-4: Box plot of infarct growth volume and reperfusion index threshold. Black bars represent medians. Circle represent outlier. High reperfusion index shows smaller infarct growth volume.

Figure 5-4 shows the association between volume infarct growth and degree of reperfusion categorised into 2 thresholds (moderate and high). Subjects who had moderate reperfusion had significant larger infarct growth (median 6.7ml; IQR: 1.85 -15.7) than subjects who had high reperfusion (median 3.5ml; IQR: 0.1 – 15.45) (p = 0.048)

5.3.7 **What are the predictors volume of infarct growth?**

Table 5-5: Multiple linear regression analysis predicting infarct growth

Predictors	Standardized Coefficients β	OR (95% CI)	p-value
Age	-0.269	0.764 (-0.869 – 0.241)	0.251
Baseline NIHSS	0.127	1.135 (-1.130 – 2.173)	0.518
HIR score	-0.028	0.972 (-39.459 – 35.475)	0.913
Mismatch volume	0.334	1.396 (-0.047 – 0.235)	0.179
Thrombolysis treatment	-0.158	0.853 (-26.509 – 15.578)	0.594
AOL score	0.201	1.222 (-11.996 – 25.367)	0.464
Reperfusion index	-0.451	0.637 (-90.324 - -3.909)	*0.034

***Indicates significant p-value <0.05**

Multiple linear regression analysis was conducted on subgroup of those who had AOL score of II or III (n=49) to predict the volume of infarct growth. The predictors of infarct growth volume are listed in Table 5-5. Reperfusion index is a significant independent predictor (OR: 0.637; CI: -90.324 - -3.909; p=0.034) for infarct growth after adjusting for age, NIHSS, collateral status (HIR), mismatch volume, use of thrombolysis and AOL score.

5.3.8 What are the predictors of early neurological improvement and 90-day good functional outcome?

Table 5-6: Multivariate logistic regression analysis predicting early neurological improvement

	Adjusted β	Adjusted OR (95% CI)	p-value
Age	-0.381	0.683 (-0.133 – 0.011	0.092
Baseline NIHSS	0.386	1.471 (-0.001 – 0.430)	0.051
HIR score	0.003	1.003 (-4.921 – 4.972)	0.991
Mismatch volume	0.130	1.138 (-0.014 – 0.024)	0.587
Thrombolysis treatment	-0.130	0.878 (-3.336 – 2.090)	0.638
AOL score	0.069	1.071 (-1.999 – 2.628)	0.780
Reperfusion index	0.113	1.119 (-4.086 – 7.330)	0.561

***Each variable is run as entered**

Table 5-7: Multivariate logistic regression analysis predicting independent recovery

Predictors	Adjusted β	Adjusted OR (95% CI)	p-value
Age	-0.019	0.982 (0.95 – 1.014)	0.264
HIR score	3.163	23.649 (0.219 – 2551176)	0.185
Mismatch volume	-0.010	0.991 (0.974 – 1.008)	0.277
Thrombolysis treatment	0.109	1.115 (0.156 – 7.992)	0.913
Reperfusion index	2.482	11.968 (0.208 – 689.592)	0.230

*** Each variable is run as entered**

In multivariate binary logistic regression analysis, none of the variables was an independent predictor of early neurological improvement (Table 5-6) or of 90-day good functional outcome (Table 5-7).

5.4 Discussion

This study investigated the relationship of reperfusion and outcome, specifically focusing on the question of whether reperfusion would modify outcome among patients with good angiographic recanalisation assessed by AOL score. Reperfusion index was significantly higher in subjects with AOL score of II or III. Among those with good recanalisation (AOL II-III), with higher reperfusion index (RI 0.71 – 1.0) had significantly smaller infarct growth volume, higher CBF, smaller ASL hypoperfusion volume and improved NIHSS compared to the group with moderate reperfusion group (RI 0.41 – 0.70). An association with functional outcome as assessed by modified Rankin Scale at day 90 could not be shown, although the point estimates of the odds ratio suggest possible relationship.

In this study, there was only one patient who did not reperfuse despite having complete recanalisation. Similarly, a previous study by Schiphorst et al., 2021 found only 1 patient out of 33 who had recanalised had no-reflow and suggested that no re-flow was maybe a rare phenomenon. Although the patient did not reperfuse, his NIHSS reduced 3 points from 8 to 5 suggesting some clinical recovery took place. This observation suggested that the reperfusion is a dynamic process which may can occur later point. This phenomenon is called as delayed reperfusion and has been studied pre-clinically in permanent and transient brain ischemia mouse models. occur due to late-phase vascular remodelling and improves peri-lesional perfusion (Durán-Laforet *et al.*, 2019) The reperfusion index measured by ASL in this study (RI of -0.19) provides a snapshot of reperfusion at the time of imaging and may not reflect the delayed reperfusion.

Quality of leptomeningeal collaterals is one of the factors that may contribute to reperfusion and thus reduce the infarct growth. It has been noted in previous studies that collateral quality determined by hypoperfusion intensity ratio (HIR) significantly predicted infarct growth (Olivot *et al.*, 2014; Tate *et al.*, 2021). The HIR calculated from these studies was defined as the ratio between Tmax>6s volume and Tmax>10s, in which a ratio of $\leq$0.4 indicated good collateral and >0.4 indicated poor collateral. Interestingly, in our study the HIR for high RI group was higher (0.42) compared to the moderate RI (0.25) although the difference was not significant. Collateral quality may therefore interact with

subsequent reperfusion, but a larger sample size may be needed to confirm this hypothesis.

This study demonstrated significant associations between reperfusion index and volume of infarct growth, even among those with good angiographic recanalisation. Higher reperfusion index resulted in smaller volume of infarct growth. In addition, reperfusion index was a significant predictor of infarct growth, but AOL score was not. The result was consistent with Eilaghi et al., 2013 in which they found that reperfusion was associated with reduced infarct growth.

Subjects who had high reperfusion index (RI: 0.71 to 1.0) had significant NIHSS reduction from baseline to follow-up compared to the group of patients with moderate reperfusion index (RI: 0.41 to 0.70). This observation was in line with Inoue et al., 2013, who found that degree of reperfusion measured using PWI was associated with favourable clinical response. Similarly, data on HERMES study showed that grades of better reperfusion measured using angiographic eTICI score were associated with better mRS outcome at 90 days (Liebeskind *et al.*, 2019). On contrary, our study revealed that reperfusion index was not significantly associated with early neurological improvement considered as a dichotomous outcome, or with 90-day good functional outcome. Nonetheless, there was a trend of higher reperfusion index with threshold RI of 0.41 and above, increased the odds of having early neurological recovery and 90-day good functional outcome.

This study provides support for tissue level reperfusion as therapeutic target, even among patients with good angiographic recanalisation based on AOL score of II or III. Replication of this study is warranted with bigger sample size to further explore the effects of underlying vascular risk factors in the model which would explain a failure to confirm the association between reperfusion index and good functional outcomes.

5.5 Conclusion

Reperfusion quality modifies outcome in patients with stroke due to vessel occlusion, even among those with good angiographic recanalisation. While complete failure to reperfusion appears to occur in only a small number of patients, reperfusion index was associated with infarct growth and neurological improvement. The degree of reperfusion could be measured using ASL reperfusion index. Reperfusion index could be a potential imaging biomarker in predicting radiological and clinical outcomes.

Chapter 6 Association of cerebral blood flow and white matter hyperintensities – An investigation using ASL.

6.1 Introduction

WMH or leukoaraiosis was first described by Hachinksi in 1987 based on Greek root, *leuko* means "white", *araios* means "rarefied, with its units far apart" and *-osis* means "the action or process of" (Hachinski, Potter and Merskey, 1987). WMH a spectrum of small vessel disease (SVD). It is commonly found in the elderly and is associated with high risk of stroke, cognitive impairment and dementia (Debette and Markus, 2010). Furthermore, the WMH progression has been associated with older age, smoking, hypertension, and baseline lesion load (van Dijk *et al.*, 2008)

MRI has been widely used in the imaging of WMH although other imaging modalities such as CTP (Li *et al.*, 2019), SPECT (Ishibashi *et al.*, 2018) and ultrasound Doppler have been performed (Turk, Zaletel and Pretnar-Oblak, 2016). In MRI, WMH appear hyperintense in T2-weighted, T2 *, FLAIR and proton density while hypointense in T1-weghted images. The radiological features of WMH are notably visible on MRI due to the disruption of the blood-brain barrier (BBB), which could lead to plasma leakage into white matter (Pantoni and Garcia, 1997). Radiological mapping of the WMH showed predominant location of the lesions in the periventricular area and deep white matter.

MRI scales for assessing the severity of WMH involvement are Fazekas score and Scheltens score (Fazekas *et al.*, 1987; Scheltens *et al.*, 1993). Scheltens score provides additional properties compared to Fazekas score in terms of a) number of lesion size, b) regional information; and c) separate scores for basal ganglia and infratentorial lesions.

It is still unclear whether reduced CBF would cause WMH progression or vice-versa. The association between the CBF and WMH burden remains debatable as described in previous systematic and meta-analysis studies (Shi and

Wardlaw, 2016; Stewart et al., 2021). These systematic and meta-analysis studies found that the CBF was lower in patients with high WMH burden when measured cross-sectionally (Bivard *et al.*, 2016; Li *et al.*, 2019) but no definite association between CBF and WMH progression when measured longitudinally (Nylander *et al.*, 2018).

CTP and DSC have been widely used to measure the CBF among patients with WMH. However, there is an increasing trend to investigate the CBF and WMH burden and progression using ASL (Stewart *et al.*, 2021). The largest perfusion analysis using ASL of periventricular small vessel (PSV) was conducted in mix-age cohort of 439 subjects (mean age of 50 years) and 61 cognitive normal elderly subjects (mean age of 73 years) (Dolui *et al.*, 2019). This ASL study found no significant difference (p=0.34) of PSV perfusion between the middle-aged cohort (mean PSV CBF of 12.99 ±5.52 ml/100g/min) while 12.29±4.99 ml/100/g/min in the elderly subjects. Therefore, the objective of this study was to:

1. Examine the association between the CBF measured using ASL with age, WMH volume, and WMH burden.

2. To identify the ASL predictors associated with WMH volume, cognitive function, and new infarct among patients with WMH.

6.2 Methods

6.2.1 Study cohort

Subjects included in this chapter were obtained from Xanthine oxidase inhibition for improvement of long-term outcomes following ischaemic stroke and transient ischaemic attack (XILO-FIST) study (Dawson *et al.*, 2018, 2023). XILO-FIST is a multicentre randomised controlled trial, which aim to assess the effect of allopurinol, a type of drug for the prophylaxis of gout, on the white matter hyperintensity progression after stroke. Subjects are aged greater than 50 years and have history of ischaemic stroke past four weeks.

6.2.2 Inclusion and exclusion criteria

The inclusion and exclusion criteria were adopted from prespecified from the XILO-FIST study. Additional exclusion criteria for this PhD work were added as listed in Table 6-1.

Table 6-1: List of inclusion and criteria

	Inclusion criteria	Exclusion criteria
• Prespecified from XILO-FIST study	• Ischaemic stroke/ischaemic lesion on brain imaging in relevant anatomical territory in patients with transient ischaemic attack • Age greater than 50 • Consent within one month of stroke	• Modified Rankin scale score of 5 • Diagnosis of dementia • Cognitive impairment deemed sufficient to compromise capacity or comply with the protocol • Dependant on daily help from others for basic activities prior to stroke • Significant co-morbidity or frailty likely to cause death within 24 months • Contra-indication to or indication for administration of allopurinol • Significant hepatic impairment • eGFR<30ml/min • Contraindication to MRI scanning • Women of childbearing potential • Prisoners • Active participation in another CTIMP or device trial or participation within the past month • eGFR<60 and Korean, Han Chinese or Thai descent
• Criteria for this PhD study	• Same as XILO-FIST study • ASL scan at week 4	• Incomplete clinical data/follow-up information • No MRI images on database • No ASL images • ASL images with poor image quality – motion artifact

eGRR: estimated glomerular filtration rate

CTIMP: Clinical trial of investigational product

6.2.3 **XILOFIST study schedule**

XILO-FIST study comprises a four-week run-in phase (week 0 to 4) and a 104-week treatment phase (Figure 6-1). The baseline assessment was conducted during the run-in phase which include the clinical evaluation and safety blood test. Follow-up assessments such as clinical evaluation, MRI brain scan and detailed cognitive function were conducted at week 104.

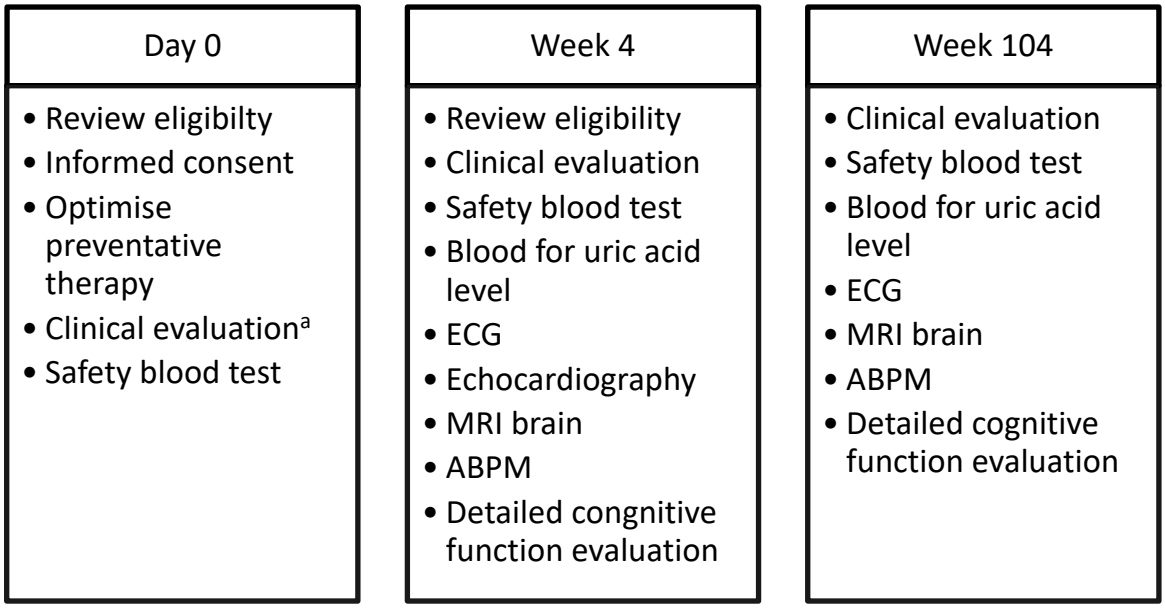

Figure 6-1: XILOFIST study schedule.
ABPM: Ambulatory blood pressure monitoring; ECG: electrocardiography; MRI: magnetic resonance imaging.
[a] Measures of stroke severity at week 4, modified Rankin scale.

6.2.4 **Imaging study**

MRI brain imaging study was conducted at baseline and follow-up. All the MRI images were acquired using 3.0T MRI PRISMA (Siemens, Erlangen, Germany). MRI brain protocols included were T1-weighted, T2-weighted, FLAIR, DWI, SWI, diffusion tensor imaging (DTI) and ASL (Table 6-2).

The PASL sequence used was a commercially available PASL PICORE Q2TIPS product sequence (Wong, Buxton and Frank, 1998b). The PASL sequence parameters were TR/TE = 2500/13, bolus duration = 700 ms, TI = 1800 ms, slice thickness = 4 mm, matrix = 64 x 64, FOV = 240 x 240 mm^2, flip angle = 90°, number of averages = 1 and 29 slices. A total of 100 ASL images (50 pairs of label and controls) and 1 calibration image (M0) were acquired for 6 minutes.

The MRI images were anonymised prior transferring to personal workstation. The MRI images were in Digital Imaging and Communications in Medicine (DICOM) format (.dcm) and converted into Neuroimaging Informatics Technology Initiative NIFTI) format (.nii) for further image processing.

Table 6-2: Sequence parameters for XILO-FIST MRI brain imaging

Sequence	T1 sagittal	T2	DWI	SWI	T2 FLAIR	DTI	ASL (PASL) PICORE Q2T
TR (ms)	2000	3000	4100	24	5000	3600	3500
TE (ms)	1.85	404	62	20	397	95	11
TI (ms)	900	-	-		1800		1800
Flip angle (°)	9	120	-				90
Number of averages	1	1	1	1	1	1	1
No of slices	176	176	27	96	160	30	20
Slice thickness (mm)	1.0	0.9	4.0	1.5	1.0	4.0	4.0
Scanning time	4.4	5.32	3.55	4.45	4.02	2.51	6.06
Bolus duration (ms)	-	-	-	-	-	-	700

6.2.5 Assessment of white matter hyperintensity burden and progression

A Fazekas' score was assigned to measure the WMH burden. The Fazekas score described the different types of hyperintensities signal abnormalities surround the ventricles and deep white matter (Fazekas, Chawluk and Alavi, 1987) (Table 6-3). Besides Fazekas score, Scheltens scale was also used to assess WMH lesion size and number based on anatomical regions (Scheltens *et al.*, 1993) (Table 6-4).

The Rotterdam progression score described the white matter lesions (on a 0 to 9 scale) in periventricular region, while the white matter lesions in the subcortical regions were described as the number and size of the lesions. Progression of the visual rating scales (Fazekas, Sheltens and Rotterdam scores) was defined as an increase of 1 point or more from baseline and follow-up scans (Prins *et al.*, 2004).

Table 6-3: Fazekas score

Periventricular hyperintensity	Description
0	Absence
1	Caps or pencil thinning
2	Smooth 'halo'
3	Irregular periventricular extending into deep white matter
Deep white matter hyperintensity	
0	Absence
1	Punctate foci
2	Beginning confluence of foci
3	Large confluent

Table 6-4: Scheltens score

Anatomical region		Score
Periventricular (PVH 0-6)	Caps – Occipital Caps – Frontal Bands – Lateral ventricles	0 = absent 1 = <5 mm 2 = >5 mm and <10 mm
White matter hyperintensities (WMH 0-24)	Frontal Parietal Occipital Temporal	0 = absent 1 = <3mm, n < 5 2 = <3mm, n > 6; 3 = 4 – 10mm, n < 5 4 = 4mm – 10mm, n >6; 5 = >11mm, n >1 6 = confluent
Basal Ganglia (BG 0-30)	Caudate nucleus Putamen Globus pallidus Thalamus Internal capsule	0 = absent 1 = <3mm, n < 5 2 = <3mm, n > 6; 3 = 4 – 10mm, n < 5 4 = 4mm – 10mm, n >6; 5 = >11mm, n >1 6 = confluent Infra-tentorial foci of hyperintensity
Infra-tentorial (ITF 0-24)	Cerebellum Mesencephalon Pons Medulla	0 = absent 1 = <3mm, n < 5 2 = <3mm, n > 6; 3 = 4 – 10mm, n < 5 4 = 4mm – 10mm, n >6; 5 = >11mm, n >1 6 = confluent

Adopted from (Scheltens *et al.*, 1993)

6.2.6 **White matter hyperintensity lesion segmentation**

The WMH were assessed by qualified and experienced radiologists following the STRIVE recommendation (Wardlaw *et al.*, 2013). The XILO-FIST study defined the WMH as hyperintense in T2-FLAIR and can appear as isointense or hypointense in T1-weghted sequences. (Dawson *et al.*, 2018). The WMH lesions were segmented by an experienced clinical imaging scientist as described in Dickie, Quinn and Dawson, 2019, (Figure 6-2). Automated extraction of WMH volumes were used by estimating the white matter area using atlas-based segmentation (Avants *et al.*, 2008). A probability map is registered to each subject using non-linear registration (Tustison *et al.*, 2014). T2-FLAIR was used to estimate the white matter area by transforming the voxels to standard z-score. The final WMH estimated were visually check by trained image analyst conforming to the STRIVE guideline.

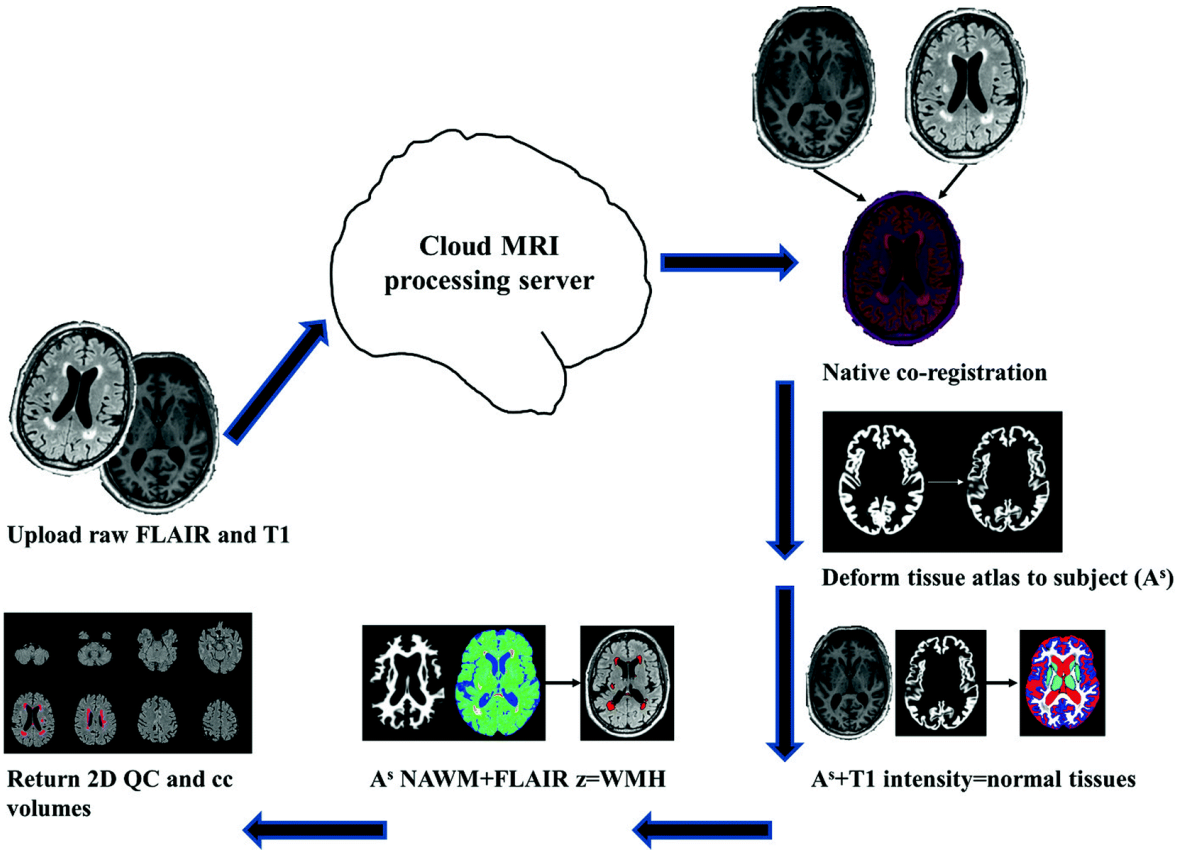

Figure 6-2: Main steps for the assessment of WMH volumes including the co-registration of T2-FLAIR and T1-weighted images, no-linear deformation registration of an atlas of tissues to subject, statistical thresholding, and visual assessment of output. Adapted from Dickie, Quinn and Dawson, 2019.

6.2.7 **ASL image processing and WMH CBF quantification**

The T1-images were processed as described in Chapter 3. Baseline ASL imaging data were carefully selected for further image post-processing and CBF quantification. ASL images with poor motion artifact were excluded from the analysis.

The WMH mask were transformed into ASL space using FLAIR matrix. The WMH mask was thresholded at value of 0.5 and binarised, to ensure definite hyperintensities were included. The CBF measurement was based on PASL sequence (Wong, Buxton and Frank, 1998b) with single compartment model using BASIL. The CBF in GM and WMH were measured in each subject by co-registering the GM and WMH mask on the CBF perfusion map on each subject.

6.3 Results

6.3.1 Study population

184 subjects were recruited for the XILOFIST study (Figure 6-3). Twenty-five subjects were excluded because of incomplete clinical data at baseline or follow-up (8 subjects), no MRI on database can be retrieved (15 subjects) and no ASL sequence on database (2 subjects)

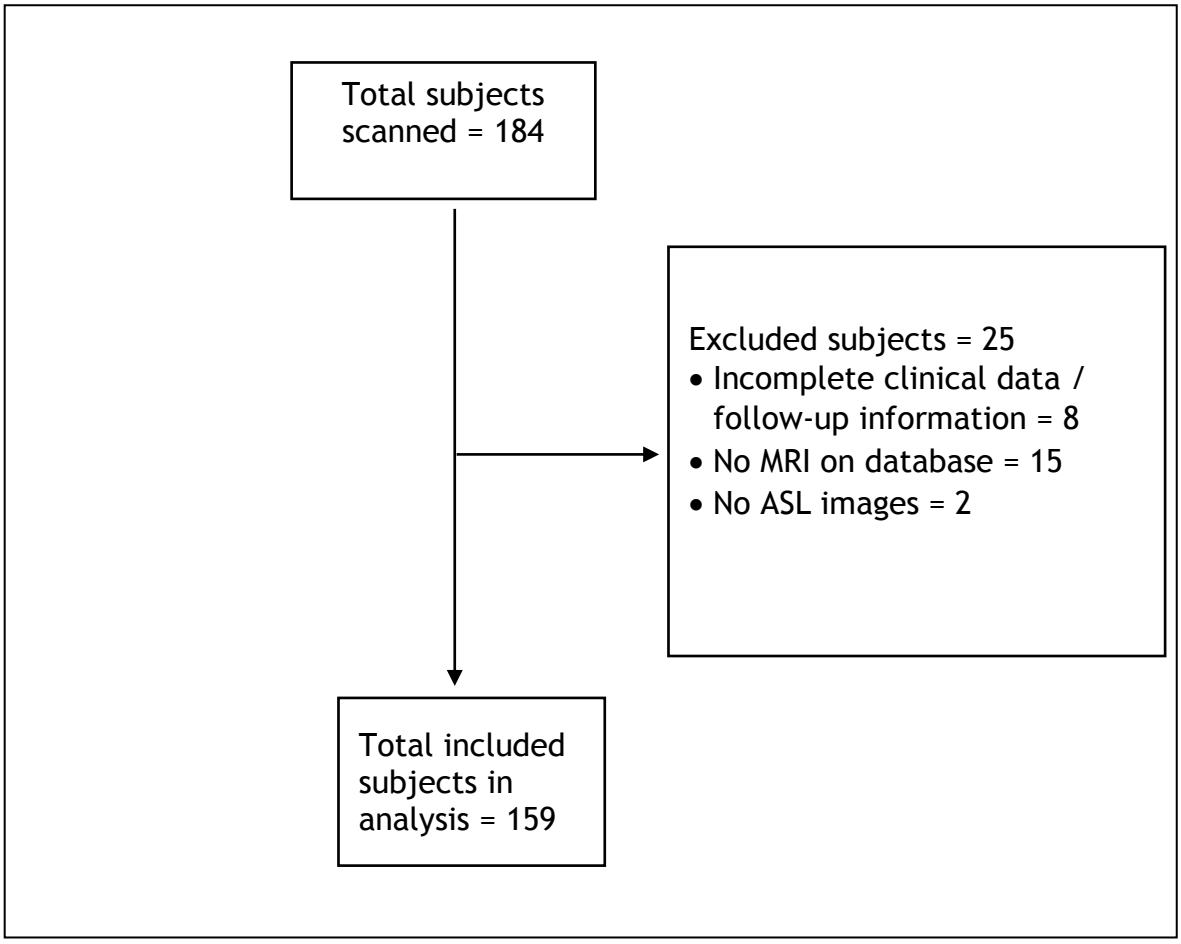

Figure 6-3: Study population

6.3.2 **Baseline and follow-up characteristics of study population**

The mean age of the study population was 65 ± 8.49 with median admission NIHSS of 1 (IQR: 0-1.75). Sixty-nine subjects (43.4%) had hypertension and 32 subjects (20.1%) had diabetes mellitus during the initial visit. 56 subjects (35.2%) had lacunar stroke. The median Fazekas score for both PVH and DWMH were 0 (IQR: 1- 2 and 1-1 respectively). The median for total Scheltens score was 11 (IQR: 7-11). Baseline and follow-up characteristics are listed in Table 6-5.

Table 6-5: Baseline and follow-up characteristics of XILOFIST cohort (n=159)

Baseline Characteristics	
Age, mean (SD), y	65 (8.49)
Gender, n (%)	
Male	108 (67.9)
Female	51 (32.1)
Systolic blood pressure, mean (SD),	139.6 (17.95)
Vascular risk factors, n (%)	
Diabetes mellitus	32 (20.1)
Hypertension	69 (43.4)
Smoker	
Current	39 (24.5)
Former	41 (25.8)
Never	79 (49.7)
Alcohol consumption	
Current	109 (68.6)
Former	10 (6.3)
Never	40 (25.2)
History of stroke	11 (6.9)
Myocardial infarction	13 (8.2)
Carotid artery disease	14 (8.8)
Peripheral arterial disease	5 (3.1)
NIHSS at admission, median (IQR)	1 (0-1.75)
mRS at admission, median (IQR)	1 (0-2)
Fazekas score, median (IQR)	
PVH	1 (1 – 2)
DWMH	1 (1 – 1)
Total	2 (2 – 3)
Scheltens score, median (IQR)	
PVH	3 (3 - 4)
WMH	6 (3 – 11)
BG	0 (0 - 1)

ITF	1 (0 – 2)
Total	11 (7 – 11)
Stroke class, n (%)	
PACS	49 (30.8)
TACS	7 (4.4)
POCS	47 (29.6)
LACS	56 (35.2)
Cardioembolic	25 (15.7)
Small vessel	44 (27.7)
Large artery	66 (41.5)
Unclassified	24 (15.1)
Rotterdam score, mean (SD)	1.47 (1.86)
Presence of new infarcts, n (%)	
Yes*	19 (11.9)
No	140 (88.1)

***Presence of new infarct subtypes were subcortical and infratentorial**

6.3.3 **MRI markers at baseline**

The volume and perfusion for both NAWM and WMH was measured at baseline (Table 6-6). The median volume of NAWM was significantly higher compared to the median volume of WMH at baseline ($p<0.001$). Similarly, the median perfusion of NAWM was significantly higher compared to the median perfusion of WMH at baseline ($p<0.001$).

Table 6-6: Baseline NAWM and WMH parameters

Baseline MRI markers	Median (IQR)	p-value
NAWM baseline volume, ml, median (IQR)	422.4 (383.8 – 451.7)	p<0.001
WMH baseline volume, ml, median (IQR)	11.9 (7.3 – 21.4)	
NAWM ASL baseline perfusion, ml/100g/min, median (IQR)	24.4 (20.5 – 28.8)	p<0.001
WMH ASL baseline perfusion, ml/100g/min, median (IQR)	11.8 (9.0 – 16.7)	

6.3.4 **Correlation of WMH volume and WMH perfusion with age**

The WMH baseline volume was positively correlated with increasing age (r = 0.372; p<0.001). In contrast, the WMH baseline CBF was negatively correlated with increasing age (r = -0.574; p<0.001).

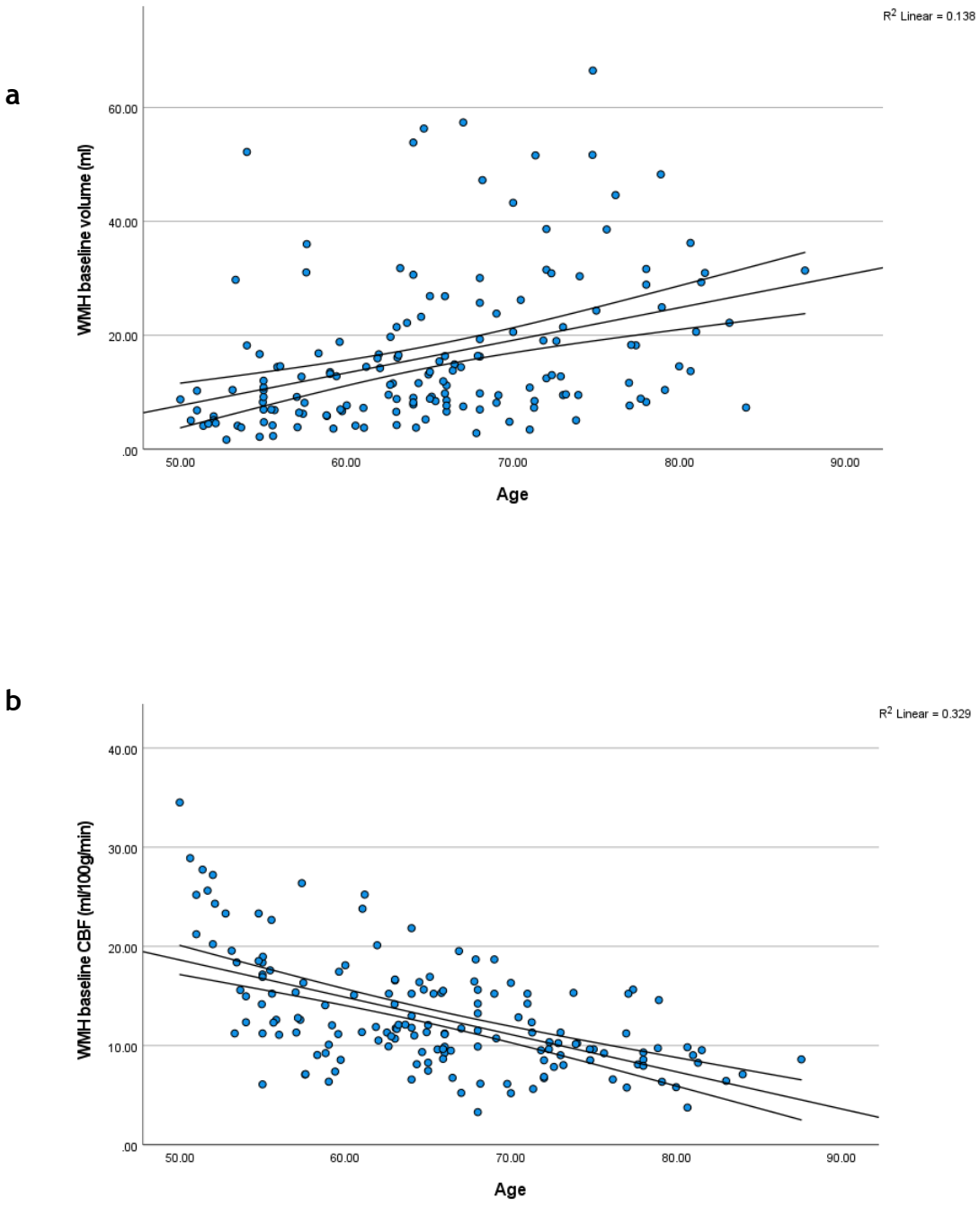

Figure 6-4: Correlation between baseline a) WMH volume and age; and b) WMH perfusion with age

6.3.5 **Correlation between WMH CBF and WMH volume**

At baseline, the was a significant negative correlation between WMH CBF and WMH volume ($r = -0.431$; $p<0.001$)

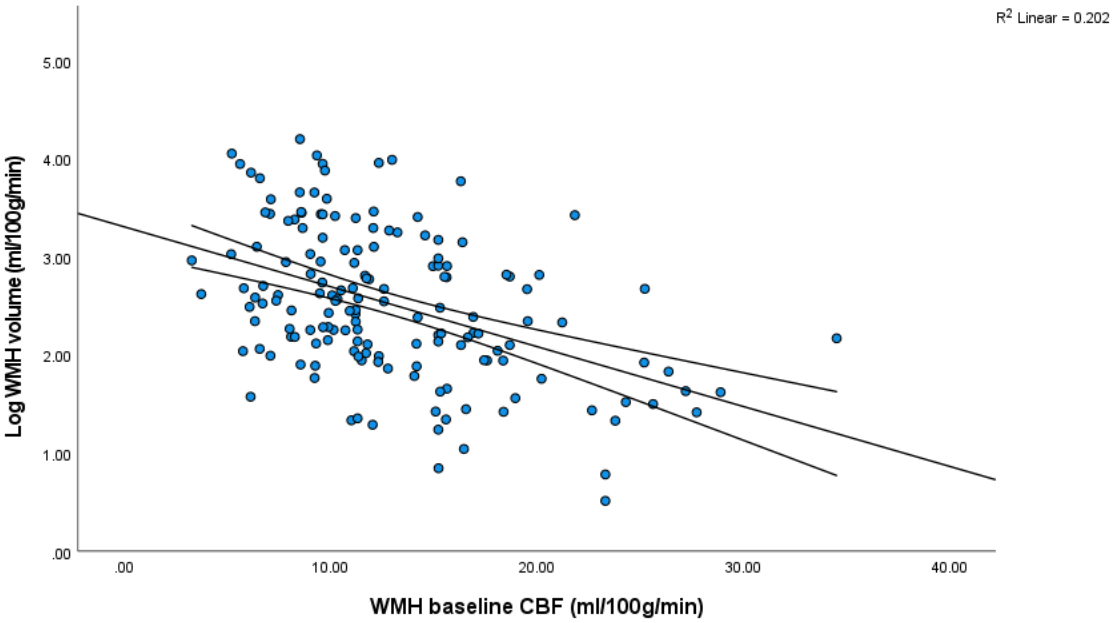

Figure 6-5: Scatterplot of relation between WMH volume and WMH CBF. Log WMH is logarithmically transformed

6.3.6 **Association WMH CBF with WMH burden**

A lower WMH and NAWM perfusion was significantly associated with increased WMH burden as scored using Fazekas score (Figure 6-6). The median WMH perfusion for Fazekas score less than 1 was 18.69ml/100g/min (IQR: 11.44 – 27.47 ml/100g/min) while the median WMH perfusion for Fazekas score more than one was 11.32 ml/100g/min (IQR: 9.03 – 15.41 ml/100g/min) (p = 0.008).

In addition, the median NAWM perfusion for Fazekas score less than 1 was 25.6/100g/min (IQR: 23.72 – 37.46 ml/100g/min) while the median NAWM perfusion for Fazekas score more than one was 23.10 ml/100g/min (IQR: 18.47 – 25.33 ml/100g/min) (p = 0.017).

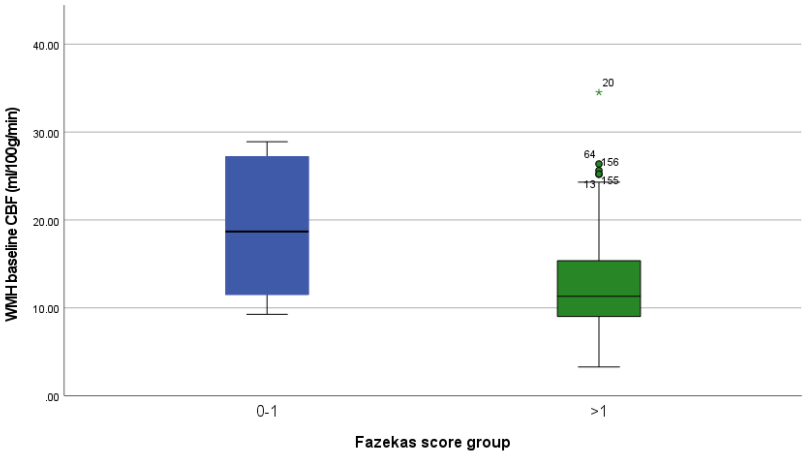

a)

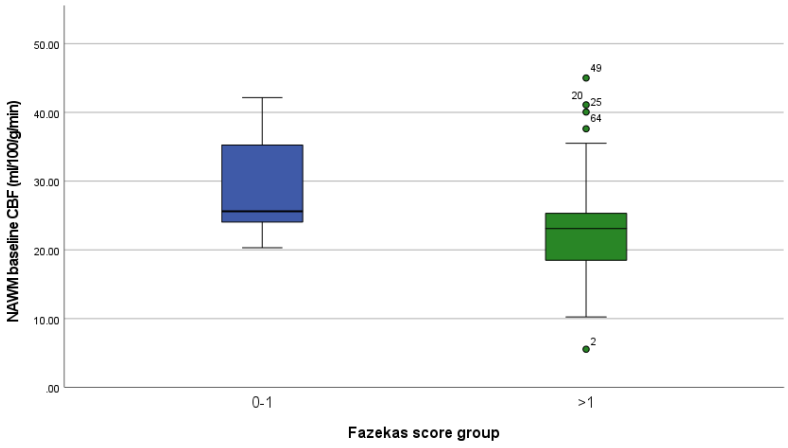

b)

Figure 6-6: Association between a) WMH and b) NAWM perfusion and WMH burden (Fazekas score). WMH and NAWM perfusion was significantly lower in group with higher WMH burden.

a

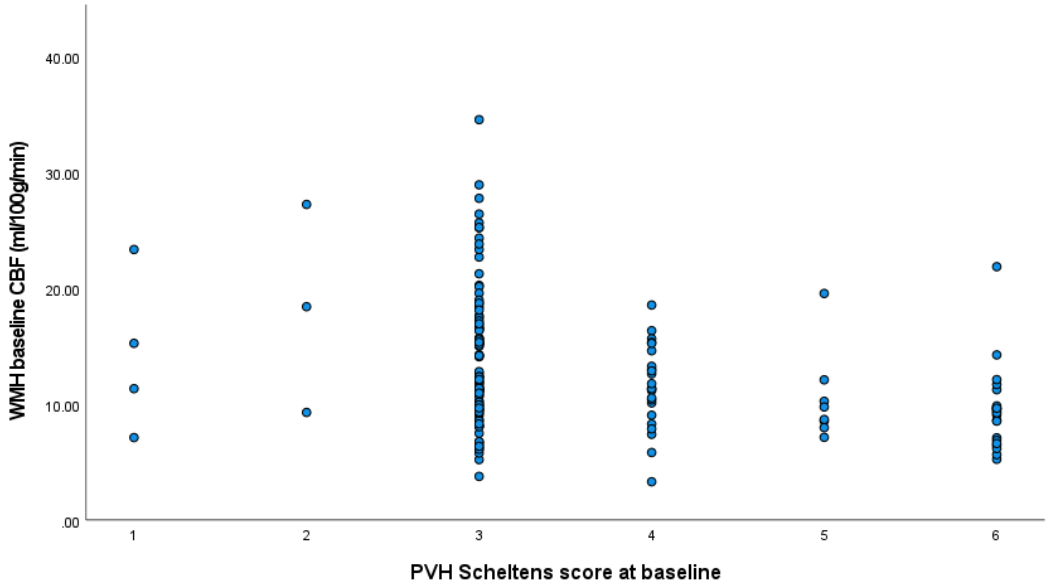
WMH baseline CBF (ml/100g/min)
40.00
30.00
20.00
10.00
.00
1
2
3
4
5
6
PVH Scheltens score at baseline

b

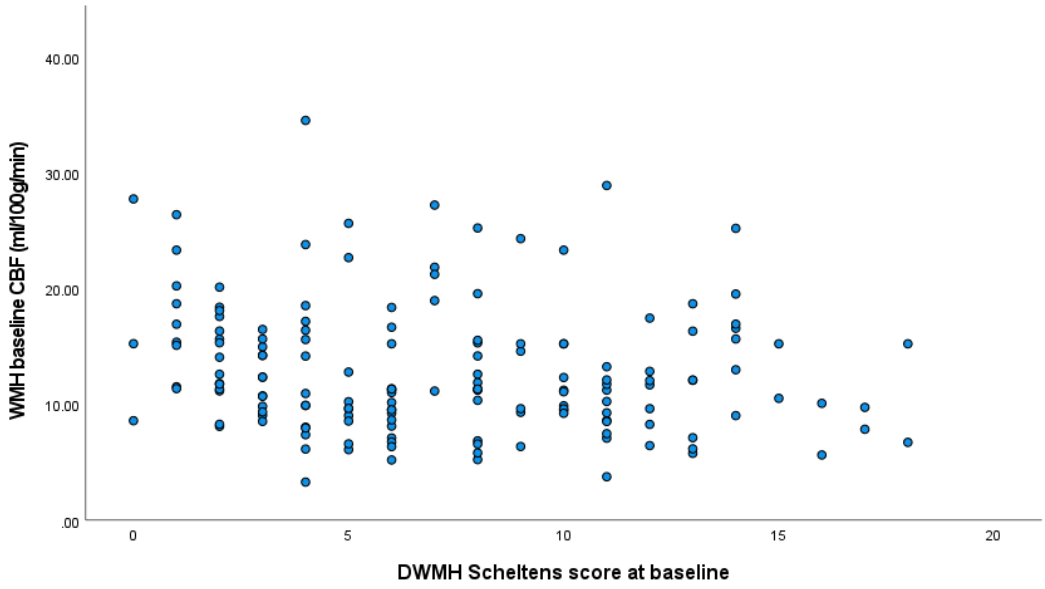
WMH baseline CBF (ml/100g/min)
40.00
30.00
20.00
10.00
.00
0
5
10
15
20
DWMH Scheltens score at baseline

c

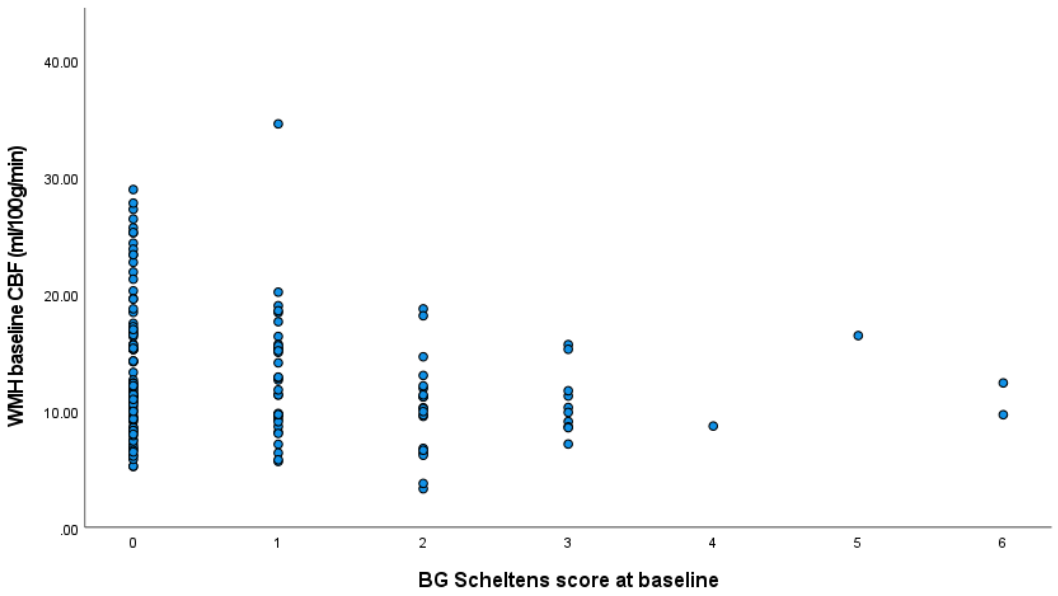

d

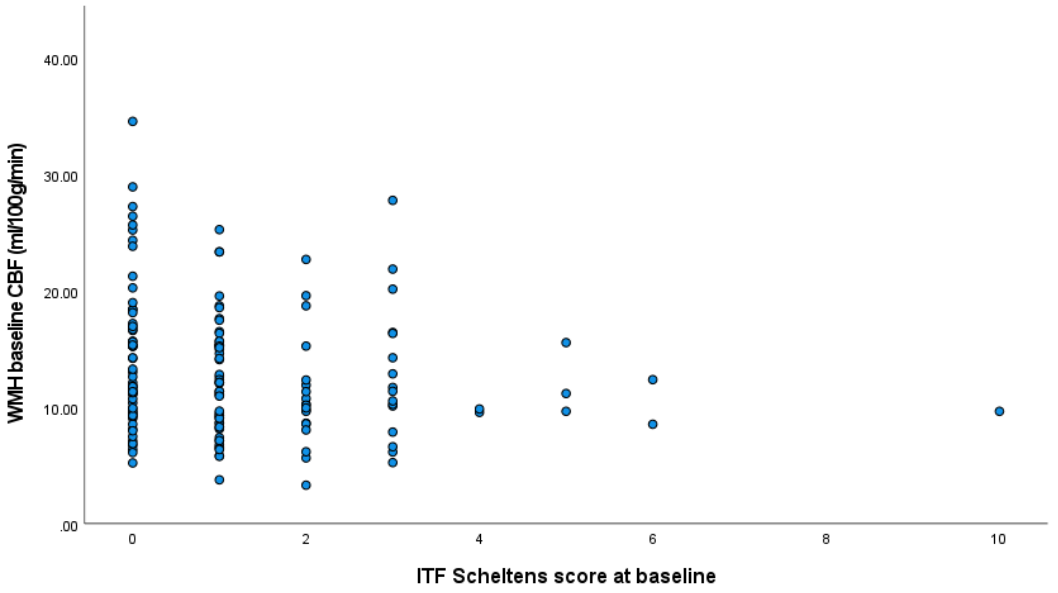

Figure 6-7: Relationship between WMH baseline CBF and components of Scheltens score at baseline.

PVH = periventricular hyperintensities; DWMH: deep white matter hyperintensities; BG = basal ganglia; ITF=infra-tentorial.

There was a significant inverse relationship between the WMH CBF and Scheltens score at different anatomical regions (Figure 6-7). The WMH CBF was inversely correlated with PVH Scheltens score (Spearman's rho=-0.333; p<0.001); DWMH Scheltens score (Spearman's rho =-0.185; p=0.020); BG (Spearman's rho =-0.186; p=0.019) and ITF (Spearman's rho =-0.162; p=0.042).

6.3.7 Predictors of follow-up WMH volume

Age (adjusted OR = 1.367; p <0.001), WMH baseline volume (adjusted OR = 0.815; p=0.020), and systolic BP (adjusted OR = 1.175; p=0.026), were significant independent predictors of follow-up WMH volume when adjusted with diabetes mellitus (Table 6-7).

Table 6-7: Multivariate linear regression analysis predicting follow-up WMH volume

Predictors	Standardized Coefficients β	Adjusted OR (95% CI)	p-value
Age	0.313	1.367 (0.229 – 0.815)	*<0.001
WMH baseline CBF	-0.204	0.815 (-0.957 - -0.081)	*0.020
Diabetes	0.075	0.842 (-0.172 – 0.054)	0.302
Systolic BP	-0.161	1.175 (0.691 – 10.669)	*0.026

***Denotes significant value at p<0.05**

6.3.8 **Predictors of new infarcts and WMH progression**

In multiple logistic regression analysis, younger age (OR 0.978, p = 0.040) and low baseline WMH CBF (OR = 0.900, p = 0.031) were an independent predictor of having new brain infarct (Table 6-8). New brain infarct was defined as areas of new cortical infarction or new lacunar infarction (Dawson et al., 2023).

Table 6-8: Multiple logistic regression analysis predicting new infarct

Predictors	β	OR (95% CI)	p-value
Age	-0.023	0.978 (0.957 – 0.999)	*0.040
WMH baseline CBF	-0.105	0.900 (0.818 – 0.991)	*0.031
Diabetes	0.599	1.820 (0.607 – 5.455)	0.285
Smoking	0.640	1.896 (0.682 – 5.267)	0.220
Hypertension	0.763	2.144 (0.739 – 6.225)	0.161
BP lowering medication	-0.200	0.818 (0.287 – 2.337)	0.708

***Indicates significant p-value <0.05**
**** Each variable is run as entered**

WMH baseline volume was a significant independent predictor with increased WMH progression (Rotterdam score) (adjusted OR = 1.017; p <0.001) when adjusted with age, WMH baseline CBF, systolic BP and blood pressure lowering therapy (Table 6-9).

Table 6-9: Multivariate linear regression analysis predicting WMH progression

Predictors	Adjusted β	Adjusted OR (95% CI)	p-value
Age	0.138	1.147 (-0.014 – 0.077)	0.172
WMH baseline CBF	0.017	1.017 (-0.062 - 0.074)	0.866
WMH baseline volume	0.409	1.505 (0.035 - 0.086)	*<0.001
Systolic BP	-0.021	0.979 (-0.019 – 0.015)	0.797
BP lowering medication	-0.014	00986 (-0.681 – 0.574)	0.866

***Indicates significant p-value <0.05**

6.3.9 **Predictors of cognitive impairment**

There was no significant independent predictor of cognitive impairment (measured by Trail test). The variables tested were age, WMH baseline volume and CBF, and NAWM baseline volume and CBF.

Table 6-10: Multivariate linear regression analysis predicting cognitive impairment

Predictors	Adjusted β	Adjusted OR (95% CI)	p-value
Age	0.171	1.186 (-0.071 – 0.755)	0.104
WMH baseline volume	0.089	1.093 (-0.108 - 0.339)	0.309
WMH baseline CBF	-0.128	0.879 (-1.088 – 0.306)	0.270
NAWM baseline volume	-0.041	0.959 (-0.065 – 0.039)	0.622
NAWM baseline CBF	0.148	1.159 (-0.191 – 0.977)	0.186

***Indicates significant p-value <0.05**

6.4 Discussion

White matter hyperintensities are common imaging findings in MRI studies among older subjects with associated risks of recurrent stroke and cognitive decline. Previous study on the effect of blood pressure lowering treatment on WMH progression reported 90% of WMH occurrence were among subjects with ischaemic strokes (Weber *et al.*, 2012). In addition, several imaging studies such as DSC and DTI have been conducted to investigate the relationship between WMH burden and progression with associated risk factors such as age, low brain perfusion and hypertension (Maniega *et al.*, 2015; Nylander *et al.*, 2018). This chapter investigated the relationship between the WMH CBF and age, WMH burden and WMH volume using ASL among subjects with a history of ischaemic stroke or TIA. Predictors for WMH progression, occurrence of new infarct and cognitive impairment were also explored.

This study confirms the relationship between baseline WMH CBF and age. The correlation analysis also showed a significant positive relationship between baseline WMH volume and age. The result of this study supported previous study showing significant association between age and WMH volume and perfusion (Habes *et al.*, 2016). The correlation analysis also demonstrated significant negative correlation between WMH CBF and WMH volume. This is consistent with results from several earlier ASL studies reporting a negative relationship between CBF and WMH volume (Brickman *et al.*, 2009; Bahrani *et al.*, 2017). Similar negative relationship between parenchymal CBF and deep WMH volume was reported in a 3.9-year longitudinal study conducted by van der Veen et al., 2015.

Low WMH CBF has been associated with progression of WMH. However, in this study, the effect of low WMH CBF has been reduced when adjusted to WMH baseline volume. In addition, the multivariate logistic regression analysis showed the high WMH volume was a significant independent predictor for WMH progression at week 104. Similar finding was found by a longitudinal study on relationship between cerebral small-vessel disease and cerebral blood flow in 575 subjects with arterial disease (van der Veen *et al.*, 2015).

In relation to this, age, WMH CBF and systolic BP was a significant independent predictor in predicting WMH volume at week 104 after adjusting for diabetes. In addition to this, WMH baseline volume significantly associated with WMH progression. This result support recent meta-analysis findings on risk factors WMH growth on 13 210 individuals which found an association between WMH baseline volume with WMH progression rate (Brown, Low and Markus, 2021). Interestingly, this study did not find any effect of blood pressure lowering medication with the WMH progression unlike reported in a meta-analysis of effects of intensive blood pressure control on the WMH (Lai *et al.*, 2020).

Nineteen (12%) new infarcts (cortical, subcortical and infratentorial) imaged by DWI in this study suggested recurrence of cerebral ischaemia among the subjects in this study. In multivariate binary logistic regression analysis, age and WMH baseline CBF were independent predictors of new infarct after adjusting to other vascular risk factors such as diabetes, hypertension, and smoking. There were limited longitudinal data supporting the relationship of WMH perfusion with recurrence stroke. Nevertheless, in one large longitudinal study, the Framingham Offspring Study, reported significant increased risk of stroke (hazard ratio = 2.28; p =0.046) among participants with high WMH volume after adjusting to age, gender, systolic blood pressure and other vascular risk factors such as smoking, and diabetes (Debette *et al.*, 2010). Similarly, Ryu et al., 2019, reported significant increased risk between WMH volume and stroke recurrence (hazard ratio = 1.03; p<0.001)

It has been described that less CBF is needed to for glucose metabolism determined by PET study related with severity of WMH in healthy subjects (DeCarli *et al.*, 1995). To support this result, a significant association between WMH burden (measured by Fazekas score) and cognitive function assessed by trail making test has been reported by Han et al., 2019. However, in this study, there were associations although not significant between older age, lower WMH CBF and higher WMH volume with trail-making test. We also did not find any significant independent predictor for cognitive impairment when tested with variables such as age, WMH CBF and WMH volume in multivariate linear regression analysis.

Three potential limitations of this study should be pointed out. First, this study used a single PLD PASL sequence instead of PCASL sequence. This is a limitation of this study as the perfusion of WMH may be underestimated because of ASL signal intensity loss along with the T1-decay (van Osch *et al.*, 2009). Using a multi-PLD PCASL sequence in future work may provide a better estimation of WMH perfusion. Next, ASL used in this study only measures the WMH and NAWM CBF. This limits the assessment of WMH progression and new infarcts as ischemic small vessel disease typically first manifests in the periventricular and subcortical white matter (Dolui *et al.*, 2019). Future longitudinal studies over several years using multi-PLD PCASL is recommended in quantifying the CBF at the periventricular regions to monitor the WMH progression and new infarcts. Finally, this study is unable to confirm the causal relationship between WMH CBF and WMH progression. Mediation analysis should be conducted to establish the causal relationship between these variables.

6.5 Conclusion

In summary, WMH perfusion was significantly associated with age and WMH volume. ASL could predict the WMH volume and new infarct at follow-up study. Therefore, ASL could serve as a potential surrogate marker for small vessel diseases represented as white matter hyperintensities.

Chapter 7 Conclusions

7.1 Summary of results

This thesis aimed to explore the clinical application of ASL as perfusion imaging among acute (WHISPER study) and chronic (XILO-FIST) ischaemic stroke cohorts. This chapter summarises the contribution of this work, and some possible future directions are suggested.

7.1.1 Agreement between different ASL labelling

The agreement of common ASL sequences, namely PCASL and PASL was investigated in Chapter 3. The grey matter and white matter perfusion were measured among acute ischaemic stroke patients. The correlation between grey and white matter was calculated, and the agreement between two ASL sequences was analysed using Bland-Altman analysis. The study was conducted on 35 subjects who satisfied the inclusion and exclusion criteria. The result of this study showed that there were significant correlations between PCASL and PASL in measuring the perfusion of grey matter ($r=0.95$, $p<0.001$) and white matter ($r=0.76$, $p<0.001$). However, the Bland-Altman analysis demonstrated a large agreement between the ASL sequences suggesting systematic errors in measuring CBF. The systematic errors are due to differences in ASL labelling efficiency, non-uniformity of perfusion signal at the top and bottom of imaging slice and perfusion-modifiers like age and patient's motion.

7.1.2 Relationship between ASL reperfusion index and follow-up clinical severity, imaging end-points and good functional outcome in acute ischaemic stroke patients

The clinical application of the reperfusion index measured by ASL was described in Chapter 4. Reperfusion index (RI) measured using ASL was correlated with radiological outcomes (infarct growth and penumbral salvage) and clinical outcome among 63 acute stroke subjects recruited from the WHISPER study. Reperfusion index of 0.41 and above was significantly associated with early neurological recovery and good functional outcome (mRS 0-2). However, RI was not significant as an independent predictor for either infarct growth and penumbral salvage after adjusting for age, baseline NIHSS, HIR score,

mismatch volume, thrombolysis treatment and AOL score, but there was a trend consistent with larger infarct growth and lower penumbral salvage with lower reperfusion index.

The main clinical application of this study is providing the quantitative indicator or threshold to define reperfusion quality assessment. RI ≤ 0 – 0.4 indicated mild reperfusion, RI 0.41 to 0.70 indicated moderate reperfusion, and RI 0.71 to 1.0 indicated high reperfusion. In addition, the results in this chapter suggested that ASL reperfusion index could serve as a potential imaging marker of tissue level reperfusion in ischemic stroke.

7.1.3 Reperfusion assessment among recanalised ischaemic stroke patients – an investigation using ASL reperfusion index

Chapter 5 describes the subsequent analysis from subgroup of patients from Chapter 4. The work in Chapter 5 focused on whether reperfusion would modify imaging and clinical outcomes among patients with good angiographic recanalisation assessed by AOL score. A total of 49 subjects who had AOL score of II or III. Among these subjects, only one patient did not reperfuse (reperfusion index -0.19) despite complete vessel recanalisation (AOL III) and showed some clinical neurological improvement after 24 hours of stroke onset. The clinical neurological improvement in this patient may be due to delayed reperfusion which is associated with improved clinical outcomes in patients with complete vessel recanalisation.

An interesting observation on the quality of collateral flow (measured using HIR) and RI was noted. The HIR for the high RI group was higher (0.42) compared to the moderate RI (0.25), although the difference was not significant. However, the RI was a significant independent predictor of infarct growth. Patients with a RI of 0.41 and below were predicted to have higher chances of larger follow-up infarct volume. Higher reperfusion index was predicted to reduce the infarct growth after adjusting for age, NIHSS, collateral status (HIR), mismatch volume, thrombolysis treatment and AOL score.

An important clinical application of these findings is to provide clinical evidence on predicting infarct growth volume in future trials based on quantitative reperfusion threshold among patients with AOL score of II or III.

7.1.4 Association of cerebral blood flow and white matter hyperintensities – an investigation using ASL

The application of ASL in chronic ischaemic stroke patients was explored in Chapter 6. In this chapter, ASL was used to measure the perfusion of WMH in 159 subjects who had suffered an ischaemic stroke within the past four weeks. Statistical analyses have been conducted to investigate the relationship between the WMH CBF and age, WMH burden and WMH volume. The correlation analysis between baseline WMH CBF and age demonstrated a significant inverse relationship between these variables. The correlation analysis also demonstrated a significant negative correlation between WMH CBF and WMH volume. Low WMH CBF has been associated with the progression of WMH. However, in this study, the effect of low WMH CBF has been reduced when adjusted to WMH volume.

The multivariate linear regression analysis showed that high WMH volume was a significant independent predictor for WMH progression at week 104. In multivariate binary logistic regression analysis, age and WMH baseline CBF were independent of predictors of new infarct after adjusting to other vascular risk factors such as diabetes, hypertension, and smoking. There were associations, although not significant, between older age, lower WMH CBF and higher WMH volume with the trail-making test.

7.2 Place in current literature

In early 2023, the International Society for Magnetic Resonance in Medicine (ISMRM) Perfusion Study Group provided updated guidelines on the consensus of using ASL in clinical setting for specific pathologies (Lindner et al., 2023). According to the guidelines, the multi-PLD PCASL with a long labelling duration is recommended for CBF assessment to mitigate transit delay effects in acute ischaemic stroke patients. The recommendation by ISMRM 2023 has been strengthened by the findings in Chapter 3, where multi-PLD PCASL showed higher perfusion CBF in grey and white matter.

Recent work by Hong et al., indicated the RI $\geq$ 0.9 measured using CTP predicted good functional outcome (mRS 0-2) in 73 ischaemic stroke patients (Hong *et al.*, 2023). The study findings were in contrast with the results in Chapter 4, in which a lower RI threshold (RI 0.41) predicted good functional outcome (mRS 0-2) because of the patients in this study had mild ischaemic stroke (lower infarct volume of 0 ml) compared to their study (infarct volume of 10 ml).

The application of ASL for the imaging of small vessel diseases WMH is underexplored. Only 16 studies using ASL as perfusion imaging were conducted in the year between 1990 until 2021 to investigate the associations between WMH burden, CBF and transit time in small vessel disease (Shi and Wardlaw, 2016a; Stewart *et al.*, 2021). Thus, the work in Chapter 6 provides additional data on the clinical application of ASL in understanding the relationship between cerebral blood flow and associated risk factors among ischaemic stroke patients with WMH.

7.3 Future recommendations

Magnetic resonance (MR) perfusion-weighted imaging (PWI) and computed tomography perfusion imaging (CTP), performed following a bolus intravenous injection of contrast agent, are now widely being used in perfusion imaging. ASL has the advantage of a non-contrast imaging method, which will benefit patients who are contraindicated to contrast imaging studies due to renal dysfunction or contrast allergy.

Since infarct growth after stroke onset is a dynamic progress, repeated perfusion imaging scanning at different time points (during baseline imaging, within 24 hours of stroke onset, and 48 hours of stroke onset) is recommended to evaluate the reperfusion status and change in clinical severity over time. Furthermore, ASL does not require any contrast media administration and no radiation makes it suitable for perfusion imaging at multiple time points. In addition, ASL reperfusion index threshold should be established according to the severity of ischemic stroke (mild to severe) to improve the understanding of reperfusion pathophysiology across different ischemic stroke patients.

Given its advantage, ASL should be the preferred imaging method to further investigate the dynamic of reperfusion mechanism in larger clinical population at multiple time points since volumes of rescuable tissue persist even at 72 hours after presentation the microcirculatory (reperfusion) is associated with periods of ischemia. This may not be ideally performed using CTP as multiple usage of CTP across different time points could contribute to high radiation dose to patients.

In addition, the application of ASL in clinical setting must be tailored to the patient's conditions. For example, longer PLD is required to quantify the cerebral blood flow in white matter hyperintensities to ensure the labelled blood can be imaged at the imaging plane. In addition, regional WMH quantification using ASL should be considered for cognitive assessments.

7.4 Closing remarks

ASL may provide an important imaging biomarker in ischaemic stroke. However, the post-processing of ASL images from the MRI scanner is a complex process which requires additional time. This may pose some challenges for the application of ASL in clinical routines. However, this PhD work is able to provide detailed steps on how to process the ASL raw images into quantitative perfusion values.

The work detailed in this thesis studies the clinical applications of ASL among acute ischaemic stroke patients and chronic ischaemic stroke patients. The reliability between commonly used ASL sequences has been demonstrated. Relationship between the ASL reperfusion index with clinical and imaging outcomes indicates the ASL reperfusion index as potential imaging marker of tissue level reperfusion in ischemic stroke. The ability of ASL as perfusion imaging among chronic stroke patients with white matter hyperintensities allows further understanding of the association between WMH perfusion and its related risk factors.

References

Aho, K. *et al.* (1980) 'Cerebrovascular disease in the community: results of a WHO collaborative study', *Bulletin of the World Health Organization*, 58(1), pp. 113–130.

Albers, G.W. *et al.* (2006) 'Magnetic resonance imaging profiles predict clinical response to early reperfusion: The diffusion and perfusion imaging evaluation for understanding stroke evolution (DEFUSE) study', *Annals of Neurology*, 60(5), pp. 508–517. Available at: https://doi.org/10.1002/ana.20976.

Albers, G.W. *et al.* (2018) 'Thrombectomy for Stroke at 6 to 16 Hours with Selection by Perfusion Imaging', *New England Journal of Medicine*, 378(8), pp. 708–718. Available at: https://doi.org/10.1056/NEJMoa1713973.

Alsop, D.C. *et al.* (2015) 'Recommended implementation of arterial spin-labeled perfusion MRI for clinical applications: A consensus of the ISMRM perfusion study group and the European consortium for ASL in dementia.', *Magnetic resonance in medicine*, 73(1), pp. 102–16. Available at: https://doi.org/10.1002/mrm.25197.

Altman, D.G. and Bland, J.M. (1983) 'Measurement in Medicine: The Analysis of Method Comparison Studies', *Source: Journal of the Royal Statistical Society. Series D (The Statistician)*, 32(3), pp. 307–317.

Ames, A. *et al.* (1967) 'Cerebral Ischemia II. The No-Reflow Phenomenon', *Am J Pathol* [Preprint], (52).

el Amki, M. *et al.* (2020) 'Neutrophils Obstructing Brain Capillaries Are a Major Cause of No-Reflow in Ischemic Stroke', *Cell Reports*, 33(2). Available at: https://doi.org/10.1016/j.celrep.2020.108260.

el Amki, M. and Wegener, S. (2017) 'Improving Cerebral Blood Flow after Arterial Recanalization: A Novel Therapeutic Strategy in Stroke', *International Journal of Molecular Sciences*, 18(12). Available at: https://doi.org/10.3390/IJMS18122669.

Astrup, J. *et al.* (1977) 'Cortical evoked potential and extracellular K+ and H+ at critical levels of brain ischemia.', *Stroke*, 8(1), pp. 51–7. Available at: https://doi.org/10.1161/01.str.8.1.51.

Astrup, J., Siesjö, B.K. and Symon, L. (1981) 'Thresholds in cerebral ischemia - the ischemic penumbra.', *Stroke*, 12(6), pp. 723–5.

Avants, B.B. *et al.* (2008) 'Symmetric diffeomorphic image registration with cross-correlation: Evaluating automated labeling of elderly and neurodegenerative brain', *Medical Image Analysis*, 12(1), pp. 26–41. Available at: https://doi.org/10.1016/j.media.2007.06.004.

Bahrani, A.A. *et al.* (2017) 'White Matter Hyperintensity Associations with Cerebral Blood Flow in Elder Subjects Stratified by Cerebrovascular Risk', *Journal of stroke and cerebrovascular diseases : the official journal of National*

Stroke Association, 26(4), p. 779. Available at: https://doi.org/10.1016/J.JSTROKECEREBROVASDIS.2016.10.017.

Baird, A.E. *et al.* (1996) 'Changes in cerebral tissue perfusion during the first 48 hours of ischaemic stroke: Relation to clinical outcome', *Journal of Neurology Neurosurgery and Psychiatry*, 61(1), pp. 26–29. Available at: https://doi.org/10.1136/jnnp.61.1.26.

Bandera, E. *et al.* (2006) 'Cerebral Blood Flow Threshold of Ischemic Penumbra and Infarct Core in Acute Ischemic Stroke', *Stroke*, 37(5), pp. 1334–1339. Available at: https://doi.org/10.1161/01.STR.0000217418.29609.22.

Banks, J.L. and Marotta, C.A. (2007) 'Outcomes Validity and Reliability of the Modified Rankin Scale: Implications for Stroke Clinical Trials', *Stroke*, 38(3), pp. 1091–1096. Available at: https://doi.org/10.1161/01.STR.0000258355.23810.C6.

Barber, P.A. *et al.* (1998) 'Spontaneous reperfusion after ischemic stroke is associated with improved outcome', *Stroke*, 29, pp. 2522–2528.

Barber, P.A. *et al.* (2000) 'Validity and reliability of a quantitative computed tomography score in predicting outcome of hyperacute stroke before thrombolytic therapy', *The Lancet*, 355(9216), pp. 1670–1674. Available at: https://doi.org/10.1016/S0140-6736(00)02237-6.

Basser, P.J. and Pierpaoli, C. (1996) 'Microstructural and physiological features of tissues elucidated by quantitative-diffusion-tensor MRI', *Journal of Magnetic Resonance - Series B*, 111(3), pp. 209–219. Available at: https://doi.org/10.1006/jmrb.1996.0086.

Belani, P. *et al.* (2020) 'Addition of arterial spin-labelled MR perfusion to conventional brain MRI: Clinical experience in a retrospective cohort study', *BMJ Open*, 10(6), p. 36785. Available at: https://doi.org/10.1136/bmjopen-2020-036785.

Bernbaum, M. *et al.* (2015) 'Reduced blood flow in normal white matter predicts development of leukoaraiosis', *Journal of Cerebral Blood Flow and Metabolism*, 35(10), pp. 1610–1615. Available at: https://doi.org/10.1038/jcbfm.2015.92.

Bivard, A. *et al.* (2013) 'Arterial Spin Labeling Identifies Tissue Salvage and Good Clinical Recovery After Acute Ischemic Stroke', *Journal of Neuroimaging*, 23(3), pp. 391–396. Available at: https://doi.org/10.1111/j.1552-6569.2012.00728.x.

Bivard, A. *et al.* (2014) 'Arterial spin labeling versus bolus-tracking perfusion in hyperacute stroke', *Stroke*, 45, pp. 127–133. Available at: https://doi.org/10.1161/STROKEAHA.113.003218.

Bivard, A. *et al.* (2016) 'Global White Matter Hypoperfusion on CT Predicts Larger Infarcts and Hemorrhagic Transformation after Acute Ischemia', *CNS Neuroscience & Therapeutics*, 22(3), p. 238. Available at: https://doi.org/10.1111/CNS.12491.

Bland, J.M. and Altman, D.G. (1999) 'Measuring agreement in method comparison studies', *Statistical Methods in Medical Research*, 8(2), pp. 135–160. Available at: https://doi.org/10.1191/096228099673819272.

Bokkers, R.P.H. *et al.* (2012) 'Whole-brain arterial spin labeling perfusion MRI in patients with acute stroke', *Stroke*, 43(5), pp. 1290–1294. Available at: https://doi.org/10.1161/STROKEAHA.110.589234.

Branston, N.M. *et al.* (1974) 'Relationship between the cortical evoked potential and local cortical blood flow following acute middle cerebral artery occlusion in the baboon', *Experimental Neurology*, 45(2), pp. 195–208. Available at: https://doi.org/10.1016/0014-4886(74)90112-5.

Brickman, A.M. *et al.* (2009) 'Reduction in cerebral blood flow in areas appearing as white matter hyperintensities on magnetic resonance imaging', *Psychiatry research*, 172(2), p. 117. Available at: https://doi.org/10.1016/J.PSCYCHRESNS.2008.11.006.

Brown, R., Low, A. and Markus, H.S. (2021) 'Rate of, and risk factors for, white matter hyperintensity growth: a systematic review and meta-analysis with implications for clinical trial design', *Journal of Neurology, Neurosurgery & Psychiatry*, 92(12), pp. 1271–1277. Available at: https://doi.org/10.1136/JNNP-2021-326569.

Campbell, B.C.V. and Khatri, P. (2020) 'Stroke', *The Lancet*, 396(10244), pp. 129–142. Available at: https://doi.org/10.1016/S0140-6736(20)31179-X.

Chalela, J.A. *et al.* (2007) 'Magnetic resonance imaging and computed tomography in emergency assessment of patients with suspected acute stroke: a prospective comparison', *Lancet*, 369(9558), pp. 293–298. Available at: https://doi.org/10.1016/S0140-6736(07)60151-2.

Chappell, M.A. *et al.* (2009) 'Variational Bayesian Inference for a Nonlinear Forward Model', *IEEE Transactions on Signal Processing*, 57(1), pp. 223–236. Available at: https://doi.org/10.1109/TSP.2008.2005752.

Chen, C. *et al.* (2017) 'Influence of penumbral reperfusion on clinical outcome depends on baseline ischemic core volume', *Stroke*, 48(10), pp. 2739–2745. Available at: https://doi.org/10.1161/STROKEAHA.117.018587.

Chen, Y., Wang, D.J.J. and Detre, J.A. (2011) 'Test-retest reliability of arterial spin labeling with common labeling strategies', *Journal of Magnetic Resonance Imaging*, 33(4), pp. 940–949. Available at: https://doi.org/10.1002/jmri.22345.

Christensen, S. *et al.* (2019) 'Persistent Target Mismatch Profile >24 Hours After Stroke Onset in DEFUSE 3', *Stroke*, 50(3), pp. 754–757. Available at: https://doi.org/10.1161/STROKEAHA.118.023392.

Clement, P. *et al.* (2018) 'Variability of physiological brain perfusion in healthy subjects – A systematic review of modifiers. Considerations for multi-center ASL

studies', *Journal of Cerebral Blood Flow and Metabolism*. Available at: https://doi.org/10.1177/0271678X17702156.

Cordonnier, C. *et al.* (2018) 'Intracerebral haemorrhage: current approaches to acute management', *The Lancet*, 392(10154), pp. 1257–1268. Available at: https://doi.org/10.1016/S0140-6736(18)31878-6.

Crisi, G., Filice, S. and Scoditti, U. (2018) 'Arterial Spin Labeling MRI to Measure Cerebral Blood Flow in Untreated Ischemic Stroke', *Journal of Neuroimaging* [Preprint]. Available at: https://doi.org/10.1111/jon.12569.

Dalby, R.B. *et al.* (2019) 'Oxygenation differs among white matter hyperintensities, intersected fiber tracts and unaffected white matter†', *Brain Communications*, 1(1), p. 395. Available at: https://doi.org/10.1093/braincomms/fcz033.

Davis, S.M. *et al.* (2008) 'Effects of alteplase beyond 3 h after stroke in the Echoplanar Imaging Thrombolytic Evaluation Trial (EPITHET): a placebo-controlled randomised trial', *The Lancet Neurology*, 7(4), pp. 299–309. Available at: https://doi.org/10.1016/S1474-4422(08)70044-9.

Dawson, J. *et al.* (2018) 'Xanthine oxidase inhibition for the improvement of long-term outcomes following ischaemic stroke and transient ischaemic attack (XILO-FIST) – Protocol for a randomised double blind placebo-controlled clinical trial', *European Stroke Journal*, 3(3), pp. 281–290. Available at: https://doi.org/10.1177/2396987318771426.

Dawson, J. *et al.* (2023) 'Xanthine oxidase inhibition and white matter hyperintensity progression following ischaemic stroke and transient ischaemic attack (XILO-FIST): a multicentre, double-blinded, randomised, placebo-controlled trial', *eClinicalMedicine*, 57. Available at: https://doi.org/10.1016/J.ECLINM.2023.101863/ATTACHMENT/6BE65F51-4F52-490F-BA41-B45ADD720BB5/MMC1.DOCX.

Debette, S. *et al.* (2010) 'Association of MRI markers of vascular brain injury with incident stroke, mild cognitive impairment, dementia, and mortality: The framingham offspring study', *Stroke*, 41(4), pp. 600–606. Available at: https://doi.org/10.1161/STROKEAHA.109.570044.

Debette, S. and Markus, H.S. (2010) 'The clinical importance of white matter hyperintensities on brain magnetic resonance imaging: Systematic review and meta-analysis', *BMJ (Online)*. British Medical Journal Publishing Group, p. 288. Available at: https://doi.org/10.1136/bmj.c3666.

DeCarli, C. *et al.* (1995) 'The effect of white matter hyperintensity volume on brain structure, cognitive performance, and cerebral metabolism of glucose in 51 healthy adults', *Neurology*, 45(11), pp. 2077–2084. Available at: https://doi.org/10.1212/WNL.45.11.2077.

Deibler, A.R. *et al.* (2008) 'Arterial spin-labeling in routine clinical practice, part 3: Hyperperfusion patterns', *American Journal of Neuroradiology*, 29(8), pp. 1428–1435. Available at: https://doi.org/10.3174/ajnr.A1034.

Detre, J.A. *et al.* (2012) 'Applications of arterial spin labeled MRI in the brain', *Journal of Magnetic Resonance Imaging* [Preprint]. Available at: https://doi.org/10.1002/jmri.23581.

Dickie, D.A., Quinn, T.J. and Dawson, J. (2019) 'The whole picture: From isolated to global MRI measures of neurovascular and neurodegenerative disease', in *Advances in Experimental Medicine and Biology*. Springer, pp. 25–53. Available at: https://doi.org/10.1007/978-3-030-31904-5_3.

van Dijk, E.J. *et al.* (2008) 'Progression of Cerebral Small Vessel Disease in Relation to Risk Factors and Cognitive Consequences', *Stroke*, 39(10), pp. 2712–2719. Available at: https://doi.org/10.1161/STROKEAHA.107.513176.

Dixon, W.T. *et al.* (1986) 'Projection angiograms of blood labeled by adiabatic fast passage', *Magnetic Resonance in Medicine*, 3(3), pp. 454–462. Available at: https://doi.org/10.1002/MRM.1910030311/FORMAT/PDF.

Dolui, S. *et al.* (2017) 'Comparison of PASL, PCASL, and background-suppressed 3D PCASL in mild cognitive impairment', *Human Brain Mapping*, 38(10), pp. 5260–5273. Available at: https://doi.org/10.1002/hbm.23732.

Dolui, S. *et al.* (2019) 'Characterizing a perfusion-based periventricular small vessel region of interest', *NeuroImage : Clinical*, 23. Available at: https://doi.org/10.1016/J.NICL.2019.101897.

Dongmei, W. *et al.* (2020) 'Mismatch of ASPECTS based on arterial spin labeling and diffusion-weighted imaging as an indicator for mechanical thrombectomy in patients with wake-up stroke', *Journal of Southern Medical University*, 40(1), pp. 1–5. Available at: https://doi.org/10.12122/j.issn.1673-4254.2020.01.01.

Durán-Laforet, V. *et al.* (2019) 'Delayed effects of acute reperfusion on vascular remodeling and late-phase functional recovery after stroke', *Frontiers in Neuroscience*, 13(JUL), p. 463096. Available at: https://doi.org/10.3389/FNINS.2019.00767/BIBTEX.

Edelman, R.R. *et al.* (1994) 'Qualitative mapping of cerebral blood flow and functional localization with echo-planar MR imaging and signal targeting with alternating radio frequency', *Radiology*, 192(2), pp. 513–520. Available at: https://doi.org/10.1148/radiology.192.2.8029425.

Eilaghi, A. *et al.* (2013) 'Reperfusion is a stronger predictor of good clinical outcome than recanalization in ischemic stroke', *Radiology*, 269(1). Available at: https://doi.org/10.1148/radiol.13122327.

Fazekas, F. *et al.* (1987) 'MR signal abnormalities at 1.5 T in Alzheimer's dementia and normal aging', *American Journal of Roentgenology*, 149(2), pp. 351–356. Available at: https://doi.org/10.2214/ajr.149.2.351.

Fazekas, F., Chawluk, J.B. and Alavi, A. (1987) 'MR signal abnormalities at 1.5 T in Alzheimer's dementia and normal aging', *American Journal of Neuroradiology*, 8(3), pp. 421–426.

Ferré, J.-C. *et al.* (2013) 'Arterial spin labeling (ASL) perfusion: Techniques and clinical use', *Diagnostic and Interventional Imaging*, 94(12), pp. 1211–1223. Available at: https://doi.org/10.1016/J.DIII.2013.06.010.

Fischer, E.G. and Ames, A. (1972) 'Studies on Mechanisms of Impairment of Cerebral Circulation Following Ischemia: Effect of Hemodilution and Perfusion Pressure', *Stroke*, 3. Available at: http://ahajournals.org.

Furlan, M. *et al.* (1996) 'Spontaneous neurological recovery after stroke and the fate of the ischemic penumbra', *Annals of Neurology*, 40(2), pp. 216–226. Available at: https://doi.org/10.1002/ana.410400213.

Gao, J. *et al.* (2017) 'Visibility of CT early ischemic change is significantly associated with time from stroke onset to baseline scan beyond the first 3 hours of stroke onset', *Journal of Stroke*, 19(3), pp. 340–346. Available at: https://doi.org/10.5853/jos.2016.01424.

Gibbs, J.M. *et al.* (1984) 'Evaluation of cerebral perfusion reserve in patients with carotid-artery occlusion', *The Lancet*, 323(8372), pp. 310–314. Available at: https://doi.org/10.1016/S0140-6736(84)90361-1.

Gouw, A.A. *et al.* (2008) 'Progression of white matter hyperintensities and incidence of new lacunes over a 3-year period: The leukoaraiosis and disability study', *Stroke*, 39(5), pp. 1414–1420. Available at: https://doi.org/10.1161/STROKEAHA.107.498535.

Guo, L. *et al.* (2014) 'Pseudo-continuous arterial spin labeling quantifies cerebral blood flow in patients with acute ischemic stroke and chronic lacunar stroke', *Clinical Neurology and Neurosurgery*, 125, pp. 229–236. Available at: https://doi.org/10.1016/J.CLINEURO.2014.08.017.

Habes, M. *et al.* (2016) 'White matter hyperintensities and imaging patterns of brain ageing in the general population', *Brain*, 139(4), p. 1164. Available at: https://doi.org/10.1093/BRAIN/AWW008.

Hachinski, V.C., Potter, P. and Merskey, H. (1987) 'Leuko-Araiosis', *Archives of Neurology*, 44(1), pp. 21–23. Available at: https://doi.org/10.1001/archneur.1987.00520130013009.

Hacke, W. *et al.* (1995) 'Intravenous Thrombolysis With Recombinant Tissue Plasminogen Activator for Acute Hemispheric Stroke: The European Cooperative Acute Stroke Study (ECASS)', *JAMA: The Journal of the American Medical Association*, 274(13), pp. 1017–1025. Available at: https://doi.org/10.1001/jama.1995.03530130023023.

Hakim, A.M. *et al.* (1987) 'The effect of spontaneous reperfusion on metabolic function in early human cerebral infarcts', *Annals of Neurology*, 21(3), pp. 279–289. Available at: https://doi.org/10.1002/ana.410210310.

Han, S.H. *et al.* (2019) 'Can the trail making test black and white predict white matter hyperintensity on MRI?', *Journal of Clinical Neuroscience*, 64, pp. 155–159. Available at: https://doi.org/10.1016/J.JOCN.2019.03.014.

Hanson, S.K. *et al.* (1993) 'Value of single-photon emission-computed tomography in acute stroke therapeutic trials', *Stroke*, 24(9). Available at: https://doi.org/10.1161/01.STR.24.9.1322.

Harston, G.W.J.J. *et al.* (2017) 'Quantification of Serial Cerebral Blood Flow in Acute Stroke Using Arterial Spin Labeling', *Stroke*, 48(1), pp. 123–130. Available at: https://doi.org/10.1161/STROKEAHA.116.014707.

Heiss, W. -D and Rosner, G. (1983) 'Functional recovery of cortical neurons as related to degree and duration of ischemia', *Annals of Neurology*, 14(3), pp. 294–301. Available at: https://doi.org/10.1002/ana.410140307.

Heiss, W.-D. *et al.* (2001) 'Penumbral probability thresholds of cortical flumazenil binding and blood flow predicting tissue outcome in patients with cerebral ischaemia', *Brain* [Preprint].

Heiss, W.D., Hayakawa, T. and Waltz, A.G. (1976) 'Cortical Neuronal Function During Ischemia: Effects of Occlusion of One Middle Cerebral Artery on Single-Unit Activity in Cats', *Archives of Neurology*, 33(12), pp. 813–820. Available at: https://doi.org/10.1001/archneur.1976.00500120017003.

Heit, J.J. and Wintermark, M. (2016) 'Perfusion computed tomography for the evaluation of acute ischemic stroke strengths and pitfalls', *Stroke*, 47(4), pp. 1153–1158. Available at: https://doi.org/10.1161/STROKEAHA.116.011873.

Heitsch, L. *et al.* (2020) 'Early Neurological Change after Ischemic Stroke Is Associated with 90-Day Outcome', *Stroke*, pp. 132–141. Available at: https://doi.org/10.1161/STROKEAHA.119.028687.

Higashida, R.T. *et al.* (2003) 'Trial design and reporting standards for intra-arterial cerebral thrombolysis for acute ischemic stroke', *Stroke*, 34(8). Available at: https://doi.org/10.1161/01.STR.0000082721.62796.09.

Hong, L. *et al.* (2023) 'Reperfusion measurements, treatment time, and outcomes in patients receiving endovascular treatment within 24 hours of last known well', *CNS Neuroscience & Therapeutics*, 29(4), pp. 1067–1074. Available at: https://doi.org/10.1111/CNS.14080.

Hossmann, K. -A (1994) 'Viability thresholds and the penumbra of focal ischemia', *Annals of Neurology*, 36(4), pp. 557–565. Available at: https://doi.org/10.1002/ANA.410360404.

Hussain, H. *et al.* (2013) 'Prevalence and Effect of "No Reflow" Phenomenon Following Endovascular Treatment Related Recanalization in Patients with Acute Middle Cerebral Artery Occlusion', *Neurology*, 80(7 Supplement).

Ikram, M.A. *et al.* (2015) 'The Rotterdam Scan Study: design update 2016 and main findings', *European Journal of Epidemiology*, 30(12), pp. 1299–1315. Available at: https://doi.org/10.1007/s10654-015-0105-7.

Inoue, M. *et al.* (2013) 'Clinical outcomes strongly associated with the degree of reperfusion achieved in target mismatch patients: Pooled data from the diffusion and perfusion imaging evaluation for understanding stroke evolution studies', *Stroke*, 44(7), pp. 1885–1890. Available at: https://doi.org/10.1161/STROKEAHA.111.000371.

Ishibashi, M. *et al.* (2018) 'Effects of white matter lesions on brain perfusion in patients with mild cognitive impairment', *Clinical Neurology and Neurosurgery*, 168, pp. 7–11. Available at: https://doi.org/10.1016/J.CLINEURO.2018.02.030.

Jahng, G.H. *et al.* (2003) 'Improved Perfusion-Weighted MRI by a Novel Double Inversion With Proximal Labeling of Both Tagged and Control Acquisitions', *Magnetic resonance in medicine : official journal of the Society of Magnetic Resonance in Medicine / Society of Magnetic Resonance in Medicine*, 49(2), p. 307. Available at: https://doi.org/10.1002/MRM.10339.

Jahng, G.H., Weiner, M.W. and Schuff, N. (2007) 'Improved arterial spin labeling method: Applications for measurements of cerebral blood flow in human brain at high magnetic field MRI', *Medical physics*, 34(11), p. 4519. Available at: https://doi.org/10.1118/1.2795675.

Johnson, C. *et al.* (2019) 'Global, regional, and national burden of stroke, 1990-2016: a systematic analysis for the Global Burden of Disease Study 2016.', *The Lancet. Neurology*, 18(5), pp. 439–458. Available at: https://doi.org/10.1016/S1474-4422(19)30034-1.

Jones, T.H. *et al.* (1981) 'Thresholds of focal cerebral ischemia in awake monkeys.', *Journal of neurosurgery*, 54(6), pp. 773–782. Available at: https://doi.org/10.3171/jns.1981.54.6.0773.

Jørgensen, H.S. *et al.* (1994) 'Spontaneous Reperfusion of Cerebral Infarcts in Patients with Acute Stroke: Incidence, Time Course, and Clinical Outcome in the Copenhagen Stroke Study', *Archives of Neurology*, 51(9), pp. 865–873. Available at: https://doi.org/10.1001/archneur.1994.00540210037011.

Kaufmann, A.M. *et al.* (1999) 'Ischemic core and penumbra in human stroke', *Stroke*, 30(5), pp. 1150–1153. Available at: https://doi.org/10.1161/str.30.5.1150/a.

Kety, S.S. and Schmidt, C.F. (1945) 'The Determination of Cerebral Blood Flow In Man By The Use Of Nitrous Oxide In Low Concentrations', *American Journal of Physiology-Legacy Content*, 143(1), pp. 53–66. Available at: https://doi.org/10.1152/ajplegacy.1945.143.1.53.

Khatri, P. *et al.* (2005) 'Revascularization End Points in Stroke Interventional Trials Recanalization Versus Reperfusion in IMS-I', *Stroke*, (36), pp. 2400–2403. Available at: https://doi.org/10.1161/01.STR.0000185698.45720.58.

Kim, S. -G (1995) 'Quantification of relative cerebral blood flow change by flow-sensitive alternating inversion recovery (FAIR) technique: Application to functional mapping', *Magnetic Resonance in Medicine*, 34(3), pp. 293–301. Available at: https://doi.org/10.1002/mrm.1910340303.

Konstas, A.A. *et al.* (2009) 'Theoretic basis and technical implementations of CT perfusion in acute ischemic stroke, Part 2: Technical implementations', *American Journal of Neuroradiology*. American Journal of Neuroradiology, pp. 885–892. Available at: https://doi.org/10.3174/ajnr.A1492.

Lai, Y. *et al.* (2020) 'Effect of intensive blood pressure control on the prevention of white matter hyperintensity: Systematic review and meta-analysis of randomized trials', *The Journal of Clinical Hypertension*, 22(11), p. 1968. Available at: https://doi.org/10.1111/JCH.14030.

Lansberg, M.G. *et al.* (2012) 'MRI profile and response to endovascular reperfusion after stroke (DEFUSE 2): A prospective cohort study', *The Lancet Neurology*, 11(10), pp. 860–867. Available at: https://doi.org/10.1016/S1474-4422(12)70203-X.

Li, R.R. *et al.* (2019) 'Analysis of correlation between cerebral perfusion and KIM score of white matter lesions in patients with Alzheimer's disease', *Neuropsychiatric Disease and Treatment*, 15, p. 2705. Available at: https://doi.org/10.2147/NDT.S207069.

Liebeskind, D.S. *et al.* (2019) 'eTICI reperfusion: defining success in endovascular stroke therapy', *Journal of NeuroInterventional Surgery*, 11(5), pp. 433–438. Available at: https://doi.org/10.1136/NEURINTSURG-2018-014127.
Limburg, M. *et al.* (1990) 'Single-Photon Emission Computed Tomography and Early Death in Acute Ischemic Stroke', *Stroke*, (21), pp. 1150–1155. Available at: http://ahajournals.org.

Lin, L. *et al.* (2017) 'Quantifying reperfusion of the ischemic region on whole-brain computed tomography perfusion', *Journal of Cerebral Blood Flow & Metabolism*, 37(6), p. 2125. Available at: https://doi.org/10.1177/0271678X16661338.

Lindner, T. *et al.* (2023) 'Current state and guidance on arterial spin labeling perfusion MRI in clinical neuroimaging', *Magnetic Resonance in Medicine*, 89(5), pp. 2024–2047. Available at: https://doi.org/10.1002/MRM.29572.

Lu, S. shan *et al.* (2020) 'Hyperperfusion on Arterial Spin Labeling MRI Predicts the 90-Day Functional Outcome After Mechanical Thrombectomy in Ischemic Stroke', *Journal of Magnetic Resonance Imaging* [Preprint]. Available at: https://doi.org/10.1002/jmri.27455.

Lyu, J. *et al.* (2022) 'Arterial Spin Labeling-Based MRI Estimation of Penumbral Tissue in Acute Ischemic Stroke', *Journal of Magnetic Resonance Imaging* [Preprint]. Available at: https://doi.org/10.1002/JMRI.28364.

Ma, H. *et al.* (2019) 'Thrombolysis Guided by Perfusion Imaging up to 9 Hours after Onset of Stroke', *New England Journal of Medicine*, 380(19), pp. 1795–1803. Available at: https://doi.org/10.1056/NEJMoa1813046.

Maniega, S.M. *et al.* (2015) 'White matter hyperintensities and normal-appearing white matter integrity in the aging brain', *Neurobiology of Aging*, 36(2), pp. 909–918. Available at: https://doi.org/10.1016/j.neurobiolaging.2014.07.048.

Marchal, G., Furlan, M., *et al.* (1996) *Early spontaneous hyperperfusion after stroke A marker of favourable tissue outcome?*, *Brain*. Available at: https://academic.oup.com/brain/article-abstract/119/2/409/382378 (Accessed: 22 October 2019).

Marchal, G., Beaudouin, V., *et al.* (1996) 'Prolonged Persistence of Substantial Volumes of Potentially Viable Brain Tissue After Stroke', *Stroke*, 27(4), pp. 599–606. Available at: https://doi.org/10.1161/01.STR.27.4.599.

Marchal, G. *et al.* (1999) 'Voxel-based mapping of irreversible ischaemic damage with PET in acute stroke', *Brain*, 122(12), pp. 2387–2400. Available at: https://doi.org/10.1093/brain/122.12.2387.

Markus, H.S. (2004) 'Cerebral perfusion and stroke.', *Journal of neurology, neurosurgery, and psychiatry*, 75(3), pp. 353–61. Available at: https://doi.org/10.1136/JNNP.2003.025825.

McCullough-Hicks, M.E. *et al.* (2021) 'The bright vessel sign on arterial spin labeling MRI for heralding and localizing large vessel occlusions', *Journal of Neuroimaging*, p. jon.12888. Available at: https://doi.org/10.1111/jon.12888.

McDonald, R.J. *et al.* (2015) 'Intracranial gadolinium deposition after contrast-enhanced MR imaging', *Radiology*, 275(3), pp. 772–782. Available at: https://doi.org/10.1148/radiol.15150025.

Mead, G.E. *et al.* (2000) 'How well does the Oxfordshire Community Stroke Project classification predict the site and size of the infarct on brain imaging?', *Journal of Neurology Neurosurgery and Psychiatry*, 68(5), pp. 558–562. Available at: https://doi.org/10.1136/jnnp.68.5.558.

Menon, B.K. *et al.* (2015) 'Multiphase CT angiography: A new tool for the imaging triage of patients with acute ischemic stroke', *Radiology*, 275(2), pp. 510–520. Available at: https://doi.org/10.1148/radiol.15142256.

Mirasol, R. v. *et al.* (2014) 'Assessing reperfusion with whole-brain arterial spin labeling a noninvasive alternative to gadolinium', *Stroke*, 45(2), pp. 456–461. Available at: https://doi.org/10.1161/STROKEAHA.113.004001.

Miteff, F. *et al.* (2009) 'The independent predictive utility of computed tomography angiographic collateral status in acute ischaemic stroke', *Brain*, 132(8), pp. 2231–2238. Available at: https://doi.org/10.1093/brain/awp155.

Moseley, M.E. *et al.* (1990) 'Diffusion-weighted MR imaging of acute stroke: Correlation with T2-weighted and magnetic susceptibility-enhanced MR imaging in cats', *American Journal of Neuroradiology*, 11(3), pp. 423–429.

Muir, Keith W *et al.* (2006) 'Imaging of acute stroke', *The Lancet Neurology*, 5(9), pp. 755–768. Available at: https://doi.org/10.1016/S1474-4422(06)70545-2.

Muir, K W *et al.* (2006) 'Visual evaluation of perfusion computed tomography in acute stroke accurately estimates infarct volume and tissue viability', *Journal of Neurology, Neurosurgery, and Psychiatry*, 77(3), p. 334. Available at: https://doi.org/10.1136/JNNP.2005.074179.

Muir, K.W. *et al.* (2007) 'Can the ischemic penumbra be identified on noncontrast CT of acute stroke?', *Stroke*, 38(9), pp. 2485–2490. Available at: https://doi.org/10.1161/STROKEAHA.107.484592.

Mutsaerts, H.J.M.M. *et al.* (2015) 'Multi-vendor reliability of arterial spin labeling perfusion MRI using a near-identical sequence: Implications for multi-center studies', *NeuroImage*, 113, pp. 143–152. Available at: https://doi.org/10.1016/j.neuroimage.2015.03.043.

Nael, K. *et al.* (2013) 'Quantitative analysis of hypoperfusion in acute stroke: arterial spin labeling versus dynamic susceptibility contrast.', *Stroke*, 44(11), pp. 3090–6. Available at: https://doi.org/10.1161/STROKEAHA.113.002377.

Nehra, A.K. *et al.* (2018) 'Accumulation of gadolinium in human cerebrospinal fluid after gadobutrol-enhanced MR imaging: A prospective observational cohort study', *Radiology*, 288(2), pp. 416–423. Available at: https://doi.org/10.1148/RADIOL.2018171105/ASSET/IMAGES/LARGE/RADIOL.2018171105.TBL4.JPEG.

Niibo, T. *et al.* (2013) 'Arterial Spin–Labeled Perfusion Imaging to Predict Mismatch in Acute Ischemic Stroke', *Stroke*, 44(9), pp. 2601–2603. Available at: https://doi.org/10.1161/STROKEAHA.113.002097.

Nylander, R. *et al.* (2018) 'Quantitative and qualitative MRI evaluation of cerebral small vessel disease in an elderly population: a longitudinal study', *Acta Radiologica*, 59(5), pp. 612–618. Available at: https://doi.org/10.1177/0284185117727567/ASSET/IMAGES/LARGE/10.1177_0284185117727567-FIG2.JPEG.

Okazaki, S. *et al.* (2017) 'Cerebral hyperperfusion on arterial spin labeling MRI after reperfusion therapy is related to hemorrhagic transformation', *Journal of Cerebral Blood Flow and Metabolism*, 37(9), pp. 3087–3090. Available at: https://doi.org/10.1177/0271678X17718099.

Olivot, J.M. *et al.* (2014) 'Hypoperfusion Intensity Ratio Predicts Infarct Progression and Functional Outcome in the DEFUSE 2 Cohort', *Stroke; a journal of cerebral circulation*, 45(4), p. 1018. Available at: https://doi.org/10.1161/STROKEAHA.113.003857.

van Osch, M.J.P. *et al.* (2009) 'Can arterial spin labeling detect white matter perfusion signal?', *Magnetic Resonance in Medicine*, 62(1), pp. 165–173. Available at: https://doi.org/10.1002/mrm.22002.

Østergaard, L. (2005) 'Principles of cerebral perfusion imaging by bolus tracking', in *Journal of Magnetic Resonance Imaging*. John Wiley & Sons, Ltd, pp. 710–717. Available at: https://doi.org/10.1002/jmri.20460.

Pantoni, L. and Garcia, J.H. (1997) 'Pathogenesis of leukoaraiosis: A review', *Stroke*. Lippincott Williams and Wilkins, pp. 652–659. Available at: https://doi.org/10.1161/01.STR.28.3.652.

Parkes, L.M. *et al.* (2004) 'Normal Cerebral Perfusion Measurements Using Arterial Spin Labeling: Reproducibility, Stability, and Age and Gender Effects', *Magnetic Resonance in Medicine*, 51(4), pp. 736–743. Available at: https://doi.org/10.1002/mrm.20023.

Petersen, E.T., Mouridsen, K. and Golay, X. (2010) 'The QUASAR reproducibility study, Part II: Results from a multi-center Arterial Spin Labeling test-retest study', *NeuroImage*, 49(1), pp. 104–113. Available at: https://doi.org/10.1016/J.NEUROIMAGE.2009.07.068.

Powers, W.J. and Raichle, M.E. (1985) 'Positron emission tomography and its application to the study of cerebrovascular disease in man', *Stroke*, 16(3). Available at: https://doi.org/10.1161/01.STR.16.3.361.

Prins, N.D. *et al.* (2004) 'Measuring progression of cerebral white matter lesions on MRI', *Neurology*, 62(9), pp. 1533–1539. Available at: https://doi.org/10.1212/01.WNL.0000123264.40498.B6.

Purushotham, A. *et al.* (2015) 'Apparent diffusion coefficient threshold for delineation of ischemic core', *International Journal of Stroke*, 10(3), pp. 348–353. Available at: https://doi.org/10.1111/ijs.12068.

Read, S.J. *et al.* (2000) 'The fate of hypoxic tissue on 18F-fluoromisonidazole positron emission tomography after ischemic stroke', *Annals of Neurology*, 48(2), pp. 228–235. Available at: https://doi.org/10.1002/1531-8249(200008)48:2<228::AID-ANA13>3.0.CO;2-B.

Rha, J.H. and Saver, J.L. (2007) 'The impact of recanalization on ischemic stroke outcome: A meta-analysis', *Stroke*, 38(3), pp. 967–973. Available at: https://doi.org/10.1161/01.STR.0000258112.14918.24.

Ringleb, P. *et al.* (2019) 'Extending the time window for intravenous thrombolysis in acute ischemic stroke using magnetic resonance imaging-based

patient selection', *International Journal of Stroke*, 14(5), pp. 483–490. Available at: https://doi.org/10.1177/1747493019840938.

Roberts, D.A. *et al.* (1994) 'Quantitative magnetic resonance imaging of human brain perfusion at 1.5 T using steady-state inversion of arterial water', *Proceedings of the National Academy of Sciences of the United States of America*, 91(1), pp. 33–37. Available at: https://doi.org/10.1073/pnas.91.1.33.

Rubiera, M. *et al.* (2005) 'Predictors of early arterial reocclusion after tissue plasminogen activator-induced recanalization in acute ischemic stroke', *Stroke*, 36(7), pp. 1452–1456. Available at: https://doi.org/10.1161/01.STR.0000170711.43405.81.

Ryu, W.S. *et al.* (2019) 'White matter hyperintensity load on stroke recurrence and mortality at 1 year after ischemic stroke', *Neurology*, 93(6), pp. E578–E589. Available at: https://doi.org/10.1212/WNL.0000000000007896.

Sacco, R.L. *et al.* (2013) 'An updated definition of stroke for the 21st century: A statement for healthcare professionals from the American heart association/American stroke association', *Stroke*, 44(7), pp. 2064–2089. Available at: https://doi.org/10.1161/STR.0b013e318296aeca.

Sarraj, A. *et al.* (2021) 'Early Infarct Growth Rate Correlation With Endovascular Thrombectomy Clinical Outcomes', *Stroke*, pp. 57–69. Available at: https://doi.org/10.1161/STROKEAHA.120.030912.

Saver, J.L. and Altman, H. (2012) 'Relationship between neurologic deficit severity and final functional outcome shifts and strengthens during first hours after onset', *Stroke*, 43(6), pp. 1537–1541. Available at: https://doi.org/10.1161/STROKEAHA.111.636928.

Scheltens, P. *et al.* (1993) 'A semiquantative rating scale for the assessment of signal hyperintensities on magnetic resonance imaging', *Journal of the Neurological Sciences*, 114(1), pp. 7–12. Available at: https://doi.org/10.1016/0022-510X(93)90041-V.

Schiphorst, A. ter *et al.* (2021) 'Tissue no-reflow despite full recanalization following thrombectomy for anterior circulation stroke with proximal occlusion: A clinical study', *Journal of Cerebral Blood Flow and Metabolism*, 41(2), pp. 253–266. Available at: https://doi.org/10.1177/0271678X20954929.

van Seeters, T. *et al.* (2015) 'The Prognostic Value of CT Angiography and CT Perfusion in Acute Ischemic Stroke', *Cerebrovascular Diseases*, 40(5–6), pp. 258–269. Available at: https://doi.org/10.1159/000441088.

Shi, Y. and Wardlaw, J.M. (2016a) *Update on cerebral small vessel disease: A dynamic whole-brain disease*, *Stroke and Vascular Neurology*. BMJ Publishing Group. Available at: https://doi.org/10.1136/svn-2016-000035.

Shi, Y. and Wardlaw, J.M. (2016b) *Update on cerebral small vessel disease: A dynamic whole-brain disease*, *Stroke and Vascular Neurology*. BMJ Publishing Group. Available at: https://doi.org/10.1136/svn-2016-000035.

Silva, A.C. *et al.* (1995) 'Multi-Slice MRI of Rat Brain Perfusion During Amphetamine Stimulation Using Arterial Spin Labeling', *Magnetic Resonance in Medicine*, 33(2), pp. 209–214. Available at: https://doi.org/10.1002/mrm.1910330210.

Soares, B.P. *et al.* (2010) 'Reperfusion Is a More Accurate Predictor of Follow-Up Infarct Volume than Recanalization: A Proof of Concept using CT in Acute Ischemic Stroke Patients', *Stroke; a journal of cerebral circulation*, 41(1), p. e34. Available at: https://doi.org/10.1161/STROKEAHA.109.568766.

Stewart, C.R. *et al.* (2021) 'Associations Between White Matter Hyperintensity Burden, Cerebral Blood Flow and Transit Time in Small Vessel Disease: An Updated Meta-Analysis', *Frontiers in Neurology*, 0, p. 621. Available at: https://doi.org/10.3389/FNEUR.2021.647848.

Strong, A.J., Venables, G.S. and Gibson, G. (1983) 'The cortical ischaemic penumbra associated with occlusion of the middle cerebral artery in the cat: I. Topography of changes in blood flow, potassium ion activity, and EEG', *Journal of Cerebral Blood Flow and Metabolism*, 3(1), pp. 86–96. Available at: https://doi.org/10.1038/jcbfm.1983.11.

Tan, J.C. *et al.* (2007) 'Systematic comparison of perfusion-CT and CT-angiography in acute stroke patients', *Annals of Neurology*, 61(6), pp. 533–543. Available at: https://doi.org/10.1002/ANA.21130.

Tate, W.J. *et al.* (2021) 'Predictors of Early and Late Infarct Growth in DEFUSE 3', *Frontiers in Neurology*, 12, p. 1117. Available at: https://doi.org/10.3389/FNEUR.2021.699153/BIBTEX.

The National Institute of Neurological Disorders and Stroke rt-PA Stroke Study Group (1995) 'Tissue Plasminogen Activator for Acute Ischemic Stroke', *N Engl J Med*, 333(24), pp. 1581–1588. Available at: https://doi.org/10.1056/NEJM199512143332401.

Turk, M., Zaletel, M. and Pretnar-Oblak, J. (2016) 'Ratio between carotid artery stiffness and blood flow – a new ultrasound index of ischemic leukoaraiosis', *Clinical Interventions in Aging*, 11, p. 65. Available at: https://doi.org/10.2147/CIA.S94163.

Tustison, N.J. *et al.* (2014) 'Large-scale evaluation of ANTs and FreeSurfer cortical thickness measurements', *NeuroImage*, 99, pp. 166–179. Available at: https://doi.org/10.1016/j.neuroimage.2014.05.044.

Vagal, A. *et al.* (2018) 'Collateral clock is more important than time clock for tissue fate a natural history study of acute ischemic strokes', *Stroke*, 49(9), pp. 2102–2107. Available at: https://doi.org/10.1161/STROKEAHA.118.021484.

van der Veen, P.H. *et al.* (2015) 'Longitudinal Relationship between Cerebral Small-Vessel Disease and Cerebral Blood Flow', *Stroke*, 46(5), pp. 1233–1238. Available at: https://doi.org/10.1161/STROKEAHA.114.008030.

Verro, P. *et al.* (2002) 'CT angiography in acute ischemic stroke: Preliminary results', *Stroke*, 33(1), pp. 276–278. Available at: https://doi.org/10.1161/hs0102.101223.

Vos, T. *et al.* (2020) 'Global burden of 369 diseases and injuries in 204 countries and territories, 1990–2019: a systematic analysis for the Global Burden of Disease Study 2019', *The Lancet*, 396(10258). Available at: https://doi.org/10.1016/S0140-6736(20)30925-9.

Wang, D.J.J. *et al.* (2012) 'The Value of Arterial Spin-Labeled Perfusion Imaging in Acute Ischemic Stroke', *Stroke*, 43(4), pp. 1018–1024. Available at: https://doi.org/10.1161/STROKEAHA.111.631929.

Wang, D.J.J. *et al.* (2013) 'Multi-delay multi-parametric arterial spin-labeled perfusion MRI in acute ischemic stroke - Comparison with dynamic susceptibility contrast enhanced perfusion imaging', *NeuroImage: Clinical*, 3, pp. 1–7. Available at: https://doi.org/10.1016/j.nicl.2013.06.017.

Wang, Xinyu *et al.* (2021) 'Can 3D Pseudo-Continuous Territorial Arterial Spin Labeling Effectively Diagnose Patients With Recanalization of Unilateral Middle Cerebral Artery Stenosis?', *Journal of Magnetic Resonance Imaging* [Preprint]. Available at: https://doi.org/10.1002/jmri.27560.

Wardlaw, J.M. *et al.* (2013) 'Neuroimaging standards for research into small vessel disease and its contribution to ageing and neurodegeneration', *Lancet Neurology*, 12(8), p. 822. Available at: https://doi.org/10.1016/S1474-4422(13)70124-8.

Weber, R. *et al.* (2012) 'Telmisartan on top of antihypertensive treatment does not prevent progression of cerebral white matter lesions in the prevention regimen for effectively avoiding second strokes (PRoFESS) MRI substudy', *Stroke*, 43(9), pp. 2336–2342. Available at: https://doi.org/10.1161/STROKEAHA.111.648576.

Williams, D.S. *et al.* (1992) 'Magnetic resonance imaging of perfusion using spin inversion of arterial water', *Proceedings of the National Academy of Sciences of the United States of America*, 89(1), pp. 212–216. Available at: https://doi.org/10.1073/pnas.89.1.212.

Wintermark, M. *et al.* (2008) 'Acute Stroke Imaging Research Roadmap', *Stroke*, (39), pp. 1621–1628. Available at: https://doi.org/10.1161/STROKEAHA.107.512319.

Wong, E. (2007) 'Vessel-encoded arterial spin-labeling using pseudocontinuous tagging', *Magnetic resonance in medicine*, 58(6), pp. 1086–1091. Available at: https://doi.org/10.1002/MRM.21293.

Wong, E.C., Buxton, R.B. and Frank, L.R. (1997) 'Implementation of quantitative perfusion imaging techniques for functional brain mapping using pulsed arterial spin labeling.', *NMR in Biomedicine*, 10(4–5), pp. 237–49.

Wong, E.C., Buxton, R.B. and Frank, L.R. (1998a) 'A theoretical and experimental comparison of continuous and pulsed arterial spin labeling techniques for quantitative perfusion imaging', *Magnetic resonance in medicine*, 40(3), pp. 348–355. Available at: https://doi.org/10.1002/MRM.1910400303.

Wong, E.C., Buxton, R.B. and Frank, L.R. (1998b) 'Quantitative imaging of perfusion using a single subtraction (QUIPSS and QUIPSS II)', *Magnetic Resonance in Medicine*, 39(5), pp. 702–708. Available at: https://doi.org/10.1002/mrm.1910390506.

Wu, W.C. *et al.* (2007) 'A theoretical and experimental investigation of the tagging efficiency of pseudocontinuous arterial spin labeling', *Magnetic Resonance in Medicine*, 58(5), pp. 1020–1027. Available at: https://doi.org/10.1002/mrm.21403.

Xing, C. *et al.* (2012) 'Pathophysiologic cascades in ischemic stroke.', *International journal of stroke : official journal of the International Stroke Society*, 7(5), pp. 378–85. Available at: https://doi.org/10.1111/j.1747-4949.2012.00839.x.

Yamamoto, D. *et al.* (2017) 'Perioperative Changes in Cerebral Perfusion Territories Assessed by Arterial Spin Labeling Magnetic Resonance Imaging Are Associated with Postoperative Increases in Cerebral Blood Flow in Patients with Carotid Stenosis.', *World Neurosurgery*, 102, pp. 477–486. Available at: https://doi.org/10.1016/J.WNEU.2017.03.037.

Yemisci, M. *et al.* (2009) 'Pericyte contraction induced by oxidative-nitrative stress impairs capillary reflow despite successful opening of an occluded cerebral artery', *Nature Medicine 2009 15:9*, 15(9), pp. 1031–1037. Available at: https://doi.org/10.1038/nm.2022.

Yonas, T. *et al.* (1991) 'CBF Measured by Xe-CT: Approach to Analysis and Normal Values', *Journal of Cerebral Blood Flow & Metabolism*, 11, pp. 716–725.

Yu, S. *et al.* (2015) 'Postischemic hyperperfusion on arterial spin labeled perfusion MRI is linked to hemorrhagic transformation in stroke.', *Journal of cerebral blood flow and metabolism : official journal of the International Society of Cerebral Blood Flow and Metabolism*, 35(4), pp. 630–7. Available at: https://doi.org/10.1038/jcbfm.2014.238.

Yu, S. *et al.* (2020) 'Reperfusion Into Severely Damaged Brain Tissue Is Associated With Occurrence of Parenchymal Hemorrhage for Acute Ischemic Stroke', *Frontiers in Neurology*, 11, p. 586. Available at: https://doi.org/10.3389/fneur.2020.00586.

Zerna, C. *et al*. (2018) ‘Current practice and future directions in the diagnosis and acute treatment of ischaemic stroke.’, *The Lancet*, 392(10154), pp. 1247–1256. Available at: https://doi.org/10.1016/S0140-6736(18)31874-9.
Zhang, L.X. *et al*. (2021) ‘Examination of optimized protocols for pCASL: Sensitivity to macrovascular contamination, flow dispersion, and prolonged arterial transit time’, *Magn Reson Med*, 00, pp. 1–12. Available at: https://doi.org/10.1002/mrm.28839.